

# CD ADAPCO

ISSUE 37

DESIGN EXPLORATION

## CFD SHAPES YOUR WORLD - FROM DIAPERS TO DENTAL IMPLANTS

### LIFE SCIENCES

Something to Smile About: Using Simulation to Improve Dental Implants!

### ELECTRONICS

Blasted by the Sun: Thermacore Cools the World's Largest Solar Telescope

### MANUFACTURING

Kimberly-Clark Puts the Elastic in Viscoelasticity!

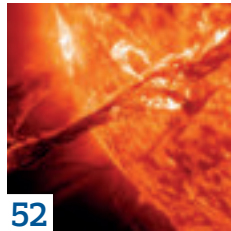
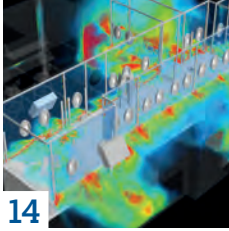


# COMING SOON **STAR-CCM+ v10**



# MULTI- DISCIPLINARY DESIGN EXPLORATION

# CONTENTS



## EDITORIAL

Dynamics welcomes editorial from all users of CD-adapco™ software or services. To submit an article:

Email: [editorial@cd-adapco.com](mailto:editorial@cd-adapco.com)

Telephone: +44 (0)20 7471 6200

## EDITOR

Anna-Maria Aurich - [anna-maria.aurich@cd-adapco.com](mailto:anna-maria.aurich@cd-adapco.com)

## ASSOCIATE EDITORS

Sabine Goodwin - [sabine.goodwin@cd-adapco.com](mailto:sabine.goodwin@cd-adapco.com)

Prashanth Shankara - [prashanth.shankara@cd-adapco.com](mailto:prashanth.shankara@cd-adapco.com)

## DESIGN & ART DIRECTION

Ian Young - [ian.young@cd-adapco.com](mailto:ian.young@cd-adapco.com)

## PRESS CONTACT

US: Lauren Gautier - [lauren.gautier@cd-adapco.com](mailto:lauren.gautier@cd-adapco.com)

Europe: Julia Martin - [julia.martin@cd-adapco.com](mailto:julia.martin@cd-adapco.com)

## ADVERTISING SALES

Geri Jackman - [geri.jackman@cd-adapco.com](mailto:geri.jackman@cd-adapco.com)

## EVENTS

US: Lenny O'Donnell - [lenny.odonnell@cd-adapco.com](mailto:lenny.odonnell@cd-adapco.com)

Europe: Sandra Maureder - [sandra.maureder@cd-adapco.com](mailto:sandra.maureder@cd-adapco.com)

## SUBSCRIPTIONS & DIGITAL EDITIONS

Dynamics is published approximately twice a year, and distributed internationally. All recent editions of Dynamics, Special Reports & Digital Reports are now available online: [www.cd-adapco.com/magazine](http://www.cd-adapco.com/magazine)

We also produce our monthly e-dynamics newsletter which is available on subscription.

To subscribe or unsubscribe to Dynamics and e-dynamics, please send an email to [info@cd-adapco.com](mailto:info@cd-adapco.com).

## ▶ INTRODUCTION

02 - Welcome to the Third Age of CFD!

Bill Clark - CD-adapco™

## ▶ FROM THE BLOG

03 - Supercharge Your Meshing with Concurrent Per-Part Meshing

James Clement - CD-adapco™

04 - Time Saving Tips!

Matthew Godo - CD-adapco™

06 - CAD Robustness & Adjoint Expressions

Joel Davidson - CD-adapco™

## ▶ LIFE SCIENCES

08 - Something to Smile About: Using Simulation to Improve Dental Implants!

Sabine A. Goodwin - CD-adapco™

Kwok-Hung (Albert) Chung & C. Wadhvani - University of Washington

14 - When CFD Secures the Manufacturing Process of Vaccines

Philippe B. Vincent & François Turgeon - Creaform

## ▶ GROUND TRANSPORTATION

20 - Overlapping Overset Meshes Open New Prospects for CFD Simulation of Moving Gear Systems

Christine Klier, Matthias Banholzer, Ludwig Berger &

Kathleen Stock - CFD Schuck Ingenieurgesellschaft mbH

26 - The Can-Am®Spyder®ST - It Actually Takes Three (Wheels) to Tango!

David Laroche - Bombardier Recreational Products Inc.

Prashanth Shankara - CD-adapco™

32 - Analysis of Pre-Ignition Initiation Mechanisms with CFD

Michael Heiss & Thomas Lauer - Vienna University of Technology

## ▶ OIL & GAS

38 - It's Getting Hot in Here! Zeeco Solves the Mystery of a Heater Malfunction using STAR-CCM+®

Zhili (Alex) Qin - Zeeco Inc

Prashanth Shankara - CD-adapco™

42 - Picking Up Bad Vibrations: Porter McGuffie Troubleshoot a Vibrating Heater

Titus Sgro - CD-adapco™

46 - Using Simulation to Assess the Fatigue Life of Subsea Jumpers

Oleg Voronkov, Alan Mueller, Alex Read

& Sabine A. Goodwin - CD-adapco™

## ▶ ELECTRONICS

52 - Blasted by the Sun: Thermacore Cools the World's Largest Solar Telescope

Stephen Ferguson - CD-adapco™

## ▶ CPI-MANUFACTURING

56 - From Gob to Bottle: Bottero Simulates the Complete Glass Forming Process

Simone Ferrari - Bottero S.p.A

## ▶ MANUFACTURING

62 - Kimberley-Clark Puts the Elastic in Viscoelasticity!

Reza R. Rend & Dwayne Jackson - Kimberley-Clark Corporation

Sabine A. Goodwin - CD-adapco™

# Welcome to the Third Age of CFD!



Today, our customers are asking for a simulation capability that will help them “see the big picture” by simulating whole systems and predicting the performance of their design in the context that it will actually be used.

**C**omputational Fluid Dynamics (CFD) is about solving difficult engineering problems, using expensive software, enormous computing resources and highly trained engineers. If the problems weren't difficult, or important, it is doubtful that anyone would devote so much effort, time and money at solving them. From the perspective of a modern engineer, it would be easy to assume that this desire to apply simulation technology to complex problems is a recent concern; that only today are we able to contemplate solving tough industrial problems, armed with a complex array of multi-physics simulation tools.

This is a misconception. Twenty years ago, commercial CFD was born from a desire to solve problems involving turbulence, heat transfer and combustion, based on the vision of a small group of pioneering researchers who were able to see beyond the meager computing resources available at the time, and to develop the methods that would ultimately revolutionize engineering.

At that time, CFD meshes could take months to construct, usually by a process of “hand-meshing” by which a (usually PhD qualified) engineer painstakingly built up meshes vertex-by-vertex. Although “automatic meshing technology” was starting to become available in the early 90s, it was far from reliable and it tended to generate more cells than the meagre computing resources of the time could handle. This was the “first age of CFD”. Getting a simulation result was

difficult and time-consuming and CFD was usually deployed at the end of the design process, as a final verification, or for troubleshooting purposes, when everything else had failed.

The arrival of cheap Linux computers reduced parallel licensing costs and the improving simulation technology opened up the “second age of CFD”, in which CFD engineers could reliably provide simulation results within reasonable timescales. Consequently, simulation began to establish itself as the core part of the design process, providing a constant stream of data that could be used to drive design decisions. Increasingly, simulation began to displace experimentation as a way of verifying designs and we began to consider problems that involved “Fluid Structure Interaction”, multiphase flow, and chemical reaction.

Which brings us to today, and the dawn of the “third age of CFD”, where lines between CFD and structural mechanics are becoming so blurred that it makes little sense calling it “CFD” at all. To meet the demands of industry, it is no longer enough to do “a bit of CFD” or “some stress analysis”. Complex industrial problems require solutions that span a multitude of physical phenomena. What our customers are really asking for today is the ability to “see the big picture” by simulating whole systems and predicting the performance of their design in the context that it will actually be used.

Whereas previous generations of engineers could take some comfort in

the “safety net” of extensive physical testing, Computer Aided Engineering is increasingly the victim of its own success as simulation continues to displace hardware testing as industry's verification method of choice. Although this increased confidence in simulation is well-deserved, it brings with it a great deal of pressure to “get the answer right” every time.

An important part of this is “automated design exploration”, in which the simulation results automatically drive design improvements, with minimal input from the engineer. With this approach, CFD is used to compile databases of simulation results that explore the complete range of usage scenarios, or it is tied to optimization technology (such as our HEEDS software) to automatically determine the best solution to a given problem.

A flick through the pages of this magazine should demonstrate just how important engineering simulation has become, not just for “high-tech” industries such as automotive and aerospace, but in designing consumer products that we use every day: from more comfortable diapers for infants to better dental implants which will allow you to keep flashing a beautiful smile in your old age.

Enjoy your read!

Bill Clark  
Executive Vice President CD-adapco™

# Supercharge Your Meshing with Concurrent Per-Part Meshing (CPPM)

JAMES CLEMENT  
CD-adapco™

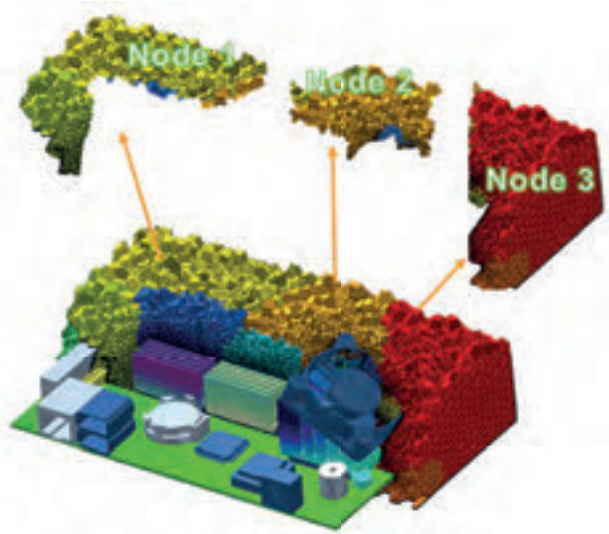


FIGURE 1: Parallel meshing

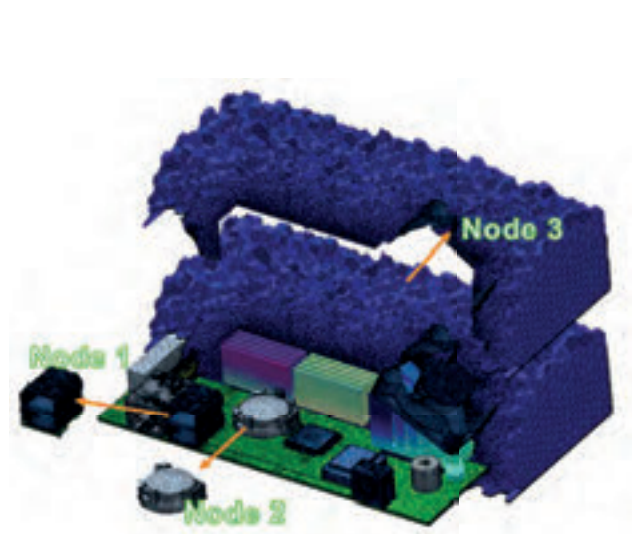


FIGURE 2: Concurrent per-part meshing

In an effort to make STAR-CCM+® even faster on a broader range of problem types, the latest version offers Concurrent Per-Part Meshing (which is a bit of a mouth full, so we'll call it CPPM instead).

Now, I'm sure you're asking yourself, "What's the difference between CPPM and regular parallel meshing?"

The answer is simple: Parallel meshing will take a single part or group of parts, split the domain into arbitrary volumes, and then distribute those volumes across nodes to mesh in parallel. CPPM allows users to mesh individual parts in serial but each part being meshed will be distributed to an individual processor. Since this process is really serial at heart, this means that it applies to not just the volume meshers but also the surface wrapper and the remesher. The CPPM option is only available when the part operation is in per-part mode, since the

parallel delineation is defined by the part itself.

So let's take an example. We want to non-conformally mesh a circuit board that contains 100 components. Historically, STAR-CCM+® would take each part and mesh it one after another on a single processor. Now with CPPM, that process can leverage as many CPUs as the user can throw at it. If we load the above simulation on 101 cores, each part will be meshed on a separate core all at the same time. So now the meshing process will only take as long as it takes to mesh the largest (mesh-count) component. To put some numbers behind this, if these 100 parts each take ten seconds to mesh in STAR-CCM+®, the meshing time with CPPM is about 10 seconds for the whole board instead of 1000 seconds. Notice earlier I mentioned that we need 101 cores to mesh each part on one core. That extra core is the "controller" core; which hides a very

powerful feature. This core acts like a head node on a queuing system, so if we have ten cores meshing 100 parts, the controller will automatically monitor each core's progress and send a new part to it when it finishes its current part. This means if a user has 99 small solid components and 1 large air domain, as the air domain meshes, the other parts will be churning out on the remaining cores without having to wait on the air domain.

Let's finish by investigating how CPPM might be used to mesh a complex problem, such as a thermal plume analysis on a helicopter. In this case, we need: a wrapped volume of the air, a wrapped volume of the internal exhaust passages and 947 solid components. In previous versions of STAR-CCM+®, this example took over seven hours to complete. Now, with concurrent meshing, this process can take as little as one and a half hours.

# Time Saving Tips!

**MATTHEW GODO**  
CD-adapco™



**M**any of us spend long hours (or what feels like long hours) in front of our STAR-CCM+® product interface and naturally, the question comes to mind – “How can I make things easier?”. After all, as engineers, we are compelled to find elegant solutions, so most of us would leap at the opportunity to reduce time-consuming interactions with the software. As luck would have it, the latest release of STAR-CCM+® is packed with a range of new time-saving features that are specifically designed to make your life easier.

Take for example "Field Functions". This feature, located under our tools node, lets you construct customized expressions. It can be used to set up your physics (by specifying initial or boundary conditions) and to assess the quality of your solution (with monitors and reports). However, it's not always straightforward to construct these formulas as they increase in complexity.

Shown in figure 1, we have an expression used to specify a toroidal initial condition for a volume fraction. To make editing easier, we've added parenthesis matching (displayed as a yellow highlight). Syntax highlighting provides you with immediate feedback on whether your expression is constructed correctly or not. Finally, a quick reference to all system functions provides the benefit of not having to search through the documentation to find what you are looking for.

Another area where significant time can be saved is in finding and grouping things. To do this, we use "Filtering", also located under our tools node. The big change for this release is that "Filtering" is now capable of supporting queries. What this means is that you can use conditional expressions to group things. This is best illustrated with the example in figure 2.

Let's say we want to create a scene containing all of our periodic surfaces. Unless we know (or remember) all the regions where they are located, it's easy to miss one. And finding them all previously meant hunting them down one by one. To save time and be confident that we've found them all, we can set up a query-based filter to first look for all things containing the name "periodic". From that list, we want to filter one more step to identify just the periodic "boundaries". The output of that query is a group of objects that can be passed to a displayer for a scene. We are just starting to expose the powerful capabilities of query-based filtering. Looking slightly ahead past the current release, we will be dramatically expanding this feature to handle more complicated use cases.

When we are collaborating or trying to learn something new, we often need to review a .sim file that was put together by someone else. Let's consider the example of polymerization kinetics that is also being introduced with this release. To set up a polymerization simulation, individual reactions need to be associated with "Field Functions". When we first look at our "Field Functions", we're confronted with a long list (figure 3). To find out whether and where a function is being used, we right-click on it. In the pull-down menu illustrations (figure 3), we can quickly determine that the reaction rate expression Kbs is not in use but the Kci is.

So, the next question now becomes "Where is this being used?" By selecting "Dependencies", we can see, in the new "Dependencies" viewer, exactly where the reaction rate expression Kci has been applied in our problem setup. I think we can appreciate that trying to find this dependency manually would have been a bit of a challenge.

Another particularly good use case for the "Dependencies" viewer is in identifying dependencies across reports, monitors and plots. If you've ever had the experience of trying to delete a monitor or report only to be confronted by the message that it is in use and can't be deleted, this feature helps tremendously. By following the "Dependencies" viewer for the report, you can navigate to either the plot or monitor that depends on it and decide whether to delete the object or not (figure 4).

Lastly, you now have an interactive colormap editor that greatly simplifies the task of creating effective visualizations. Colormaps are fundamental to how we present and communicate our information. This feature lets you create, modify, copy/paste and import/export your own colormaps. Where this feature is particularly useful is when it is used in combination with volume rendering.

In the colormap editor shown in figure 5, control points can be used not only to change the color along the map (the control points at the bottom), but also to change its level of transparency (control points on top). To create this particular illustration, changes to transparency are made step by step. The resulting image is assessed and transparency control points are added and modified as needed. Changes can be previewed interactively, making it easy to quickly arrive at the desired end result.

While batch operation is a requirement for high productivity in CAE analysis, there is still a need for manual interaction. Checking the problem setup, quickly identifying changes from one simulation file to another, and critically assessing the results all require skill and judgment. We expect that these changes will increase your productivity and improve your overall experience in working.

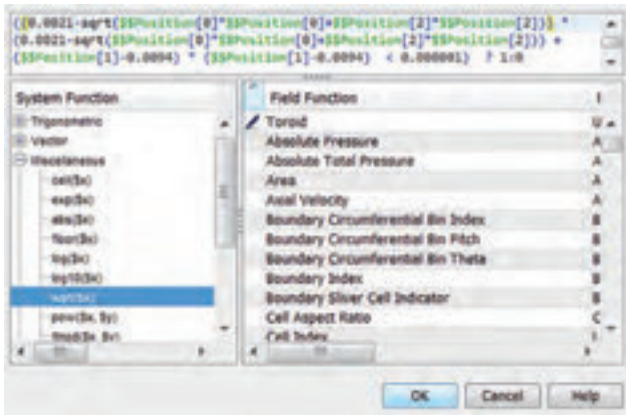


FIGURE 1: Improved construction of formula syntax for "Field Functions"

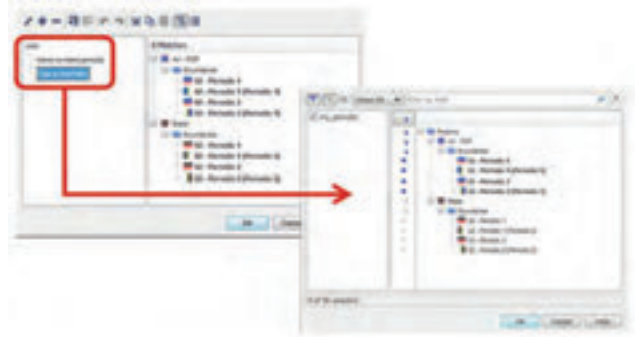


FIGURE 2: Filtering supporting queries



FIGURE 3: "Field Functions" dependencies

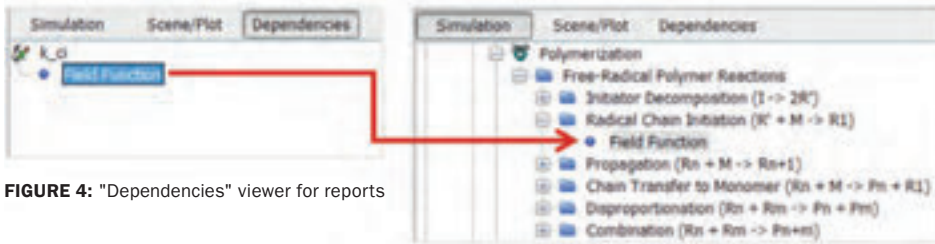


FIGURE 4: "Dependencies" viewer for reports

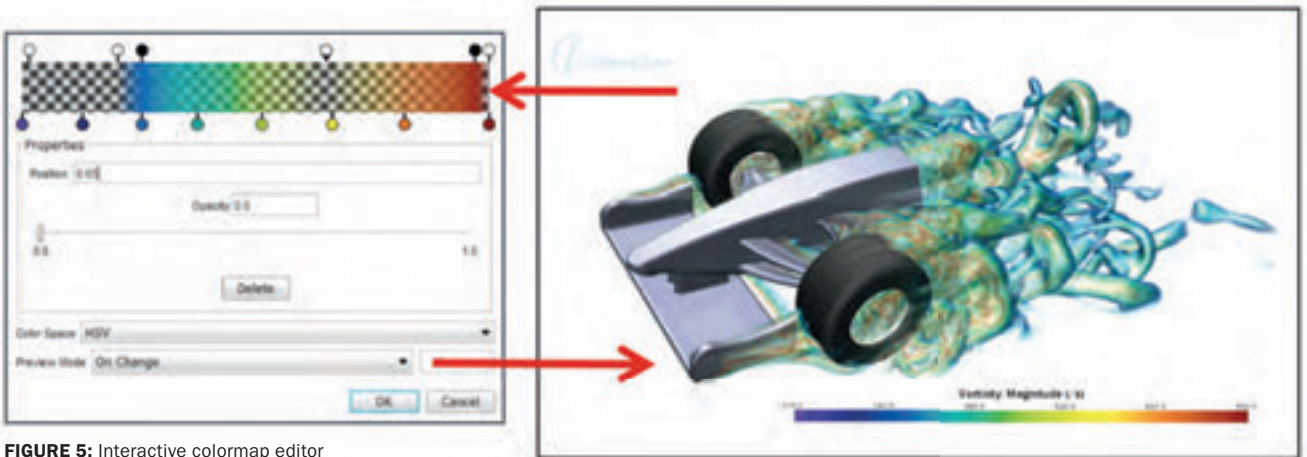


FIGURE 5: Interactive colormap editor

# CAD Robustness & Adjoint Expressions

JOEL DAVISON  
CD-adapco™

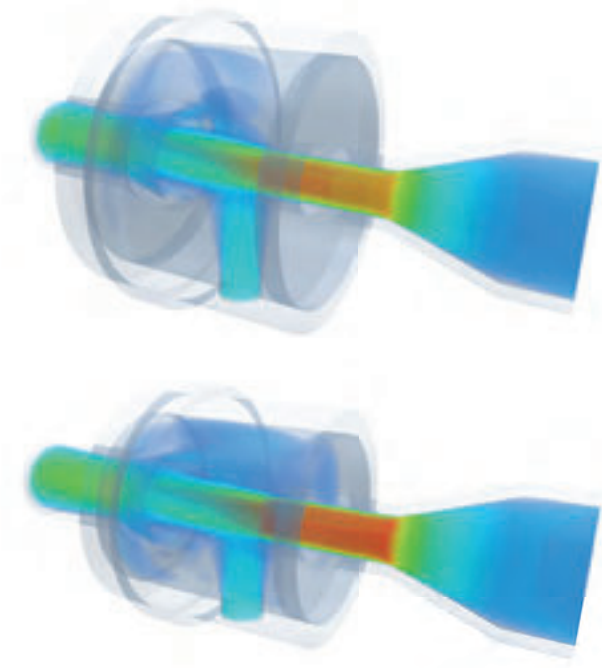


FIGURE 1: STAR-CCM+®/Enabling Optimate™ for inhaler design

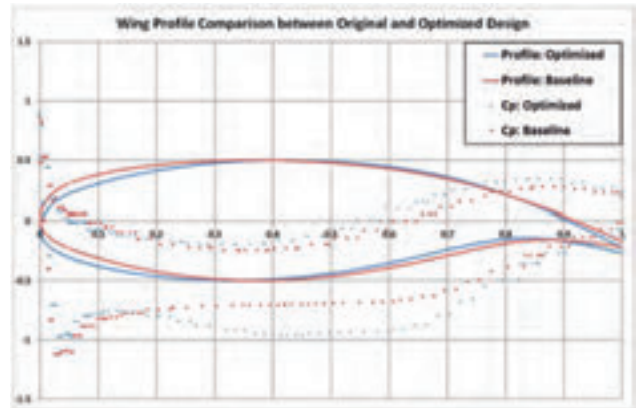


FIGURE 2: Adjoint solver optimization on airfoil profile

**D**uring the opening session of the STAR Global Conference earlier this year, Didier Halbronn, CD-adapco™ Vice President of European Sales, spoke about our ongoing commitment in the field of Multidisciplinary Design Exploration (MDX). In this article, I want to highlight a couple of new features in STAR-CCM+® that approach this in different ways.

## ENSURING ROBUST CAD

One of the challenges of parametric optimization is ensuring that the CAD model is tolerant to the full range of variations that the product is likely to encounter (both in its operational life and during the optimization process). As model sophistication grows and parameters may become interrelated, it is hard to know up front how robust your model is to variation and how many regeneration failures you may have.

Too many CAD regeneration failures and you can't have confidence that your design truly is the optimum or that the relationships between inputs and outputs in your Design of Experiments (DOE) are valid. While the CAD regeneration step is usually short, the simulation that follows it may be more time-consuming and if you don't have confidence in the result due to the number of failures, a lot of time may be wasted.

To alleviate this issue, the new release of STAR-CCM+®/Enabling Optimate™ and Optimate™+ has the option to perform a CAD robustness study. This study, performed before the full analysis, allows you to quickly check the robustness of your design ensuring that time isn't spent performing simulations that may be wasted due to failed geometry regeneration. Not only does it save you time, it also gives you confidence that you can truly find better designs faster.

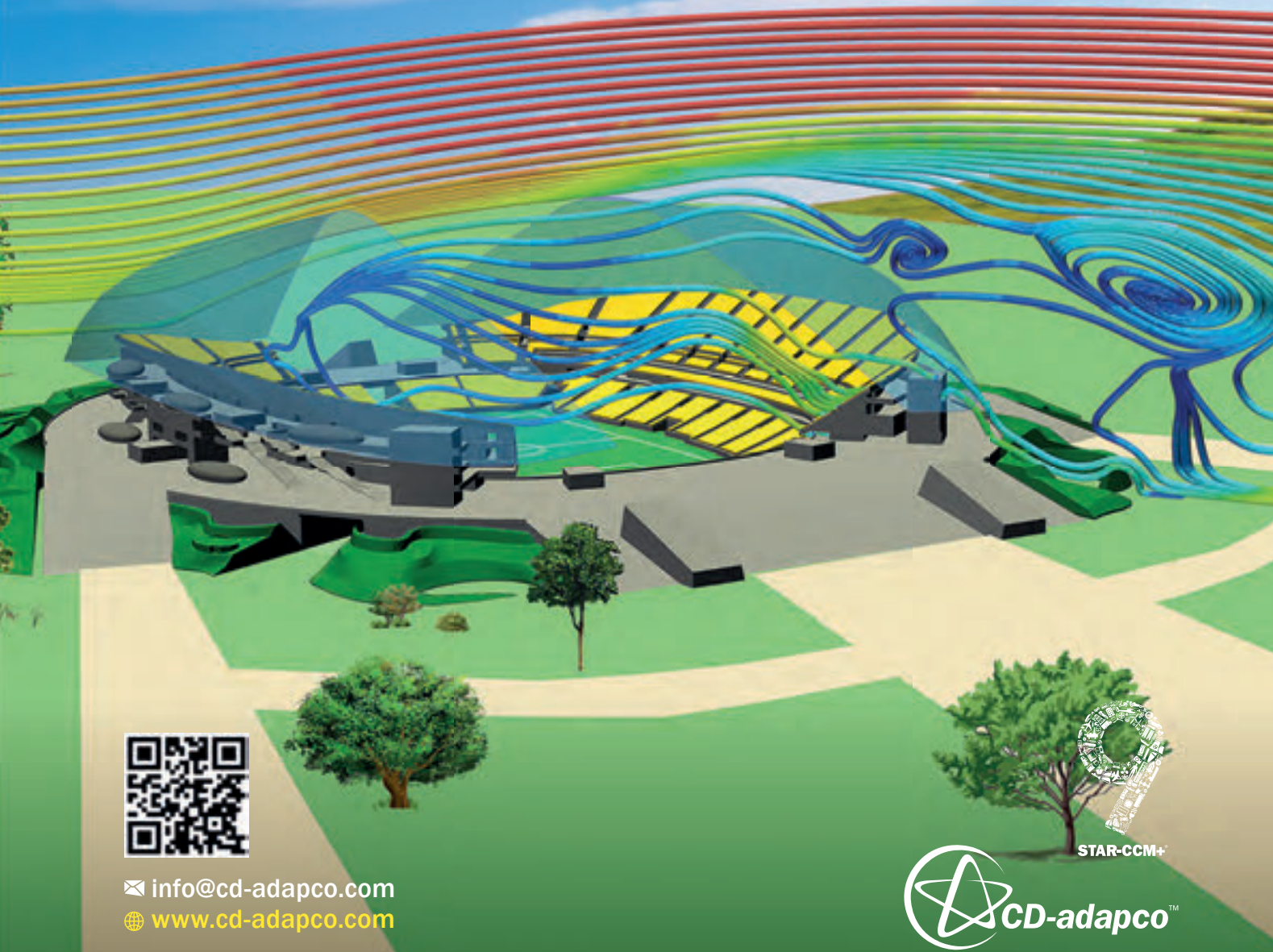
## TYING OBJECTIVES TOGETHER

While STAR-CCM+®/Enabling Optimate™ and Optimate™+ provide a compelling solution for parametric optimization and sensitivity analysis, it is not the only tool we have for MDX. For non-parametric studies, where geometry modification is not constrained by a CAD model, the STAR-CCM+® adjoint solver is a powerful method for exploring your design space in a more free-form way.

The adjoint solver gives you information about how changing the shape, flow field and boundary conditions for your design will affect your cost functions, which represent your engineering objectives. In common with parametric optimization, you will often want to look at a combination of different objectives and how sensitive they are to your design. With this latest release of STAR-CCM+®, this is now possible with adjoint as well.

# SIMULATING SYSTEMS

FLOW – THERMAL – STRESS – EMAG – ELECTROCHEMISTRY – CASTING – OPTIMIZATION  
REACTING CHEMISTRY – VIBRO-ACOUSTICS – MULTIDISCIPLINARY CO-SIMULATION



✉ [info@cd-adapco.com](mailto:info@cd-adapco.com)  
🌐 [www.cd-adapco.com](http://www.cd-adapco.com)



**CD-adapco™ GLOBAL ACADEMIC PROGRAM – MORE THAN JUST LICENSES!**

Recognizing the importance of supporting the global academic engineering community, CD-adapco™ provides students and academic institutions the opportunity to take advantage of its Global Academic Program. Our "More Than Just Licenses!" philosophy is dedicated to ensuring students, professors and graduates have access to the latest info, training and support to guarantee success in academia and beyond. Thousands of academics in hundreds of academic institutions all around the world have implemented STAR-CCM+® into their undergraduate, graduate and postgraduate curriculum and / or research teams.

The CD-adapco™ Global Academic Program has produced hundreds of new engineers with STAR-CCM+® experience ready to join your team. Contact your local sales representative today to find out how you can put the CD-adapco™ Academic Program to work for you!

# Something to Smile About: Using Simulation to Improve Dental Implants!

**SABINE A. GOODWIN**  
CD-adapco™

**KWOK-HUNG (ALBERT) CHUNG & C. WADHWANI**  
University of Washington

## INTRODUCTION

**C**ements are commonly used in dentistry, but there is very little knowledge of how their flow patterns influence the performance of dental systems. One area in dentistry where shape optimization should be considered is cementing of implant restorations. It has been shown that extrusion of excess cement at the crown-abutment margin during the seating of a cement-retained crown over an implant is a major cause of peri-implant disease [1-4]. Recent advances in simulation are now enabling an increased level of insight into the details of the cement flow in these complex systems, opening the door for addressing the potential health issues associated with them and developing innovative implant designs.

## SYSTEMS CONTROL SOLUTION

The cements used in dentistry are non-Newtonian and shear-thinning in nature [5]. This means that as more stress is applied, the cement starts to flow more readily. The stress in the system and therefore the implant shape is expected to significantly influence the flow patterns of cement including the volume of extrusion of cement into the surrounding tissue and the magnitude of extrusion forces. These parameters have a significant impact on the surrounding periodontal tissue [3, 4] and may lead to long term peri-implant



**FIGURE 1:** Parameterized model of implant abutment and crown

disease, a destructive inflammatory condition affecting the gums.

The problem of peri-implant disease as it relates to cement extrusion must be addressed from a “systems control” solution. Understanding cement flow patterns, appropriate placement sites and controlling volumes are all critical for finding ways to address the ongoing health issues associated with cement-retained implant restorations. Crude models have been used to gain

some understanding of cement flow, including using clear plastic beakers to visualize the behavior and studying implant abutments with cast crowns. Using a “design-build-test” principle in which the effects of design changes are quantified by experimental tests on physical prototypes is often costly and time-consuming [5, 6]. Simulation, on the other hand, opens the door for virtual prototyping and the dental industry is now beginning to better understand their complex systems by taking advantage of the benefits numerical simulation has to offer. This is destined to result in a paradigm shift within the dental field.

## NUMERICAL APPROACH

STAR-CCM+® was used to perform numerical simulations on the complete implant abutment, cement and crown system.

Realistic implant abutment and crown forms from scanned stereo lithographic (STL) files provided data points for parameterization of the implant shape (figure 1) and a polyhedral mesh was developed utilizing the overset meshing technology available in STAR-CCM+® to simulate the relative motion of the crown as it travels over the implant. The Volume of Fluid (VOF) multiphase model was used to simulate the flow of cement in the system as it is particularly

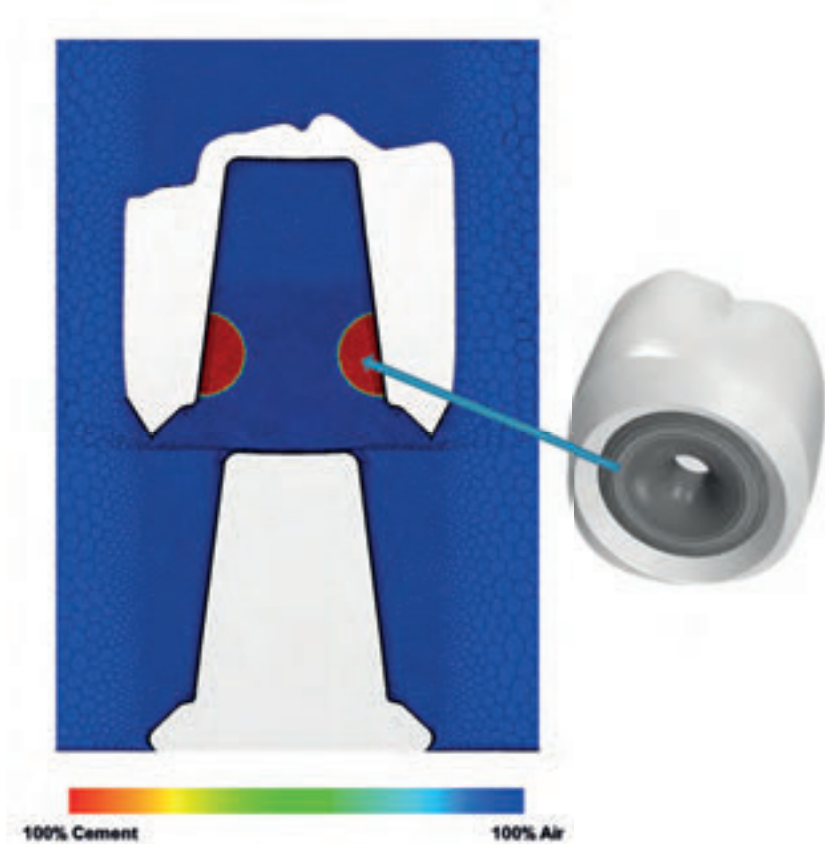


FIGURE 2: Mesh and cement loading for simulations with STAR-CCM+®

well-suited for immiscible fluids (like cement and air) and it enables capturing the position and shape of the interface between the dental cement and surrounding air as the crown is seated. RelyX™ cement (3M ESPE) was chosen for this study and its non-Newtonian properties were simulated using the Herschel-Bulkley model for non-Newtonian fluids in STAR-CCM+®.

Figure 2 depicts a cross-sectional cut through the overset mesh, showing volume fraction of cement at the start of the simulation, with red representing 100% cement and blue representing 100% air. In this case, 35mm<sup>3</sup> of cement was loaded near the crown margin, in a ½ toroid shape [7].

**OBSERVATIONS IN THE LAB**

Recently, Wadhvani et al [6] have studied how implant abutments can be modified to control cement flow patterns and minimize cement extrusion. The in vitro study was performed on three types of abutments shown in figure 3 (top row):

- A Closed Abutment (CA), with the screw access channel sealed off.

- An Open Abutment (OA) with the screw access channel left open.
- An Internal Vent Abutment (IVA) with two additional round vents placed in the axial walls of the OA, 180° apart.

Figure 4 shows how much cement was retained in each system in the lab, clearly indicating that the amount of excess cement extruded at the crown-abutment margin was greatest for the CA, followed by the OA and the IVA. The photographs in figure 3 (bottom) also reveal that there is a better infill of the screw access channel with the IVA abutment as compared to the OA abutment.

**SIMULATE THE SYSTEM WITH STAR-CCM+®**

Numerical simulations enable the engineer to build a virtual laboratory, providing insight into a product’s performance before tests need to be carried out. State-of-the-art visualization tools available in STAR-CCM+® offer a wealth of detailed information not readily available from laboratory tests or from observations in the dentist’s chair, including visualizing the flow of cement in the system (figure 5).



FIGURE 3: Abutment modifications (top) and effects of modifications on cement retention (bottom)

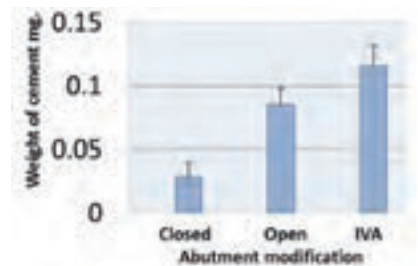


FIGURE 4: Experimental data showing amount of cement retained in each system during laboratory experiments (CA, OA, IVA)

Using STAR-CCM+®, the effects on the cement flow patterns were studied by varying four variables in the system:

1. Implant abutment design,
2. Cement application site,
3. Speed of crown seating and
4. Amount of cement in the system.

**Implant Abutment Design**

First, the three types of abutments were analyzed and simulation results were compared to the findings from the experimental study [6]. This served as a validation of the numerical methods used. Figure 6 shows the geometry of the three models (CA, OA, IVA) in STAR-CCM+®.

Figure 7 depicts the solutions obtained with STAR-CCM+® for each of the abutment modifications, showing the volume fraction of cement at the starting and ending positions for each of the systems. In this simulation, the cement was loaded in the shape of a ½ toroid near the margin of the crown and the crown traveled at a speed of 7 mm/sec. The amount of cement in the system was identical for each of the three abutment modifications shown (~35 mm<sup>3</sup>). Numerical



FIGURE 5: 3-D images generated in STAR-CCM+® showing the details of cement flow during crown seating on the CA



FIGURE 6: Geometries for each type of abutment: CA, OA, IVA

simulations for each of these geometries showed realistic cement flows and predicted the trends observed in previous studies. As observed in the lab, the simulations predicted that the amount of excess cement extruded from the system is significantly larger with the CA system as compared to the OA or IVA system. The IVA is observed to be the best performer, with almost no cement entering into the surrounding environment. The simulations also support the observation that there is a better infill of the screw access channel with the IVA system compared to the OA system.

#### Cement Application Site

STAR-CCM+® was used to evaluate how cement application site affects cement flow patterns. Figure 8 displays the results of two simulations where the same amount of cement (~35 mm<sup>3</sup>) was loaded in a ½ toroid shape near the margin of the crown in the first case and in the occlusal half of the crown in the second case. Five cross sectional frames are shown as the crown is seated on the CA. Results indicate that when cement is applied high up in the crown, the occlusal space fills up much faster as compared to the case where

it is loaded at the crown margin. Once the occlusal space is completely filled, pressure on the cement below it increases significantly. As a result, the extrusion of cement happens much earlier when loaded in the occlusal half of the crown; it leaves the system even before the crown fully seats. In the final position, this causes an incomplete margin seal, a greater extrusion site and an increased mixing of air and cement as it exits the system.

#### Speed of Crown Seating

Simulations were performed with three different speeds of crown seating to assess the effect of speed on cement flow patterns for each abutment modification. Figure 9 shows the final position for the CA, when the crown is seated in 0.25 sec versus 1 sec. It shows visually that the crown should not be seated too rapidly if the seal is to be maintained. Figure 10 shows the results for the IVA system. In this case, a higher seating speed is beneficial, as it enables filling up the screw access hole completely, before cement is extruded in the surrounding environment. A similar behavior for the OA system was observed.

#### Amount of Cement in the System

The effect of overloading the crown with cement has also been evaluated. Figure 11 shows the IVA system with cement loaded in a toroid shape containing 30mm<sup>3</sup>, 35mm<sup>3</sup> and 45mm<sup>3</sup> of cement. These results indicate that loading the crown with too much cement causes cement to be forced out at the crown-abutment margin, yet resulting in an incomplete fill of a screw access hole when internal venting is used. Similar results were obtained for the CA and the OA system.

#### CONCLUSION

STAR-CCM+® was used to analyze the complex flow fields associated with cementation of implant restorations, opening the door for virtually addressing the health problems associated with extrusion of cement into the soft tissue surrounding the implant. Great insight was gained into the cement flow patterns for various cement application techniques and abutment modifications. Simulations with STAR-CCM+® predicted the patterns observed in recent experimental test making it well-poised for future studies. This is destined to result in a paradigm shift in the dental field.

#### THE TEAM

Dr Wadhvani is a specialist dentist (Prosthodontist) conducting research on implant restorations. He is a fellow of the ITI (International Team Implantology) and lectures nationally and internationally on dental implants. He has received awards for his research work which he conducts with several dental schools including: University of Washington, University of Texas and University of California San Francisco.

Dr Chung graduated from the National Defense Medical Center, TAIWAN with a DDS degree. He received his PhD degree in Biomaterials from the Northwestern University in Chicago and a certificate in Advanced Prosthodontics from the University of Texas, Health Science Center in San Antonio. He was appointed by the University of Washington as a full Professor of Restorative Dentistry Department in 2006. Dr Chung is a Fellow of Academy of Dental Materials and published more than 95 articles in peer-reviewed journals and has lectured both nationally and internationally.



FIGURE 7: Simulations with STAR-CCM+® showing volume fraction of cement in CA, OA and IVA systems

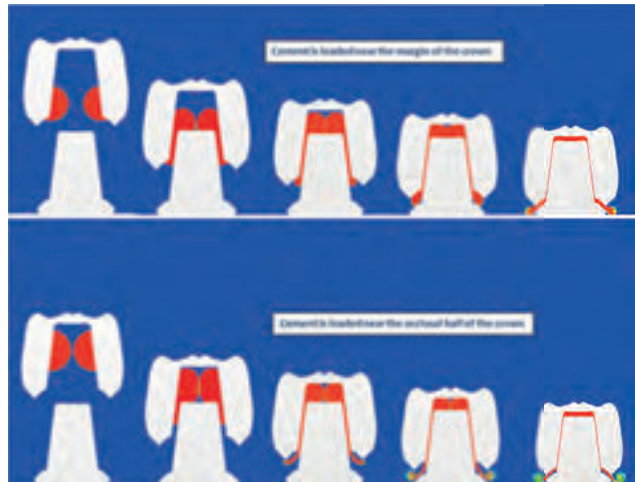


FIGURE 8: Cross sectional frames showing cement flow for two types of cement loading: near the margin of the crown and near the occlusal surface of the crown



FIGURE 9: Effect of speed of seating on cement flow in the CA system

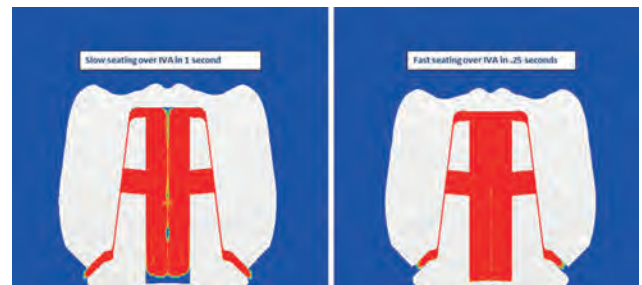


FIGURE 10: Effect of speed of seating on cement flow in the IVA system

## REFERENCES

- [1] Pauletto, N.; Lahiffe, B.J.; Walton, J.N.: Complications associated with excess cement around crowns on osseointegrated implants: A clinical report. *Int. J. Oral Maxillofac Implants* 1999; 14: 865-868.
- [2] Gapski, R.; Neugeboren, N.; Pomerantz, A.Z.; Reissner M.W.: Endosseous implant failure influenced by crown cementation: A clinical case report. *Int. J. Oral Maxillofac Implants* 2008; 23: 943-946.
- [3] Wilson, T.G.: The positive relationship between residual excess cement and peri-implant disease: prospective clinical endoscopic study. *J. Periodont* 2009; 80: 1388-1392.
- [4] Wadhvani, C.; Rapoport, D.; La Rosa, S.; Hess, T.; Kretschmar, S.: Radiographic detection and characteristic patterns of residual excess cement associated with cement-retained implant restorations: A clinical report. *J. Prosthet Dent.* 2012 Mar; 107(3): 151-157.
- [5] Wadhvani, C.; Chung, K.H.: The role of cements in dental implant success, Part 2. *Dent. Today*, 2013 Jun; 32(6): 46, 48-51.
- [6] Wadhvani, C.; Piñeyro, A.; Hess, T.; Zhang, H.; Chung, K.H.: Effect of implant abutment modification on the extrusion of excess cement at the crown-abutment margin for cement-retained implant restoration. *Int. J. Oral Maxillofac Implants* 2011; 26: 1241-1246.
- [7] Wadhvani, C.; Hess, T.; Piñeyro, A.; Opler, R.; Chung, K.H.: Cement application techniques in luting implant-supported crowns: A quantitative and qualitative survey. *Int. J. Oral Maxillofac Implants.* 2012; 27(4): 859-864.

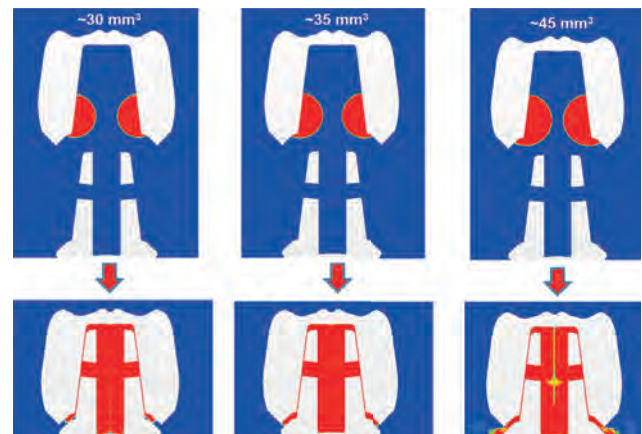


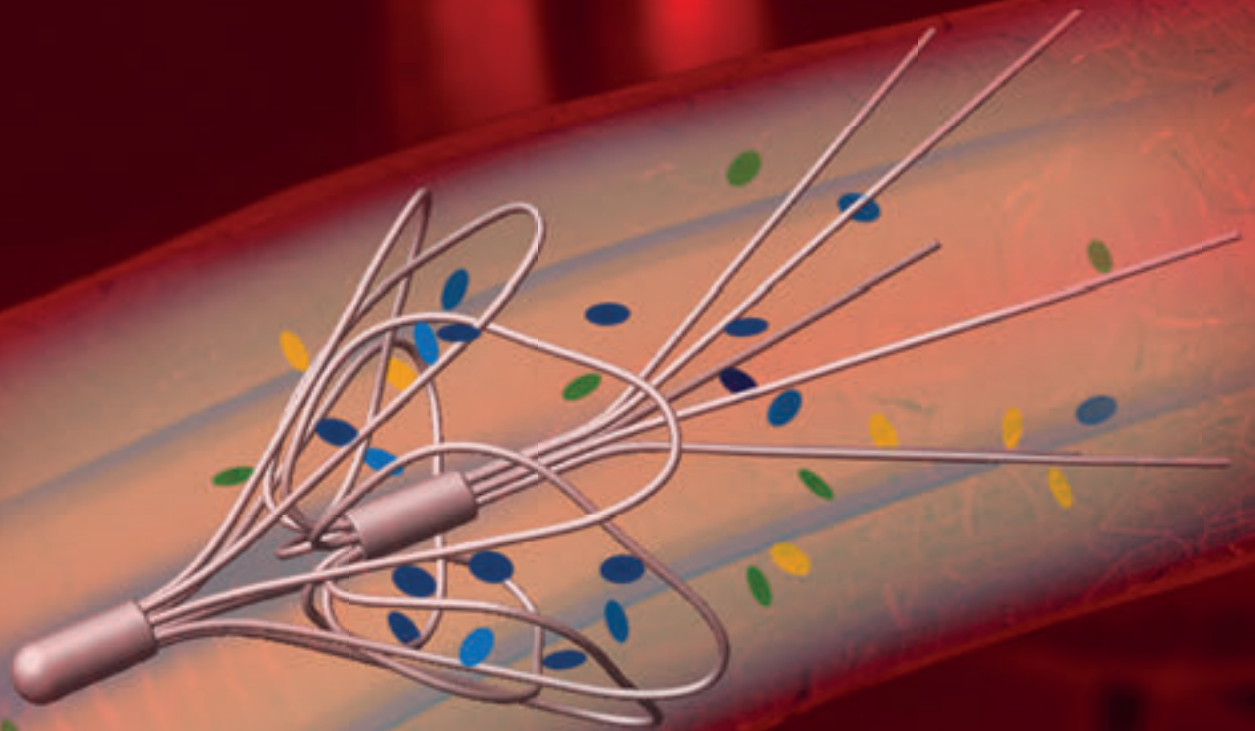
FIGURE 11: Effect of amount of cement for the IVA system

“Dentistry as a profession is centuries old and is a combination of art and science. Dental implants require a higher science-based knowledge to be successful. STAR-CCM+® is an effective simulation tool that can be used to predict behavior thus evaluating dental systems like never before. The possibilities are endless!”

DR CHANDUR WADHWANI  
University of Washington

# SIMULATING SYSTEMS

FLOW – THERMAL – STRESS – EMAG – ELECTROCHEMISTRY – CASTING – OPTIMIZATION  
REACTING CHEMISTRY – VIBRO-ACOUSTICS – MULTIDISCIPLINARY CO-SIMULATION



✉ [info@cd-adapco.com](mailto:info@cd-adapco.com)  
🌐 [www.cd-adapco.com](http://www.cd-adapco.com)



STAR-CCM+



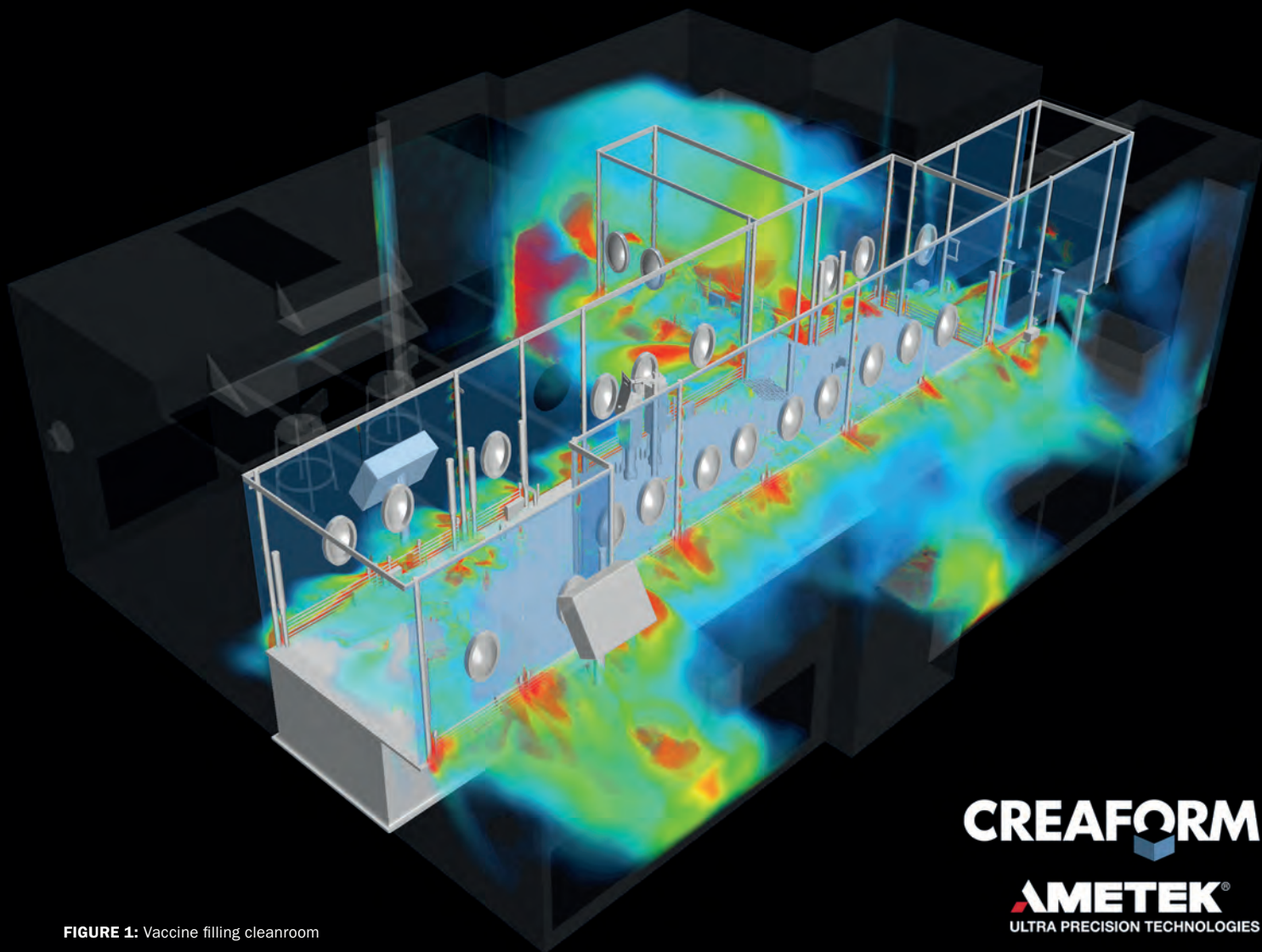


FIGURE 1: Vaccine filling cleanroom

**CREAFORM**

**AMETEK**<sup>®</sup>  
ULTRA PRECISION TECHNOLOGIES

# WHEN CFD SECURES THE MANUFACTURING PROCESS OF VACCINES

Bringing Vaccine Manufacturing Validation to the Next Level using CFD: Creaform Upgrades the Regulatory Compliance Process of Pharmaceutical Environments

**PHILIPPE B. VINCENT & FRANÇOIS TURGEON**  
Creaform

Creaform was asked to assist in the design of a cleanroom, by performing a complete 3D reconstruction of the geometry of the room, and using this to carry out detailed CFD simulations. The cleanroom in question is used in the manufacturing of influenza vaccine, and the aim of the study was to design an efficient aerodynamic barrier that would mitigate the risk of contamination. The demonstration was convincing and CFD simulations shed light on phenomena that traditional smoke tests, still used for regulatory compliance of pharmaceutical environments, had never been able to resolve before.

## INTRODUCTION

**T**he pharmaceutical cleanroom in this study is a critical environment requiring a high level of protection against contamination. While the cleanroom itself is a grade B environment, the interior of the RABS (Restricted Access Barriers) is protected with screened barriers and HEPA (High-Efficiency Particulate Air) clean-air filtration, such that it is rated as a grade A critical zone. The vaccine filling machine had to be incorporated in the RABS, leading to many specific flow interactions which could not be predicted prior to installation, neither by the manufacturer nor the integrator.

The RABS provide vaccine protection against contamination using a physical and aerodynamic barrier. The extent of separation between the process and the contamination sources, like people, determines the grade level of the protected zone. Grade B environment is already a decent class of cleanroom, and further zoning with restricted access barriers, like the glass doors with gloved access, defines a grade A critical zone.



**FIGURE 2:** Room scan using Creaform's handheld MetraSCAN

It was therefore necessary to thoroughly understand the fluid flow behavior in order to ensure proper flow path around non-sterile components of the machine. Not only was the regulatory compliance of the cleanroom at stake, but with the amazing production rate of the line (hundreds of vial fillings per minute), a contamination would represent a considerable financial loss because it leads to the waste of vaccine doses.

In that context, Creaform's 3D modeling and Computational Fluid Dynamics (CFD) solutions came in very handy. Using basic STL files such as the ones created by 3D scanners, the engineering team numerically reproduced the cleanroom in Computer Aided Design (CAD) software and performed a series of CFD simulations using STAR-CCM+®.

## THE STAKEHOLDERS

### CREAFORM

Creaform's mission is to develop, manufacture and market cutting edge portable 3D measurement and analysis technologies that increase productivity. Through its expertise and the passion and commitment of its employees, Creaform helps companies from the manufacturing industry to seamlessly create, simulate, verify and collaborate in 3D, significantly enhancing their turnaround times and profitability. Through its 3D Engineering

Services department, Creaform develops CFD simulation techniques in multiple fields like transport, energy, environment, civil works, electronics and HVAC.

For the project discussed here, Creaform was responsible for the CAD reproduction of the entire pharmaceutical production line and surrounding cleanroom, the CFD simulation of the air flow with RABS and HVAC systems in operation, and the assessment of aerodynamic deflectors to optimize flow behavior around non-sterile components.

### LAPORTE CONSULTANTS INC.

Laporte is a consulting firm specialized in bio-pharmaceutical, food & beverage and industrial engineering. Its employees have experience in a wide array of services in the process, building and infrastructure, automation, packaging and regulatory compliance fields.

In the context of this project, Laporte was in charge of the process design, installation and commissioning for the pharmaceutical facility upgrade. These tasks include the HVAC design and the integration of the filling machine in the RABS system. Laporte was also responsible for the preliminary smoke tests used for regulatory compliance.

### COMPUTATIONAL GEOMETRY

A typical headache when carrying out a CFD analysis is not having the geometry available. An even bigger headache is

not having confidence in the numerical geometry because the as-built drawings are incomplete or the geometry has changed over time. This situation brings the engineers to constantly question the CFD results. Creaform, by supplying efficient 3D scanning solutions, ensures high quality numerical reproduction. Creaform also manufactures fast, portable and easy to use scanners that provide metrology-grade accuracy and resolution. For CFD applications in the HVAC industry, it is quite common for Creaform's engineers to combine the scan of an entire room acquired by a mid-range scanner with the precise scan of specific parts using one of Creaform's handheld scanners (see figure 2). The result is a clean STL file such as the one built for the pharmaceutical cleanroom.

The numerical geometry of the cleanroom includes the walls and furniture, the HEPA filtration, the HVAC system, the physical barrier with gloved access (windows surrounding the production line), the control panels as well as the RABS itself with the accumulation table for vials, the conveyor, the filling needles, the capping machine and many measurement instruments, all of which were accounted for in the CFD simulations thanks to the wrapping capabilities of STAR-CCM+®.



FIGURE 3: Hexahedral mesh of vials conveyor

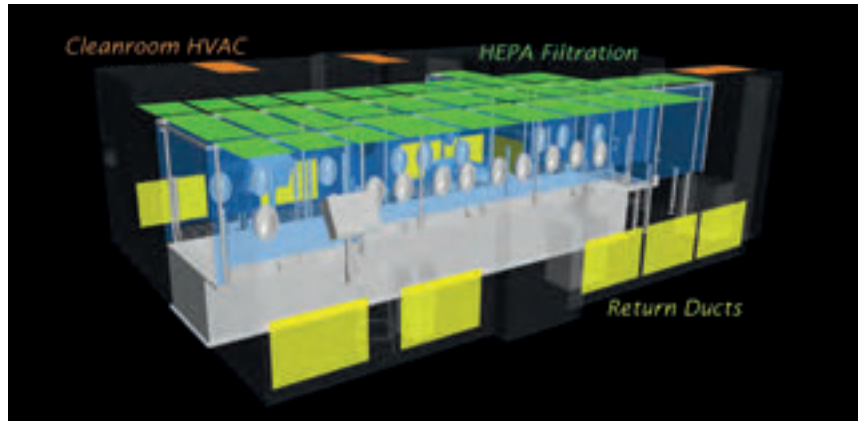


FIGURE 4: Principal boundary conditions

Creaform provides, amongst other services, consultation in numerical simulations and uses STAR-CCM+® in its software arsenal as it allows to quickly treat about any geometry, including raw scans. Our experts can work around with the scans and any other available data to numerically reconstruct the geometry and then perform the CFD simulations, cutting down costs and intermediaries.

## SIMULATIONS

Precise and representative boundary conditions are critical for the cleanroom simulation. They were carefully determined using very recent data acquisition:

- Laminar flow equipment performance evaluation providing air velocity profiles for each diffuser of the HEPA filtration system;
- Ventilation balancing measurements for the HVAC system including return ducts;
- Precise pressure gaging in adjacent rooms for secondary air flow rates through wall openings for conveyor and through the door contour.

Turbulence modeling was achieved with the RANS approach and more specifically with the SST (Menter)  $k$ - $\omega$  model, thus limiting the results to steady state. The All  $y$ + Wall Treatment was used because many near wall cells fell within the buffer region of the boundary layer. The control over the entire surfaces to force viscous sublayer resolution was computationally expensive and judged unnecessary. Indeed, calculation of viscous forces is not required and flow separation occurs at cutting edges, so its prediction is trivial. Consequently, the mesh is polyhedral and does not make use of prism layers. The prioritized cell refinement was the one allowing to capture the surface details of the machine components, resulting in a cell count of

5.6 million for initial runs (setup check and initial solution) and of 18.4 million for final runs. Simulations made use of the coupled flow model with a 2nd order discretization.

## RESULTS

### OVERALL PRESSURE DISTRIBUTION

Ideal flow conditions just above the conveyor level consist of a perfectly vertical flow. Pressure distribution in the horizontal plane is thus very important and must be as uniform as possible inside the RABS. The first CFD simulation of the cleanroom showed a small pressure gradient that was sufficient to induce a longitudinal component to the velocity vectors inside the RABS. Laporte engineers designed deflectors to redistribute the pressure in the capping section and removed the partition that provoked a pressure increase in the vials accumulation section. Combined with the modular adjustment of the HEPA filtration, these modifications significantly improved the pressure distribution in the RABS (see figure 5). The CFD simulation correlates well with the smoke tests performed with the new design and confirmed the improvement efficiency.

### TRANSVERSE FLOW

With the longitudinal flow corrected, Laporte and Creaform focused on transverse velocity components in the vicinity of non-sterile machine

components. The CFD simulations highlighted two similar undesired situations: one around the needles holder and one around the capping arm. Both components are non-sterile and the air draft from underneath the physical barrier induces a significant transverse velocity component. As can be seen in Figure 6 (a), this phenomenon drives particles in contact with the arm directly toward the vials that are conveyed at the level of the toothed plate. The aerodynamic deflector visible on Figure 6 (b) was tested in simulation and provoked the shift of the air draft towards the machine floor. It caused the streamlines in the vicinity of the arm to reach the underside of the conveyor, keeping the potentially contaminated particles far from the vials. A similar deflector was used at the level of the needles holder. Once designed by Laporte and outsourced for machining, these deflectors were tested in situ with smoke and turned out to perform very well as predicted by the CFD analysis.

### IMPINGING FLOW

A third undesired situation addressed by CFD simulations is the one caused by impinging flow on non-sterile surfaces: the accumulation table and the conveyor discs. In both cases, the parts expose a horizontal surface directly to the vertical flow, inducing stagnation points and undesirable vortices.

On the table at the beginning of the production line, opened vials accumulate

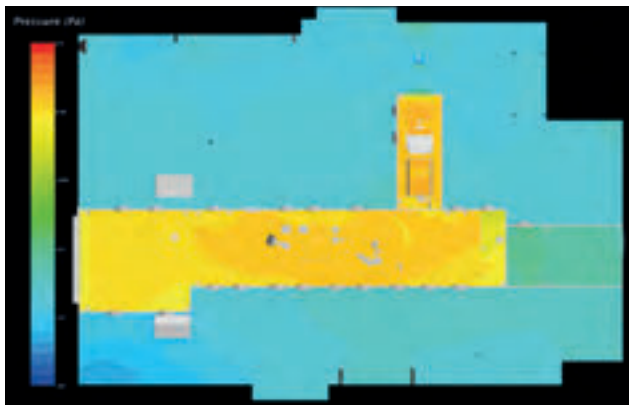


**FIGURE 5:** Pressure distribution in horizontal plane – before (above) and after (below) design adjustments

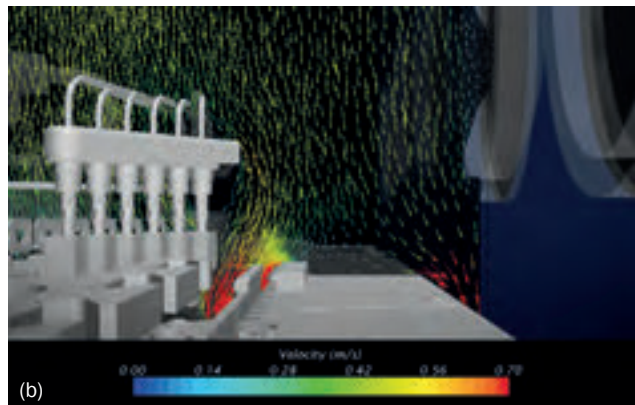
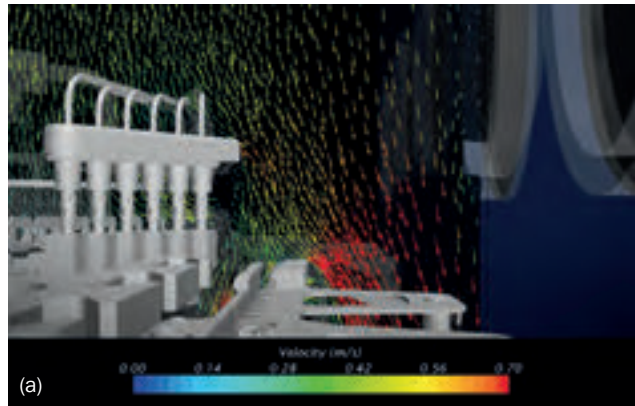


**FIGURE 6:** Velocity vectors in section plane at capping arm elbow - original design (above), modified design with aerodynamic deflectors (below)

## "Creaform's integrated solutions of scanning, CAD reconstruction and CFD analysis gave visual and precise answers about intangible air flow questions."

**GILLES GRENON**

Laporte Consultants Inc.

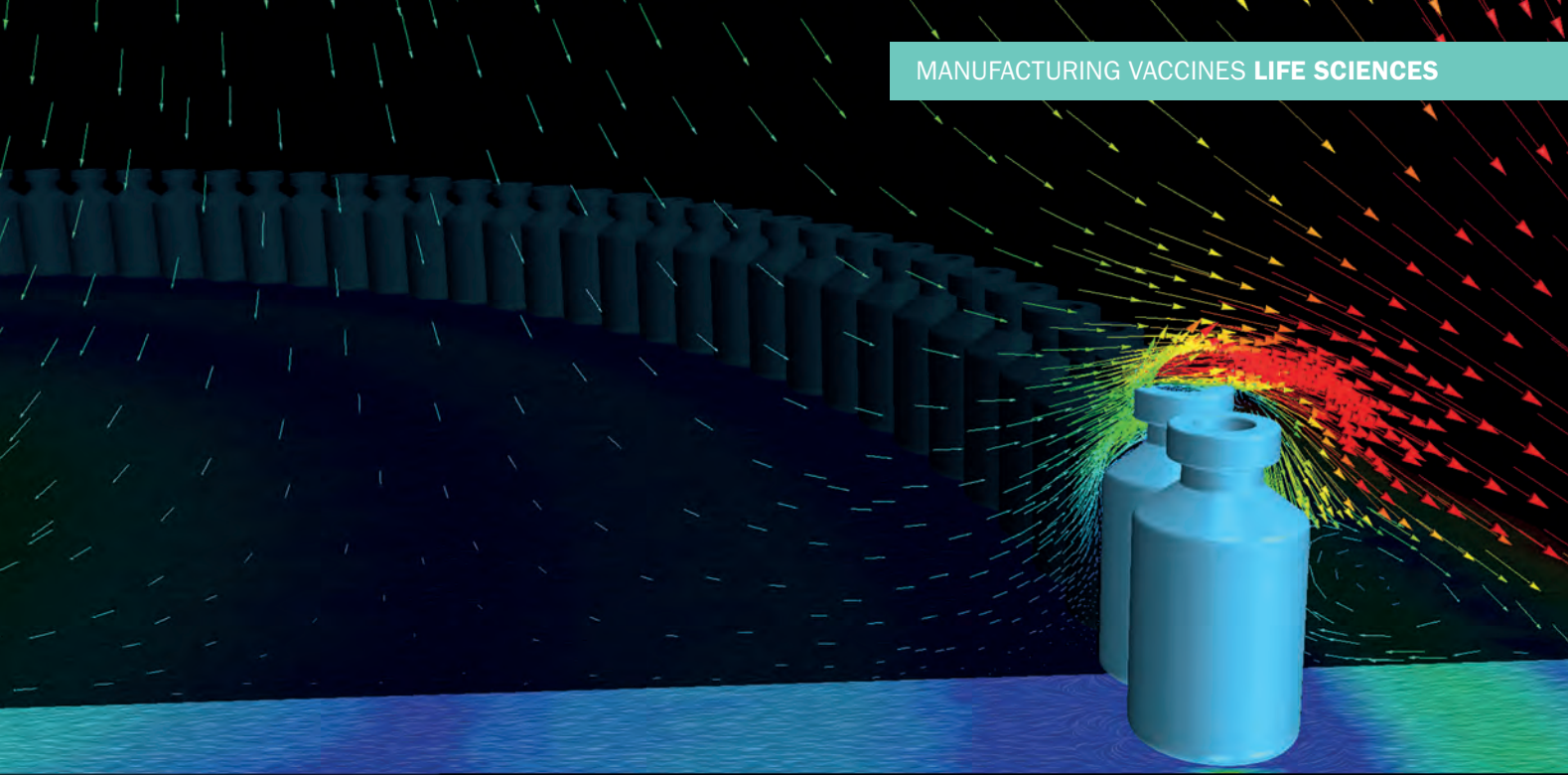
and form a circular pattern near the exterior edge of the table. This table is designed with a central hole, allowing for a proportion of the impinging flow to evacuate without touching the vials. Nevertheless, some streamlines evacuate through the exterior edge, passing through a series of vials as can be seen on figure 7. Many fixes to decrease head losses for the flow through the central hole have been tested in simulation with mixed success. The attention was then focused on determining the actual risk of contamination for the evacuation through the exterior edge, and a particular simulation of the flow around the vials was performed. This detailed simulation, with actual vials modeled, used the global simulation fields to determine

boundary conditions. It showed that in steady-state, the entire flow in contact with the table would evacuate through the vials' shoulders (see figure 8), thus limiting the contamination risks. Laporte also proposed a specific cleaning procedure for the accumulation table.

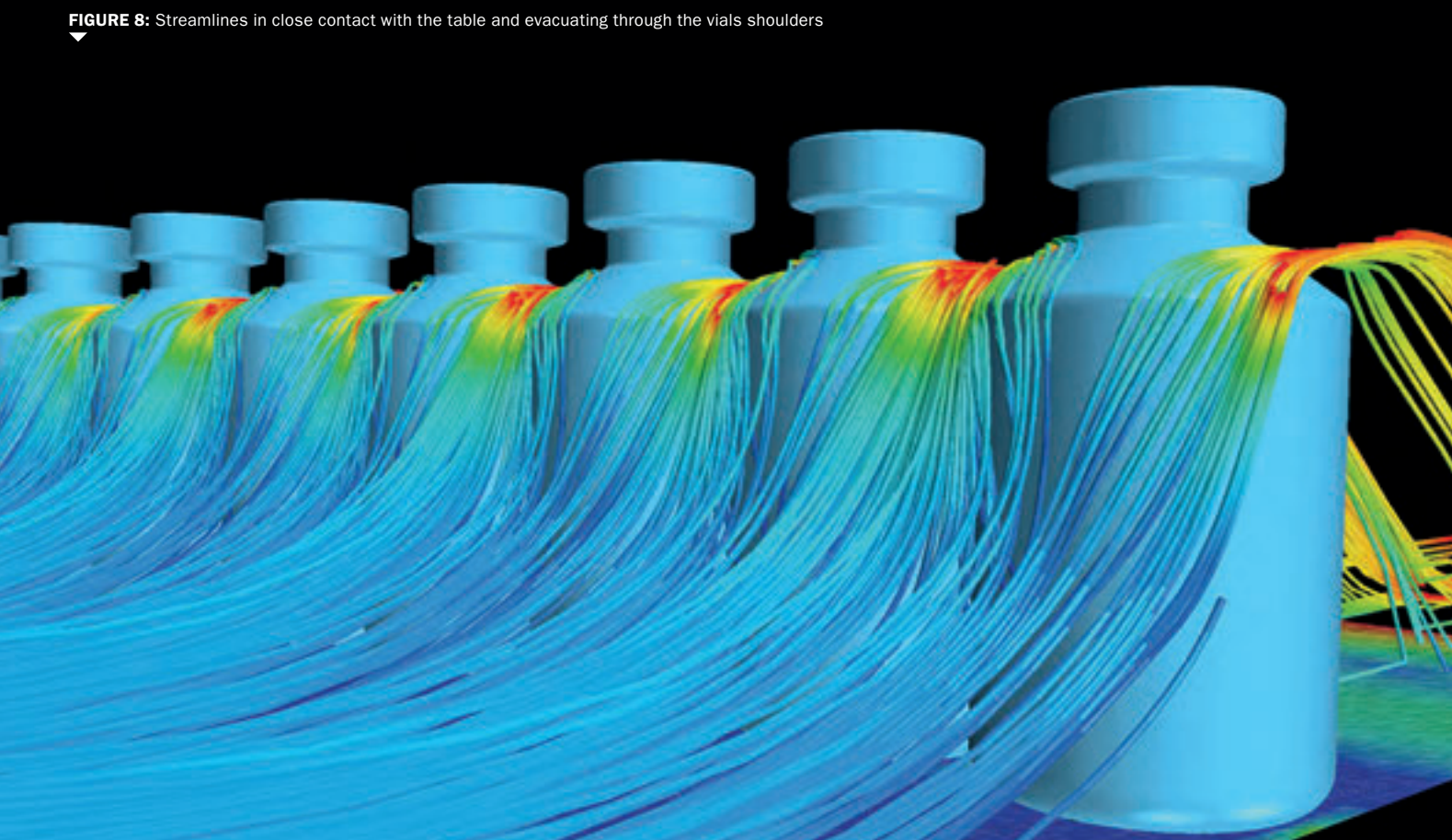
As for the non-sterile conveyor discs, they would induce a stagnation point surrounded by vortices that would eventually transport particles over the vials path. Thus, their initial design as solid discs was questioned and Laporte ultimately remanufactured the discs and added holes, allowing for a much better evacuation towards the machine floor. The modification was tested with the CFD model and with smoke ejections and both methods confirmed the suppression of the issue.

### CONCLUSION

The project was a convincing demonstration of the complementarity of the reverse engineering solutions and CFD capabilities of Creaform's Engineering Services team, equipped with STAR-CCM+®. The project was also a clear demonstration of the innovative mind of Laporte, who adopted CFD in its cleanroom commissioning in order to gain predictive insight to complement the traditional smoke tests. The CFD results presented here are currently used in combination with the smoke test videos to demonstrate the effectiveness of the aerodynamic barrier in front of regulatory agencies. So far, the feedback is very positive as CFD really helps to visualize the flow features. It is Creaform's will to make CFD a prevalent tool for future pharmaceutical production lines.



▲  
**FIGURE 7:** Impinging flow on accumulation table



▼  
**FIGURE 8:** Streamlines in close contact with the table and evacuating through the vials shoulders



# OVERLAPPING OVERSET MESHES OPEN NEW PROSPECTS FOR CFD SIMULATION OF MOVING GEAR SYSTEMS

CHRISTINE KLIER, MATTHIAS BANHOLZER, LUDWIG BERGER & KATHLEEN STOCK  
CFD Schuck Ingenieurgesellschaft mbH

**A** common difficulty in the simulation of complex fluid flow problems is that not every geometry can be well represented using a single, contiguous grid. This is especially true for the case of relative motion between components. Overset grids can be used to track relative motions with computational efficiency and recent advances in high performance Computational Fluid Dynamics (CFD) software like STAR-CCM+® have enabled the coupled simulation of multiphase fluid flows and rigid body motions using overlapping overset grids. A CFD method was developed and applied for the simulation of oil flow in a multiple rotating spur-gear system with emphasis on predicting the flow fields and pressure torques in the gearbox and between intermeshing gear regions. The multiphase flow in this problem was simulated using the Volume of Fluid (VOF) method and the results indicated that the applied CFD method offered a convenient and efficient way to study different oil filling levels in a gearbox with respect to their influence on oil flow and on the volume fraction of oil on gear flanks.

## INTRODUCTION

Problems that arise when gear lubrication becomes insufficient are well known by every bicycle rider as well as car driver. Replacement of bearings, pistons, piston-rings and gearwheels is not only time-consuming but expensive and therefore

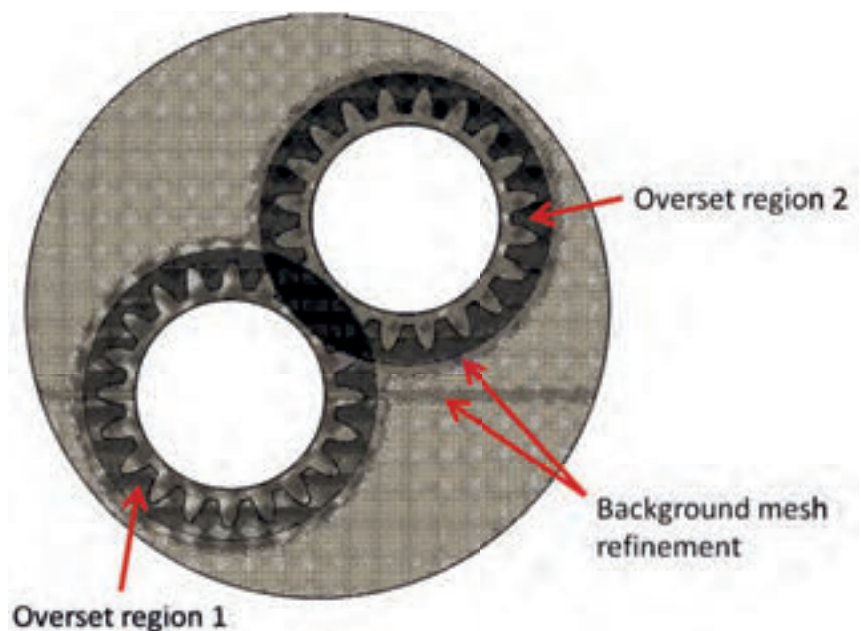


FIGURE 1: X-cut plane section through the gear housing showing mesh details of the model

gear lubrication is a significant concern for a wide range of industries that use power transmission. Prototype testing of gear-boxes does not always provide the necessary detailed information required for complex modern gears as they often carry greater loads with high rotational speeds. CFD model prediction is thus an effective tool for optimization of oil flow around the rotating components in a gear-box. The results from CFD simulations can help improve the

efficiency of transmissions, reduce the friction between the gearwheels (pitting), minimize load-independent spin power losses, and assess oil splashing effects on gear housing.

The newly enhanced overset meshing capability that allows for multiple overlapping overset zones in STAR-CCM+®, coupled with multiphase flow based on the VOF method, offers the necessary simulation environment for handling complex simulation problems such as

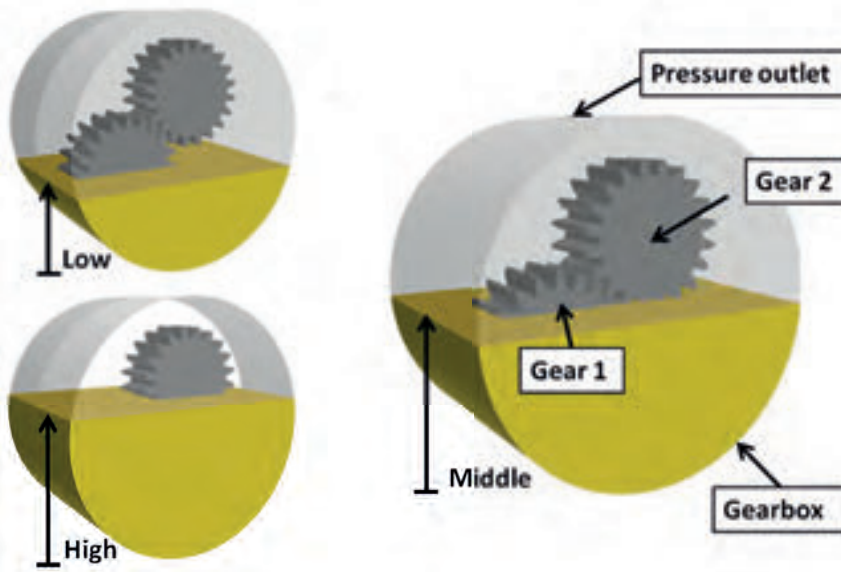


FIGURE 2: Initial distribution of the three different oil filling levels

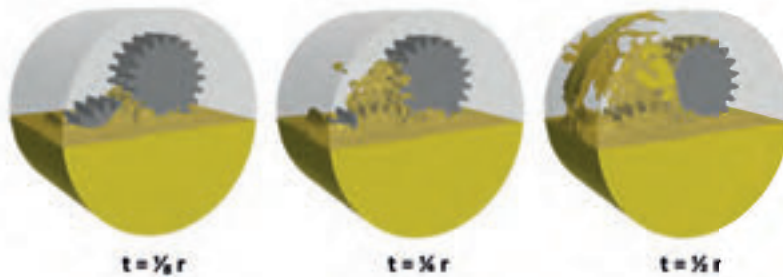


FIGURE 3: Oil distribution changes in time for the middle oil level

Gearbox and gearwheels were simulated including a symmetry plane boundary condition according to the mesh plane section shown in figure 1. The geometry was laid out as follows:

- Gear housing diameter ( $d$ ) = 280 mm, length ( $l$ ) = 200 mm
- Two gearwheels of each  $d = 130$  mm,  $l = 58$  mm.

The mesh (figure 1), consisting of polyhedral cells with five prism layer cells on wheel and housing surfaces, comprised of a total of about 5.4M cells. Furthermore, mesh refinement regions were defined to ensure adequate grid spacing in the overlapping zones.

The smallest gap between the two rotating gearwheels was set to be around 1.5 mm.

Due to high temperature operating conditions in many applications of gear lubrication, the decision was made to set fluid density and viscosity values based on oil at 100°C.

Three different initial oil level distributions were defined by the user field function functionality in STAR-CCM+®.

As shown in figure 2, for the low oil level, the first gear head was half covered by the oil sump while for the middle oil level, the teeth of the second gear head already extended to the sump and for the high oil level, the first gear head was completely covered by oil.

One further detail of the set-up to be noted concerns the rotation rate of the gear system: To keep simulation time to a minimum, the rotation rate was set to a constant 2000 revolutions per minute (rpm).

In practice, the rpm of gear systems frequently increases with time. To assess the importance of this effect, the influence of a linear ramp for the rotation rate was studied for the middle oil level and compared to the oil distribution in the box and on gear flanks for the case with constant revolution rates.

To assess the importance of this effect, the influence of a linear ramp for the rotation rate was studied for the middle oil level and compared to the oil distribution in the box and on gear flanks for the case with constant revolution rates.

To assess the importance of this effect, the influence of a linear ramp for the rotation rate was studied for the middle oil level and compared to the oil distribution in the box and on gear flanks for the case with constant revolution rates.

To assess the importance of this effect, the influence of a linear ramp for the rotation rate was studied for the middle oil level and compared to the oil distribution in the box and on gear flanks for the case with constant revolution rates.

### RESULTS: CFD ANALYSIS OF A ROTATING SPUR GEAR SYSTEM

As a consequence of the high computational demand of this simulation, only two full revolutions ( $r$ ) of the gears were simulated for all cases. At that point, the flow field had not quite reached steady state conditions but the oil was already forced out of the gear teeth regions as a result of the high rotational kinetic energy in the system.

In our opinion, important flow processes have already occurred at that point in time, determining oil distribution on gear flanks, friction between gearwheels, and oil distribution in the gearbox. Figure 3 shows the oil distribution in the gearbox for the middle oil level after 1/8, 1/4,

1/8, 1/4, 1/2, 3/4, and 1 full revolution. The oil distribution is shown as a yellow area within the gearbox housing, and the gears are shown in grey.

1/8, 1/4, 1/2, 3/4, and 1 full revolution. The oil distribution is shown as a yellow area within the gearbox housing, and the gears are shown in grey.

rotating gear systems. This case study shows that this coupled approach can be successfully used to simulate oil flow in a rotating spur-gear system in a reasonable time with satisfactory results for evolving flow and pressure fields, and for oil distribution in the box and on gear flanks. Three various levels of oil and the influence of the rotational speed on lubrication were tested.

### METHOD: COUPLED SIMULATION OF MULTIPHASE FLOW AND MULTIPLE BODY MOTION

The VOF method, which uses the Eulerian framework, was used to set up the multiphase flow simulation in this model. With this approach, the volume fraction continuity equation is solved for each Eulerian phase, while the immiscible fluid phases in the VOF model share velocity, pressure, and temperature fields which saves computational time compared

to the multiphase segregated model, another Eulerian approach available in the STAR-CCM+® simulation environment. Air entrapments and turbulence regimes, which are important in a gearbox with high rotational speeds, and oil splashing can be well represented by this approach. For the simulation of multiple body motions, overset meshes (also known as Chimera grids) were used. The relative motion of one or more bodies, including arbitrary or tangential motions of objects in close proximity [1], can be simulated using this capability in STAR-CCM+®. Each moving body is defined as a separate region and is represented by its own grid. The newest enhancement in STAR-CCM+® allows for overset zones to also overlap with each other, an indispensable capability for the simulation of rotating intermeshing gears. While the solution is computed on all grids simultaneously [2], a background mesh serves as reference grid for all motions.

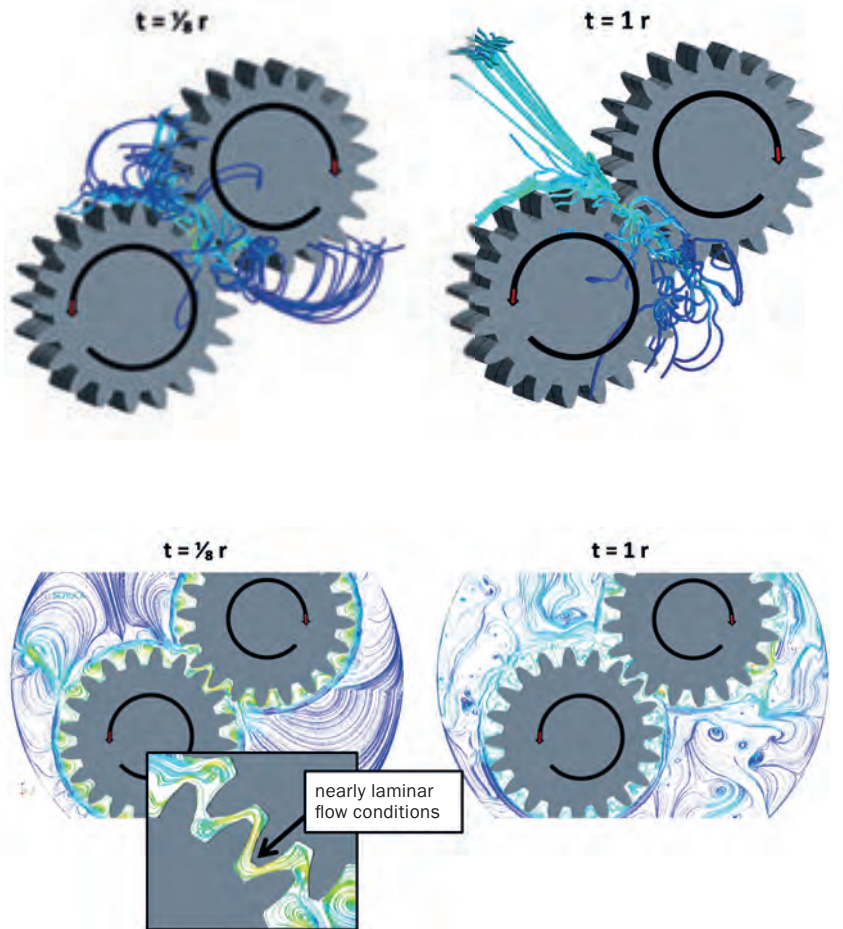


FIGURE 4: Streamlines showing transient flow features between the intermeshing gears (top) and transient velocity flow field changes in the gearbox (bottom)

and  $1/2 r$  and this gives a good indication of how much oil was already splashed out of the oil sump after a short time interval. Furthermore, the results from the simulation enable a detailed transient assessment of the velocity streamlines and flow fields (figure 4) as well as pressure distribution in the system (figure 5), shown for the middle oil level. The streamlines in figure 4 (top image) represent transient flow features between the intermeshing gears and thus give some indication on whether the oil flow is still sufficient for lubrication. Figure 4 (bottom image) demonstrates changes in the velocity flow field with time. At the beginning of the simulation ( $1/8 r$ ), the field was characterized by circulation between adjacent gear teeth and nearly laminar flow conditions in the intermeshing gear region. However, after  $1 r$ , turbulent structures already dominate the flow field in the gearbox.

The pressure conditions in figure 5 indicate that initially, most of the oil amount remains in the oil sump and thus, high amounts of oil could be squeezed into the interstitial gear region. After  $1 r$ , the oil splashing already has pressure effects on the gearbox housing, while the low pressure conditions in the intermeshing gear region indicate oil suction into the gap.

The challenge of optimizing lubrication and of finding the best oil filling height is the minimization of splashing effects (displaced oil volume), torques, and friction (shown in table 1) while maximizing the oil film on gear flanks. The simulation results enabled a qualitative and quantitative assessment of the best filling level of oil in the system. In all cases (low, middle and high oil level), the inclusion of air bubbles in interstitial gear regions becomes obvious at the latest after  $1/2 r$  (figure 6). Figure 7 depicts the oil distribution in the box and on gear flanks after  $1/3 r$  and  $1 r$  for the middle oil level. The diagram in figure 8 compares the Volume Fractions (VF) of oil on gear flanks for the three different filling heights, indicating that the highest oil level resulted in the highest VF of oil on the gear flanks. On the other hand, the increase/decrease of the VF curves was not proportional between the different filling levels (figure 8) and the middle filling level resulted in good values when compared to the highest level for gear 1. The comparison in table 1 also indicated that the middle level resulted in small oil splashing effects compared to the available oil amount in the system. Pressure, torque and friction

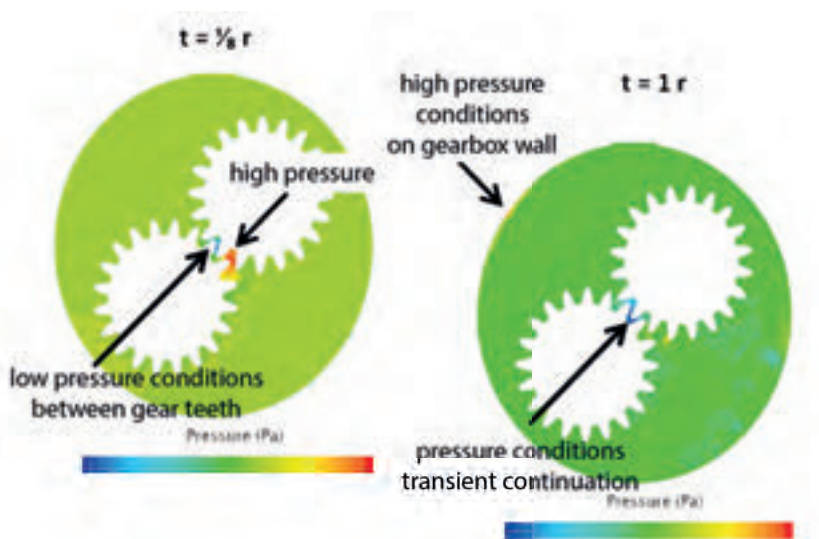


FIGURE 5: Pressure condition changes in time in the gearbox.

conditions were also comparably low for this filling depth.

The effect of including a linear ramp of the rotational frequency in the simulations was also studied and showed only a small influence on the oil fraction on the gear flanks (results not shown).

**CONCLUSION AND FUTURE WORK**

Transient flow fields, pressures and torques in the gearbox and in the intermeshing gear region have been efficiently and effectively studied using the presented CFD method. The applied method offered a convenient way to study the influence of different oil filling heights on the oil flow in the gearbox and on the volume fraction of oil on the gear flanks. Due to their high specific heat capacity, liquid lubricants also fulfill important functions concerning the cooling system of a gearbox. Future work will therefore include simulations of oil temperature and heat dissipation in the gearbox as well as heat conduction at the gearbox wall and at the gear flanks. These results served as a case study and experimental data will be essential for further model validation.

**REFERENCES**

[1] Eppel, Deborah: "Epicyclic Gear Simulation with Overlapping Overlap Mesh", Dynamics, Issue 35, p 5, 2013.  
 [2] Schreck, Eberhard; Perić, Milovan and Snyder, Deryl: "Overlap Grids Technology in STAR-CCM+®: Methodology and Applications", [http://www.cd-adapco.com/conference\\_video/overlap-grids-technology-star-ccm-current-state-future-developments](http://www.cd-adapco.com/conference_video/overlap-grids-technology-star-ccm-current-state-future-developments)

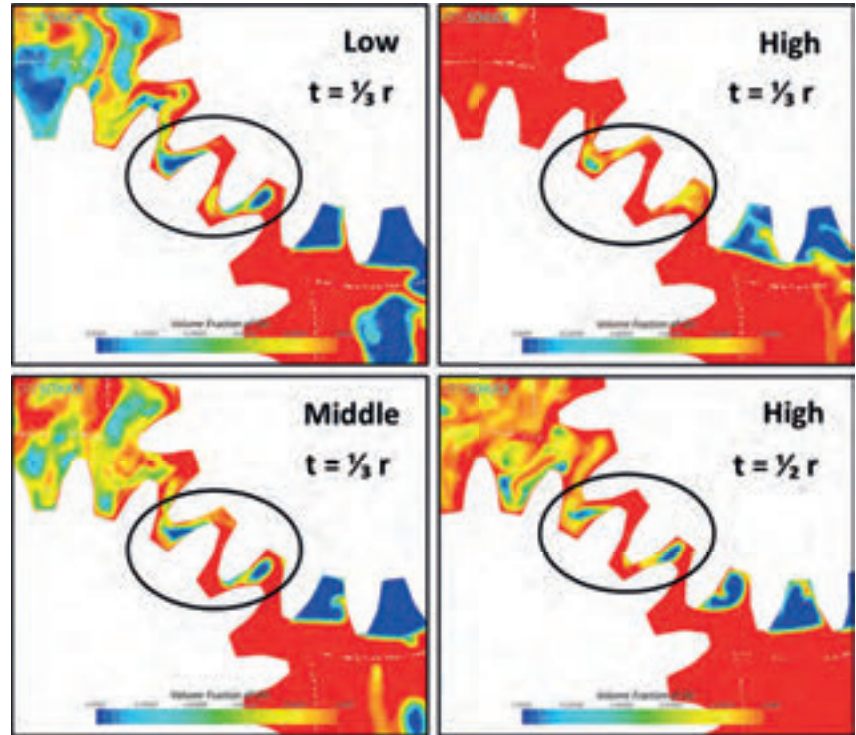


FIGURE 6: Volume fraction of oil between the intermeshing gears and for the three different oil filling levels at 1/3 r (additionally for filling level high at 1/2 r)

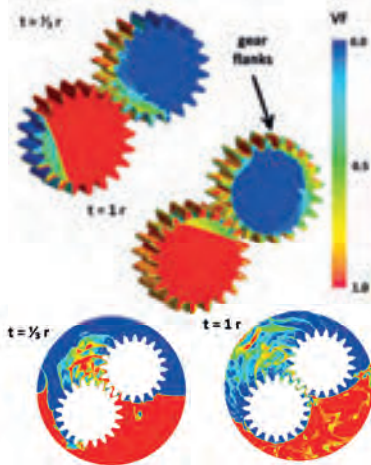


FIGURE 7: Volume fraction of oil on gear flanks (top image) and in the gearbox (bottom image) after 1/3 and 1 r

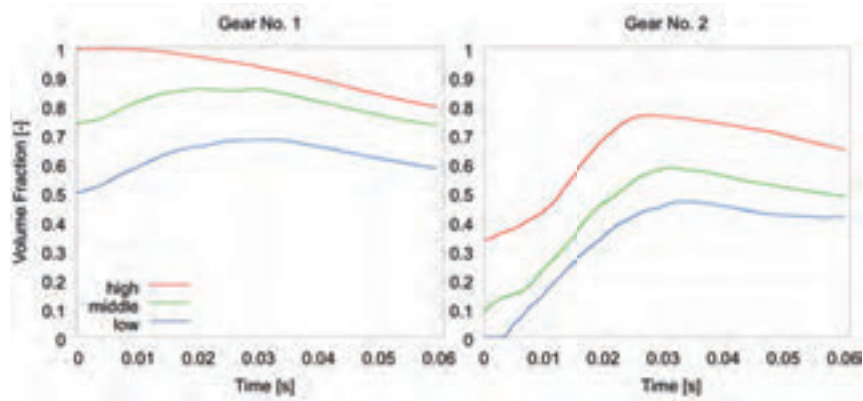


FIGURE 8: Temporal development of the volume fraction of oil on the flanks of Gear 1 and Gear 2

	oil amount [%]	avg. pressure gearbox (1r - 2r) [%]	torque (at 2r) [%]		friction (at 2r) [%]		displaced oil volume (at 2r) [%]
			G1	G2	G1	G2	
Low	32	100	100	100	100	100	4.5
Middle	46	+ 18	+ 233	+ 141	+ 72	- 13	4.2
High	58	+ 34	+ 455	+ 497	+ 272	+ 59	8.9

TABLE 1: Comparison of available oil amounts (in relation to gearbox volume), average pressure in the gearbox (between the time interval 1 and 2r), torque and friction conditions on the flanks of Gear 1 (G1) and Gear 2 (G2) (respectively, at 2r), and oil amount (in relation to gearbox volume) splashed over the initial filling level in the box (at 2r) for the three different filling levels

# SIMULATING SYSTEMS

FLOW – THERMAL – STRESS – EMAG – ELECTROCHEMISTRY – CASTING – OPTIMIZATION  
REACTING CHEMISTRY – VIBRO-ACOUSTICS – MULTIDISCIPLINARY CO-SIMULATION



✉ [info@cd-adapco.com](mailto:info@cd-adapco.com)

🌐 [www.cd-adapco.com](http://www.cd-adapco.com)



STAR-CCM+



GROUND TRANSPORTATION IT TAKES THREE TO TANGO



# THE CAN-AM® SPYDER® ST – IT ACTUALLY TAKES THREE (WHEELS) TO TANGO!

**DAVID LAROCHE**  
Bombardier Recreational Products Inc.

**PRASHANTH SHANKARA**  
CD-adapco™



FIGURE 1: Initial designs of the Can-Am® Spyder ST roadster

## INTRODUCTION

The birth of the Can-Am® Spyder® roadster defined new paradigms. Combining the open-air benefits of a motorcycle with many of the convenient features of a traditional roadster created a totally new product category of on-road power sport vehicles.

This unique three-wheel vehicle architecture brings stability at rest and in motion, with the right balance between performance and peace of mind. This makes the Spyder® roadster user-friendly, and the road accessible

to many people who want to enjoy the open-air experience.

The rider-active ergonomic is tailored to facilitate body involvement and to allow the rider to adapt to each specific riding experience. The straddle-type seating creates a great symbiosis between man and machine. The overall dynamic behavior is exhilarating yet reassuring for winding roads, commuting and touring.

The craftsmanship is pushed to new limits, giving its utmost attention to detail so that customers can enjoy every

thrilling second of the Can-Am® Spyder® global experience.

## PROJECT SPYDER® ST

First introduced in 2007, the initial version of the Can-Am® Spyder®, designated RS, was a sport version offering exhilarating riding for recreational sport driving enthusiasts. In 2010, the touring version, Spyder® RT, was introduced merging the performance of the RS with a comfortable, long-distance riding experience. In 2013, the Spyder® ST was brought to market, creating an evolution of the Spyder® RS



FIGURE 3: Trimmed hexahedral mesh on the ST model with rider and under hood

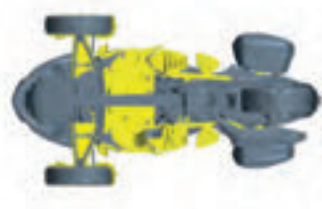
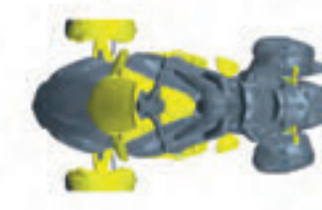


FIGURE 2: Can-Am® Spyder® ST showing optimized components (in yellow)

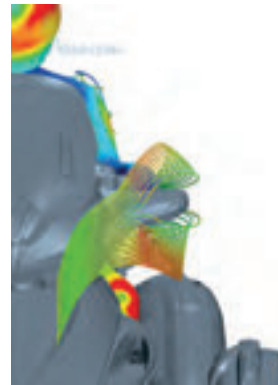
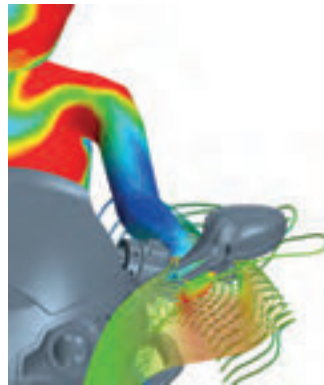
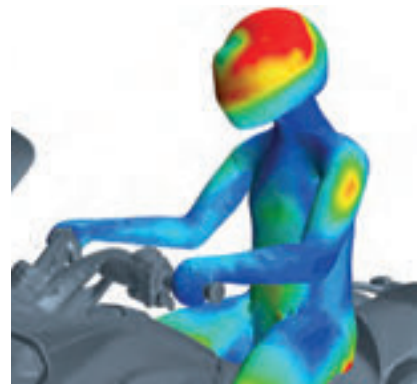


FIGURE 4: Comparison of wind protection between model and optimized design

with sport touring characteristics and improved thermal comfort. With ample storage and wind protection combined with the ergonomics necessary to handle tight corners as easily as long journeys, the ST is a stylish, sporty design completely at home for a quick ride to the market or breezing down the highway on a Sunday afternoon.

The entire vehicle was designed and engineered through virtual product development with the help of engineering simulation. The engineering team at BRP

worked in collaboration with the vehicle design studio from day one to develop the vehicle. The most important weapon in their arsenal during the design stages was STAR-CCM+®, CD-adapco™'s multi-purpose, multi-physics Computer Aided Engineering (CAE) tool offering the power of accurate, efficient numerical simulation at their fingertips.

### SIMULATING SYSTEMS

Over the years, the world of simulation has progressed to the point where

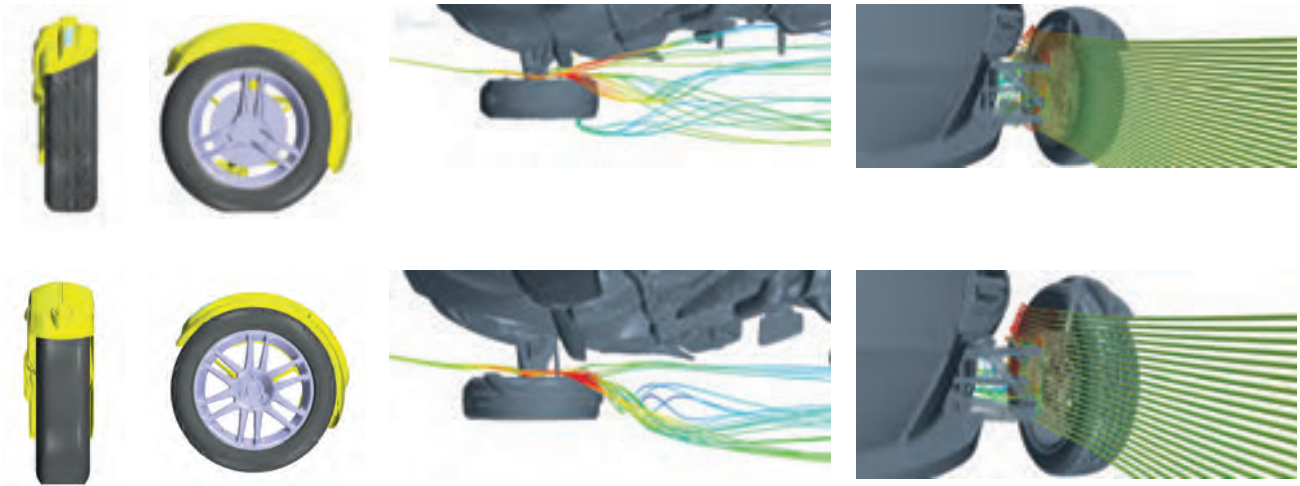


FIGURE 5: Comparison of flow around front fender between original (top) and optimized (bottom) design

## Following the idea of simulating the entire system as a whole, BRP has successfully used state-of-the-art numerical simulation to design and engineer a world-class product with minimal testing.

standalone simulations of a single component or physical process are no longer the name of the game. The evaluation of the performance of the entire system and the interaction of various sub-systems with one another and the system as a whole is a design challenge that can be tackled successfully with modern simulation tools. For the development of the Spyder® ST, BRP relied on STAR-CCM+® to simulate the different designs and systems of the roadster from day one, including aerodynamics, underhood cooling and thermal comfort. The advanced multi-physics capabilities of STAR-CCM+® allow the engineers to include all these relevant phenomena in the same simulation, thereby accounting for their interaction with each other and influencing the design of the Spyder® roadster from the beginning.

Based on previous versions of the Spyder® RS, two different initial designs for the Spyder® ST were in competition (figure 1) with different upper fairing, headlamp, mirror geometries and fender variants. These designs also had increased luggage capacity compared to the RS model and improved ergonomics from a relaxed seating position. Clay models of the two designs from the styling studio were built and 3D laser scanning techniques were then applied to create 3D CAD model for the STAR-CCM+® simulations. The simulation results were then used to optimize the initial designs

which were passed on to the design studio. This iterative process was carried out until the design and engineering requirements were met before a single prototype was made or tested, which is the real value of numerical simulation.

Figure 2 shows the components (in yellow) of the two designs optimized through STAR-CCM+®. The 3D CAD models of designs A & B were imported into STAR-CCM+® and a virtual wind tunnel was built around the model. The entire domain was then discretized using trimmed hexahedral cells inside STAR-CCM+®. The model included the Spyder®, underhood components, rotating wheels, moving ground, radiator, oil cooler and exhaust heat generation. The discretized domain consisted of 20 million trimmed hexahedral cells and is seen in figure 3.

### WIND PROTECTION

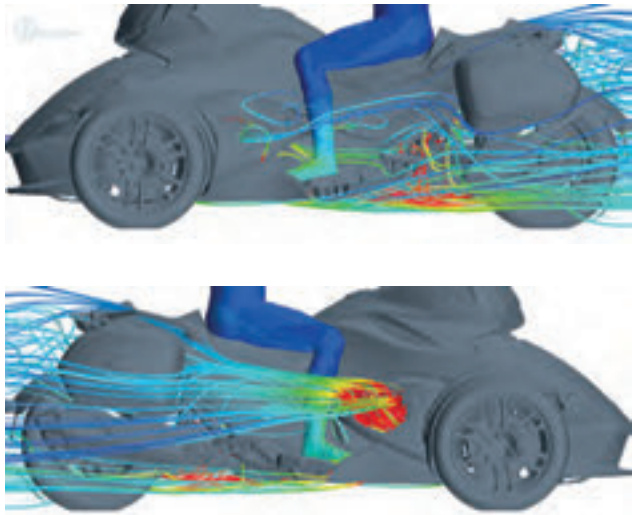
The first area of focus in the numerical analysis was wind protection for the rider. The iterative process adopted for the simulation resulted in an optimized design that offered an improvement in wind protection for the rider in three main different areas: head, hands and knees. Figure 4 shows the comparison between the original clay model design and the optimized design from STAR-CCM+®. Areas of red show regions on the rider's body resulting in discomfort while blue areas indicate the

opposite end of the spectrum with lower discomfort for the rider. The optimized design shows major reduction in rider discomfort. The accuracy of STAR-CCM+® and ability to be a design tool rather than a supplement was proven when the optimized design from STAR-CCM+® was tested on the track. Experimental from track validation confirmed the findings from STAR-CCM+® indicating better wind protection for the rider. The windshield in the final design showed minimal buffeting while still offering a clear view of the road ahead over the top of the windshield.

### AERODYNAMIC PERFORMANCE

An important design modification from an aerodynamic perspective was on the front fender. The front fender design on the Can-Am® Spyder® roadster has remained the same since the first Spyder® version in 2008. The numerical simulations delivered a complete database of the individual drag contribution of the different components of the roadster Spyder®. An analysis of these results showed that the front fender was a major contributor of drag. With this new knowledge in hand, BRP designed a new front fender that was improving the flow around the tires and creating less drag. Simulations showed that the new front fender resulted in a drag reduction between 3% and 5% depending on the Can-Am® Spyder® models, thereby

Spyder ST



Spyder RS

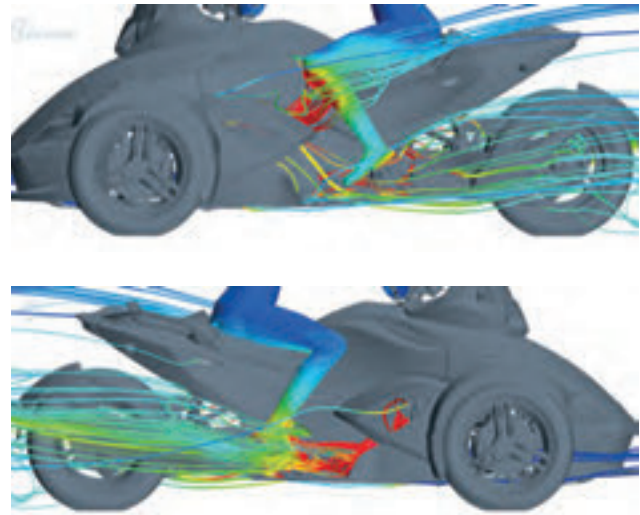


FIGURE 6: Thermal comfort comparison between BRP's Can-Am® Spyder® RS and ST models

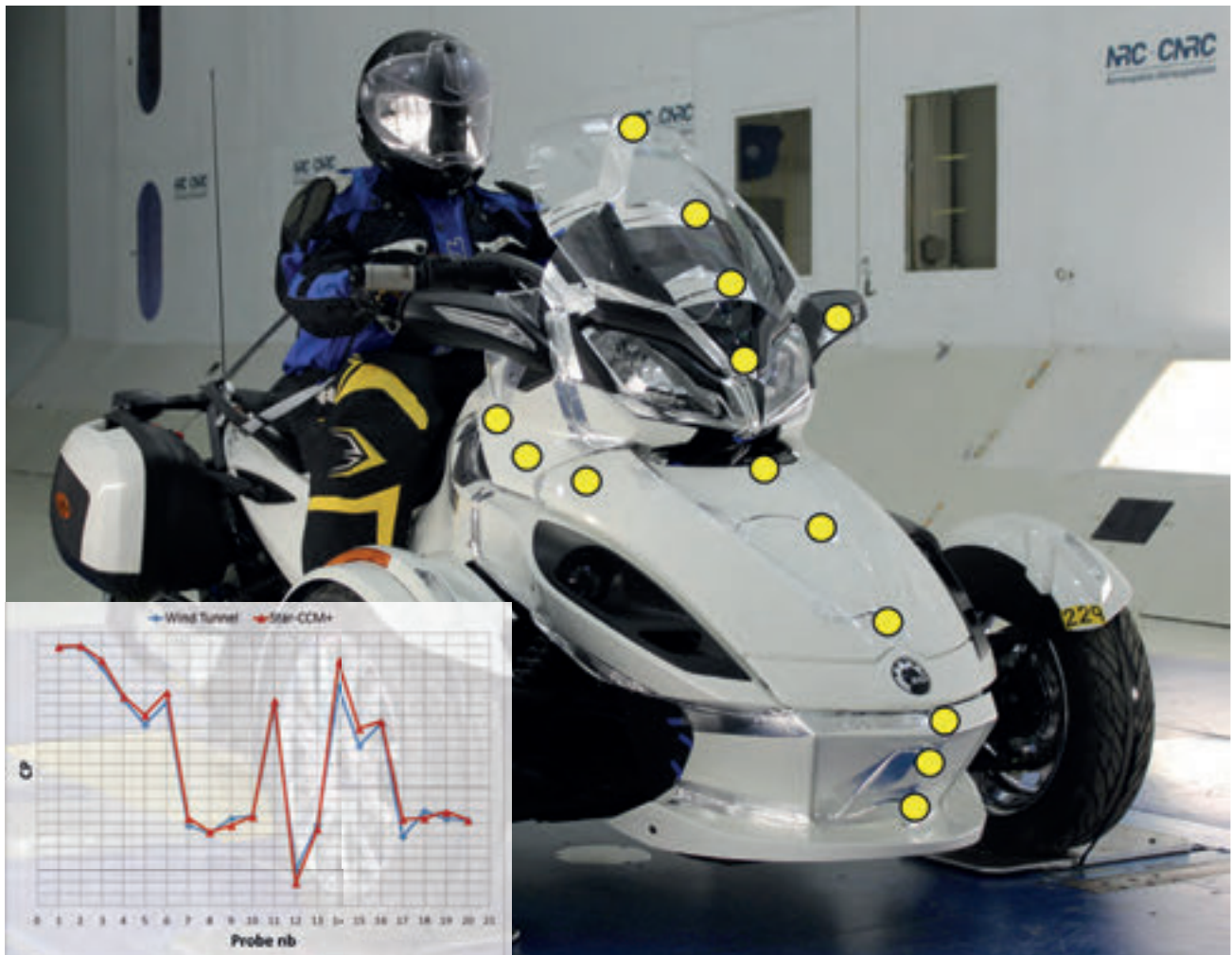
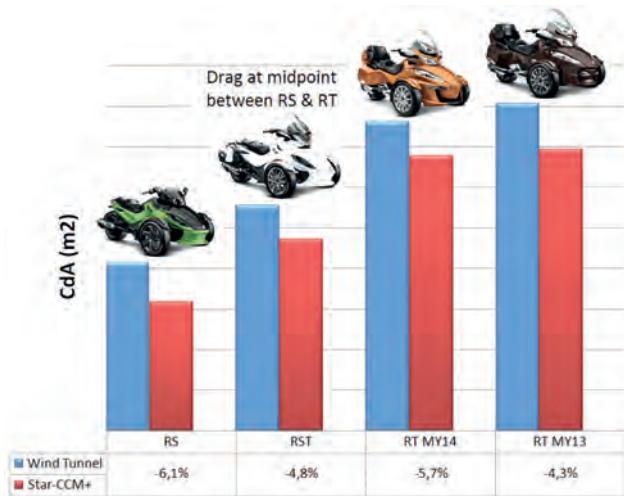


FIGURE 7: Comparison of pressure coefficient at different probe locations from STAR-CCM+® and test (table on the left), pressure probes (yellow dots) on the vehicle



**TABLE 1:** Drag comparison between STAR-CCM+® and experiments for Can-Am® Spyder® variants

For the development of the Spyder® ST, BRP relied on STAR-CCM+® to simulate the different designs and systems of the roadster from day one, including aerodynamics, underhood cooling and thermal comfort.

improving fuel mileage of the vehicle. The findings from STAR-CCM+® were confirmed by experimental testing of the new fender in wind tunnel. Figure 5 shows the comparisons between the old and new fender showing smoother, less turbulent airflow around the fender resulting in lesser drag.

## THERMAL COMFORT

In addition to the design improvements for wind protection and aerodynamics, STAR-CCM+® also helped BRP to improve the thermal comfort of the rider. Feedback from the customers of the Can-Am® Spyder® RS model indicated that the right foot of the rider was getting hot due to the high temperature air flow from the radiator impinging on the right foot. The engineers of the Spyder® ST set out to improve the rider experience by eliminating this discomfort. The Spyder® RS was simulated using STAR-CCM+® to identify the thermal areas of concern on the right foot. Figure 6 (left) shows areas of red on the rider's right foot confirming the high temperature flow here. In addition, the simulations also highlighted another area of concern around the rider's left knee which showed increased temperatures. Modifications to the body panels were made to reduce the heat on the rider knee and foot while maintaining the current cooling capacity of the radiator. The newer design reduced thermal discomfort on the rider's body as seen in figure 6 showing reduced areas of red (hot) and increased blue regions (cool) on the leg.

## WIND TUNNEL TESTS

The final design based on STAR-CCM+® was tested in Ottawa CNRC 9m x 9m wind tunnel for validating the performance. Drag was measured on all Can-Am® Spyder® models, past and present for comparison. Pressure was measured on the Spyder® ST at 20 different points using pressure. Figure 7 shows good correlation of the pressure coefficient between STAR-CCM+® and experiments. From table 1, it can be seen that STAR-CCM+® performed a good job of predicting the drag on all models without any experimental data to guide the simulations. The results showed that the drag from the Spyder® ST met the initial design requirement of being at the midpoint of the drag on Spyder® RS and RT.

## CONCLUSION

The Can-Am® Spyder® ST roadster, aerodynamically engineered solely using STAR-CCM+®, successfully met all the following design requirements:

- Better wind protection with minimal buffeting
- Drag at midpoint between RS and RT
- Better thermal comfort for the rider

Following the idea of simulating the entire system as a whole, BRP has successfully used state-of-the-art numerical simulation to design and engineer a world-class product with minimal testing. The final product is a sports-touring version of the Can-Am® Spyder® that offers the excitement of the open road to everyone. One thing is certain: When you get adoring waves and smiles from strangers while riding this roadster, just remember that it's not you; it's the Spyder® that's turning heads.

Founded by J.-Armand Bombardier, the inventor of tracked vehicles for transportation on snow covered terrain; the company was first named L'Auto-Neige Bombardier Limitée. In 1967, L'Auto-Neige Bombardier Limitée became Bombardier Limited. In December 2003, the recreational products segment of the company is sold to members of the Bombardier family, Bain Capital and the Caisse de dépôt et placement du Québec. The new company is named Bombardier Recreational Products Inc. In 2013, BRP became a public company, listed on the Toronto Stock Exchange (TSX:DOO).

Headquartered in Valcourt, Québec, Canada, BRP is a global leader in the design, development, manufacturing, distribution and marketing of powersports vehicles and propulsion systems. Its portfolio includes Ski-Doo® and Lynx® snowmobiles, Sea-Doo® watercraft, Can-Am® all-terrain and side-by-side vehicles, Can-Am® Spyder® roadsters, Evinrude® outboard engines and Rotax® engines for karts, motorcycles and recreational aircraft as well as inboard jet propulsion systems for boats. BRP supports its line of products with a dedicated parts, accessories and clothing business. With annual sales of over CA\$3 billion from 105 countries, the company employs approximately 7,100 people worldwide.

**CD-adapco™ GLOBAL ACADEMIC PROGRAM – MORE THAN JUST LICENSES!**

Recognizing the importance of supporting the global academic engineering community, CD-adapco™ provides students and academic institutions the opportunity to take advantage of its Global Academic Program. Our "More Than Just Licenses!" philosophy is dedicated to ensuring students, professors and graduates have access to the latest info, training and support to guarantee success in academia and beyond. Thousands of academics in hundreds of academic institutions all around the world have implemented STAR-CCM+® into their undergraduate, graduate and postgraduate curriculum and / or research teams.

The CD-adapco™ Global Academic Program has produced hundreds of new engineers with STAR-CCM+® experience ready to join your team. Contact your local sales representative today to find out how you can put the CD-adapco™ Academic Program to work for you!

# ANALYSIS OF PRE-IGNITION INITIATION MECHANISMS WITH CFD

**MICHAEL HEISS & THOMAS LAUER**  
Vienna University of Technology

**F**or downsized SI-engines at high loads and particularly at low engine speeds, spontaneous auto-ignitions randomly occur before the regular spark timing, leading to severe engine damage. These pre-ignitions are limiting the fuel efficient combustion process and therefore it is crucial that the underlying mechanisms are understood.

Experimental and numerical investigations were carried out at the Institute for Powertrains and Automotive Technology at the Vienna University of Technology. An optical access was installed on the test engine to enable high-speed imaging. CFD simulations were carried out in order to evaluate droplet impingement and wall film formation on the piston and liner. Virtual particles released from wetted areas on the piston crown close to the liner showed a good correlation with the location of the recorded light emissions initiating pre-ignitions.

Additionally, the detachment of soot particles from the combustion chamber walls caused by the high-frequency pressure oscillations during a pre-igniting cycle was modeled in CFD based on the video observations. Particles that remained in the combustion chamber after gas exchange heated up during the subsequent regular combustion cycle, and therefore became critical for follow-up pre-ignition events in the next cycle. Thus, the initiation for pre-ignitions by droplets and particles could be confirmed.

## INTRODUCTION

CO<sub>2</sub> emissions from anthropogenic sources are suspected to have an impact on global warming. Governments around the globe react by defining targets for the reduction of greenhouse gases and CO<sub>2</sub> fleet emission. This is particularly a challenge for vehicles that are propelled by gasoline engines. A

step towards a more efficient working process is the downsizing of gasoline engines using high boost pressures and direct injection. It allows the shifting of operating points to higher engine loads with a higher efficiency.

Experience with highly boosted engines has shown that at high loads and particularly at low engine speeds, spontaneous self-ignitions randomly occur before the regular spark timing followed by a mega-knock that may lead to engine damage in serious cases. Recent experimental studies revealed that oil/fuel droplets or deposits are a possible source of pre-ignition [1-3].

It is the aim of the presented work to analyze the mechanisms that initiate pre-ignition using different measuring techniques and CFD simulations.

## EXPERIMENTAL SETUP AND OPTICAL DIAGNOSTICS

A turbocharged 4-cylinder DI test engine with 1.4 l displacement and a central 6-hole injector was set up on a test bench. The engine was operated at an engine speed of 2,000 rpm, a boost pressure of 2.1 bar and a brake mean effective pressure of 21 bar. A video access was installed on cylinder 4 for high-speed imaging of pre-ignition and two bores were applied to the cylinder head for the light source and the camera.

As previously stated, pre-ignitions frequently occur within clusters of three to five events alternating with regular combustion cycles. The first observed pre-ignition of a cluster showed distinct differences in light-emissions for several events. During the first pre-ignition cycle, a light source occurred spontaneously and immediately ignited the entire mixture. Due to the fact that there was no previous light emission, it is likely that the first pre-ignition

was triggered by oil/fuel droplets that reached their critical condition for self-ignition at the moment when they became visible. Figure 1 (a) shows an initial pre-ignition event.

It was common to all pre-ignitions that in the subsequent regular burning cycle, glowing particles were observed, particularly during the final combustion phase, see figure 1 (b). Obviously, these particles are deposits. The videos suggest that some of these particles remain in the combustion chamber and are heated up during the following regular combustion, at which point the time is sufficient for the heat transfer between gas and particle. Subsequent pre-ignitions are usually repeated three to five times until no major deposits were present in the combustion chamber.

## SIMULATION OF THE WALL FILM FORMATION AND DROPLET TRACES

CFD simulations were carried out in order to analyze the wall film formation on the piston and the liner and hence the behavior of droplets that are released from the film. Fuel components with high boiling temperatures were considered by introducing a five-component surrogate fuel. The mass fractions of the constituents were chosen to fit the measured distillation curve assuming an ideal gas and liquid [4, 5].

The prediction of wall film formation on surfaces with a temperature in the range of the fluid's boiling temperature requires a multi-regime impingement model that takes into account the wall temperature and the droplets' stability. In this work, an adapted Bai-Gosman model was used [6]. The spray was modeled with a Lagrangian approach using the measured droplet spectrum as a boundary condition and the Reitz-Diwakar model for secondary break-up. The turbulent flow field was modeled

with a 2-equation k-ε model.

The simulation of an injection event revealed a distinct wetting of the piston crown. Mixing of fuel and lube oil and the accumulation of the fuel-oil-mixture in the piston crevice is therefore probable. The crevice volume was not modeled in detail. Therefore, droplets with an assumed diameter of 500 μm were released in regions with intensified wall wetting to mimic droplet stripping and the droplet traces in the combustion chamber as seen in figure 2. The trajectories were calculated up to the crank angle where the pre-ignitions were typically observed. A reasonable correlation between the endpoints of the trajectories and the locations of pre-ignitions from the video observations (yellow symbols) could be found and this supports the assumption of stripped droplets from wetted crevice areas as a source of pre-ignitions.

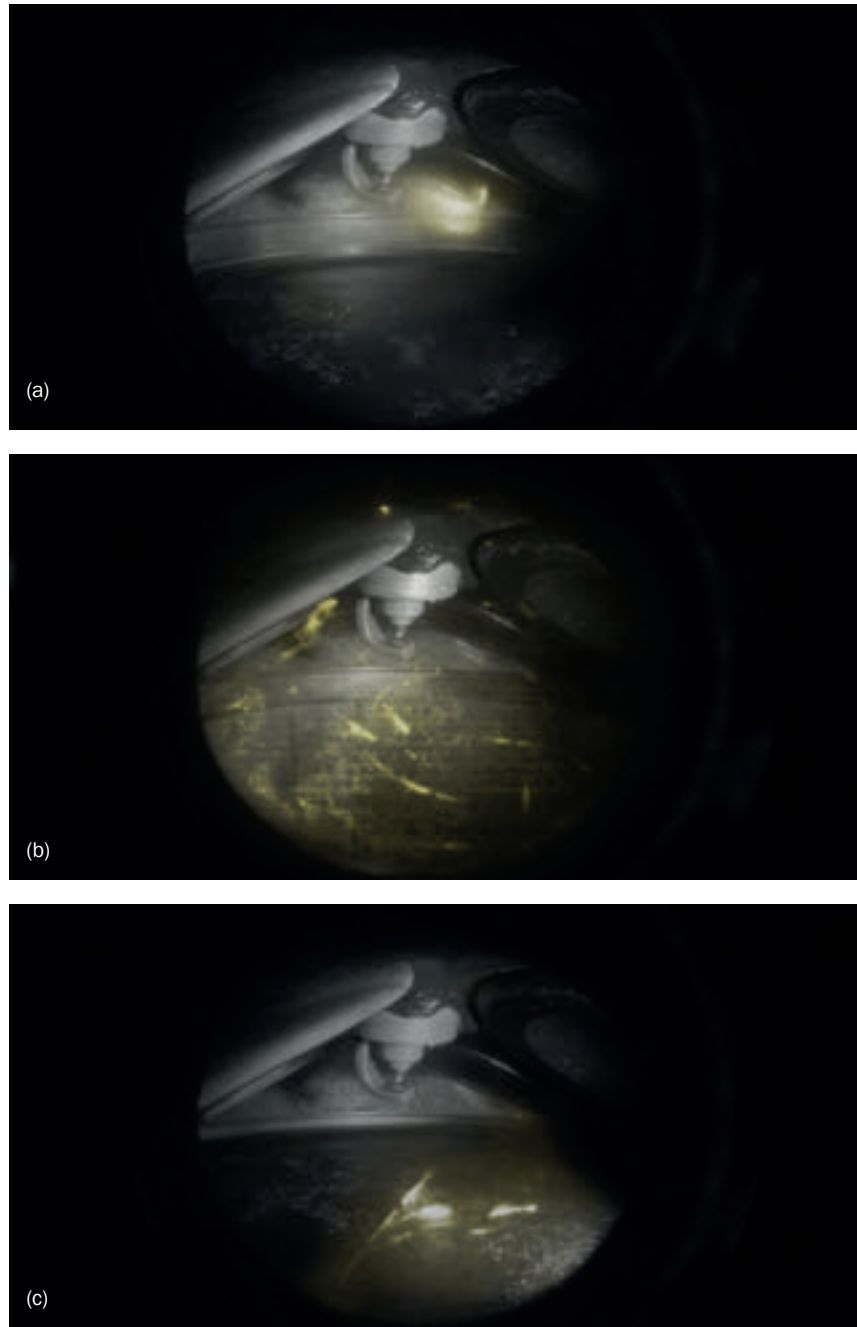
**INVESTIGATIONS ON FOLLOW-UP PRE-IGNITIONS**

The optical investigations suggested that the follow-up pre-ignitions are triggered by glowing particles. They frequently occur after a regular combustion cycle. For a more elaborate analysis of the underlying mechanisms, a CFD simulation was carried out for the first pre-ignition, the subsequent regular combustion cycle and the first follow-up pre-ignition. For the combustion, a 3-zone enhanced coherent flame model was used. Its model parameters were adapted to match the measured burn rates.

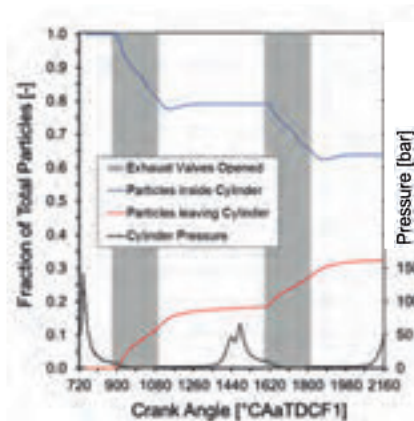
Particles were released briefly after the first mega-knock event from the discs of the exhaust valves and the crevice volume, where a formation of solid deposits due to intensive wall wetting or high temperatures is likely. The initial properties of the particles are summarized in table 1. Their initial speed after being detached by the pressure oscillations and their diameter were varied to study the impact of both parameters on their further behavior. The particles' initial temperature was chosen to be a typical cylinder wall temperature.

Figure 3 shows the number of particles that remain inside the combustion chamber until the first follow-up pre-ignition event occurs. For a better visualization, the cylinder pressure is plotted on the 2<sup>nd</sup> ordinate and the opening of the exhaust valves is illustrated with shaded bars.

It becomes obvious that more than 60% of the originally released particles



**FIGURE 1:** High-speed images of pre-ignition events: (a) Initial pre-ignition event; (b) Follow-up event with glowing particles; (c) Progress of one subsequent pre-ignition event due to a glowing particle



**FIGURE 3:** Evolution of the number of particles over three cycles

Total number	6,000 particles
Diameter	50 μm ≤ d ≤ 500 μm
Velocity	0 m/s ≤ vinit ≤ 10 m/s
Temperature	500 K

**TABLE 1:** Specification of inserted particles

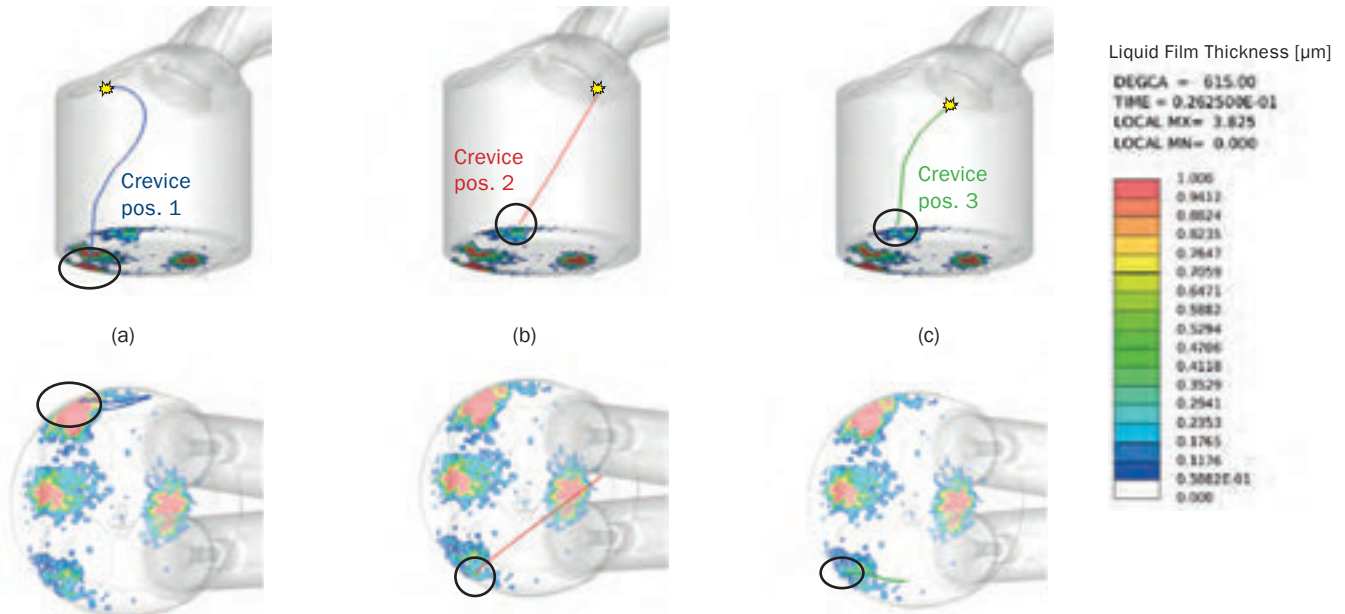


**FIGURE 2:** Trajectories of droplets (colored lines) released from wetted crevice areas in comparison with recorded origins of pre-ignitions (yellow symbols)

remain in the combustion chamber. It could be further shown that a disproportionately high amount of small particles leave the combustion chamber whereas the bigger particles remain inside. This outcome is qualitatively in good agreement with the observations at the engine test bench and can be argued with the fact that the bigger particles do not follow the flow field instantaneously due to their higher inertia.

In order to study the heating and the thermal inertia of the particles, the properties of solid soot were assigned. The particles were assumed to be spherical without any temperature distribution inside the particle. Furthermore, no exothermal reactions were considered.

It could be shown with this simplified approach that the small particles are immediately heated above the self-ignition temperature of soot that was assumed to be 900 K. Furthermore, the investigations revealed that the

bigger particles significantly increase in temperature during the regular burning cycle and distinctly exceed the self-ignition limit in the third cycle. In figure 4, the temperature curves of the five hottest particles are plotted. Additionally, the self-ignition limit of soot is added to the diagram.

Although no exothermic reactions were included (and this is considered a severe simplification), it becomes clear that the temperature of the particles increases steadily if they survive the exhaust stroke of the first pre-ignition event. Therefore, the observation of an alternating succession of cycles with pre-ignition and regular combustion can be explained with the intensive heating of the remaining particles during the regular combustion.

### CONCLUSIONS

CFD simulations were carried out in order to explain the underlying mechanisms of pre-ignition events and their alternating occurrence at the test bench. This study confirmed that the stripping of

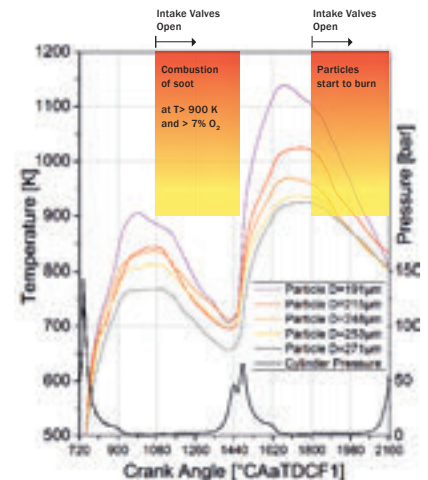


**FIGURE 4:** Temperature history of the hottest particles at compression start of the 3rd cycle

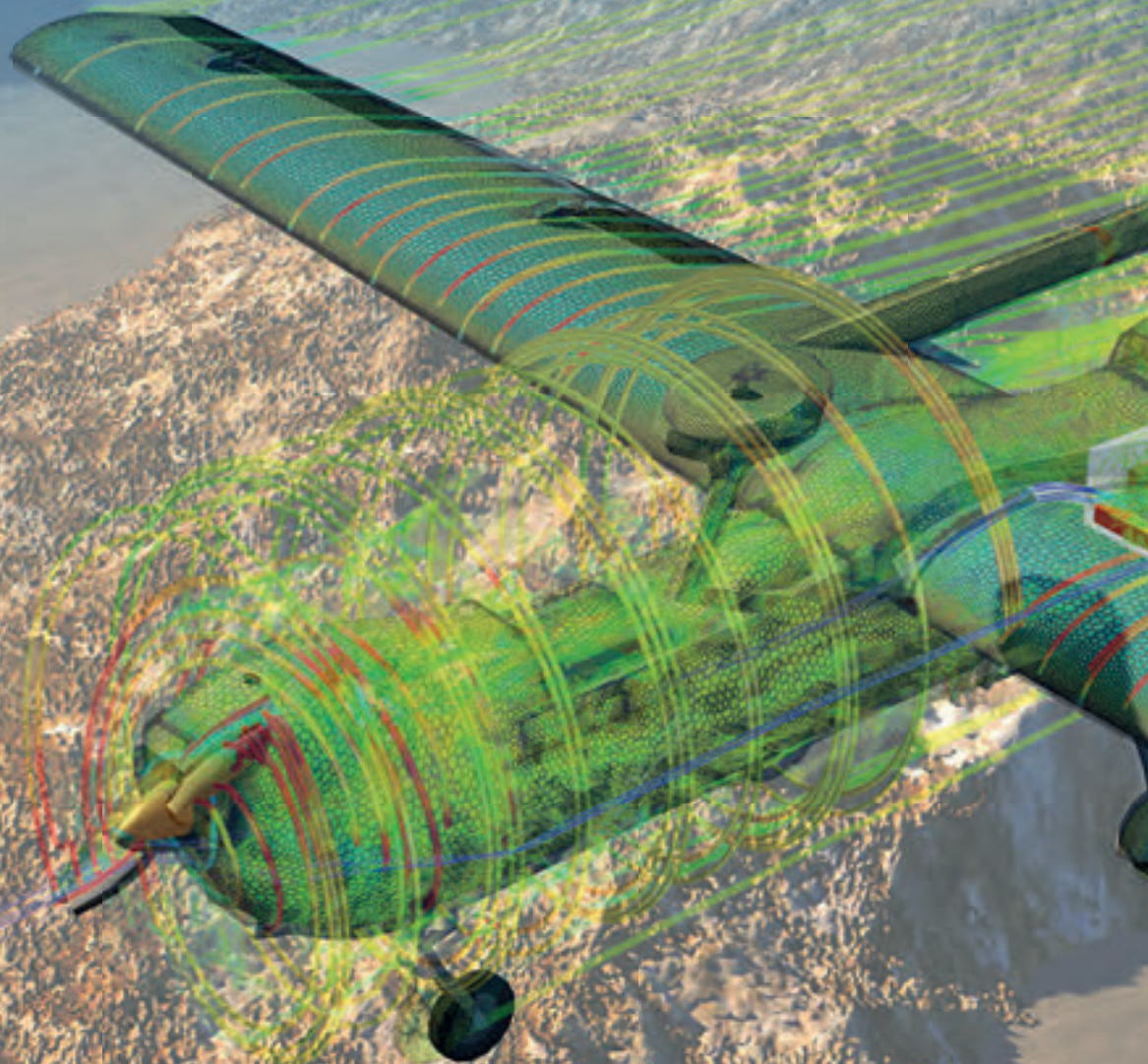
droplets and the detachment of deposits are possible causes for pre-ignitions. However, further model details like the exothermic reactions on the particles' surfaces must be considered for future work.

### REFERENCES

1. Takeuchi, K.; Fujimoto, K.; Hirano, S.; Yamashita, M.: Investigation of Engine Oil Effect on Abnormal Combustion in Turbocharged Direct Injection - Spark Ignition Engines. In: SAE Technical Paper: 2012-01-1615
2. Yasueda, S.; Takasaki, K.; Tajima, H.: Abnormal Combustion caused by Lubricating Oil in High BMEP Gas Engines. In: MTZ Industrial (2013), Vol. 3, pp. 34-39
3. Zahdeh, A.; Rothenberger, P.; Nguyen, W.; Anbarasu, M.; Schmuck-Soldan, S.; Schaefer, J.; Goebel, T.: Fundamental Approach to Investigate Pre-Ignition in Boosted SI Engines. In: SAE Technical Paper: 2011-01-0340
4. Lauer, T.; Heiß, M.; Bobicic, N.; Holly, W.; Pritze, S.: A Comprehensive Simulation Approach to Irregular Combustion. In: SAE Technical Paper 2014-01-1214
5. Batteh, J. J.; Curtis, E. W.: Modeling Transient Fuel Effects with Alternative Fuels. In: SAE Technical Paper: 2005-01-1127
6. Heiss, M.; Lauer, T.: Simulation of the Mixture Preparation for an SI Engine using Multi-Component Fuels. STAR Global Conference 2012, Amsterdam: 2012

# SIMULATING SYSTEMS

FLOW – THERMAL – STRESS – EMAG – ELECTROCHEMISTRY – CASTING – OPTIMIZATION  
REACTING CHEMISTRY – VIBRO-ACOUSTICS – MULTIDISCIPLINARY CO-SIMULATION



✉ [info@cd-adapco.com](mailto:info@cd-adapco.com)

🌐 [www.cd-adapco.com](http://www.cd-adapco.com)



STAR-CCM+





# IT'S GETTING HOT IN HERE! ZEECO SOLVES THE MYSTERY OF A HEATER MALFUNCTION USING STAR-CCM+®

ZHILI (ALEX) QIN  
Zeeco Inc.

PRASHANTH SHANKARA  
CD-adapco™



FIGURE 1: X-cut plane section through the gear housing showing mesh details of the model

## INTRODUCTION

In engineering consulting, troubleshooting the problems faced by your customer in an efficient, timely manner is the bread and butter of the business. As such, it is highly critical to be equipped with the right tools in addition to having competent engineers tackling the problem. This article showcases one such example where a modern numerical simulation software in the hands of good engineers transforms into an efficient, effective

virtual troubleshooting tool. Zeeco Inc. is a provider of combustion and environmental solutions, involved in the engineering design and manufacturing of burners, flares and incinerators. In addition, Zeeco also offers engineering consulting to their clients. One such customer came to Zeeco with a problematic heater that was suffering from low performance. This article highlights how Zeeco used CD-adapco™'s flagship software, STAR-CCM+®, to

**“STAR-CCM+®  
is an efficient  
and cost-saving  
engineering  
tool for  
troubleshooting”**

ZHILI (ALEX) QIN  
Zeeco

virtually troubleshoot the heater and identify the cause of the heater's inefficient operation.

## INDUSTRIAL HEATER – THE ISSUES

The problematic industrial heater is shown in figure 1. The modeled system included burners on both sides at the bottom and a radiant section on top with process tubes running along the length and breadth of the heater. The convection section and stack were not included in the model. The process tubes carried processed fluids that entered the heater at the top and exited at the bottom. A combustion air distribution duct was attached to the burners to distribute the air equally to each of the burners for combustion. The walls of the heater are made of firebrick and ceramic fiber module.

The heater had the following issues while in operation and Zeeco was tasked with finding the cause and providing solutions for these:

- **Coking:** Coking is the formation of coke on the inside of the heater tubes, reducing their heat transfer capacity. The process tubes carried hydrocarbon fluid and the heavier species in the fluid were prone to coking. During operation, it was noticed that there was coking inside the process tubes.
- **Run Length:** The heater was initially designed to run for 9-10 months. Due to problems with the coking, the heater only ran for 3-4 months after which the heater had to be shut down to clean the coking inside the tubes.
- **Thermal Behavior:** The temperature readings on the tube metal showed non-uniform temperatures and heat flux distributions at the tube surface.

Visual troubleshooting of the heater and its various components is extremely difficult and impractical because there is no easy way to access to the interior of the system. Zeeco decided to turn to virtual simulation to gain insight into the heater performance. STAR-CCM+®, CD-adapco™'s multi-physics simulation software, was used as a troubleshooting tool for this purpose.

## CFD SETUP OF THE HEATER

A CAD model of the heater geometry was prepared for analysis using Solidworks. The computational model included the heater radiant section with process tubes, burners and air distribution ducts. The domain was discretized in STAR-CCM+® using trimmed hexahedral cells (figure 2) and Navier-Stokes equations were solved in these cells. Only half the heater was



FIGURE 2: Initial distribution of the three different oil filling levels

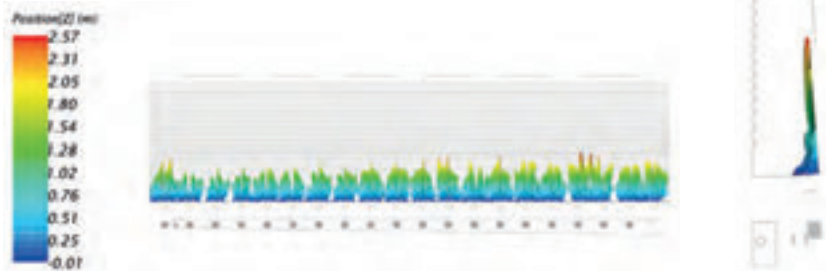


FIGURE 3: Oil distribution changes in time for the middle oil level

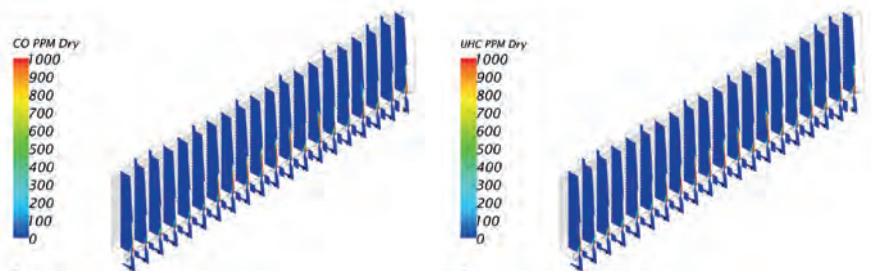


FIGURE 4: (a) Streamlines showing transient flow features between the intermeshing gears and (b) transient velocity flow field changes in the gearbox

modeled with around 13M cells and symmetry condition was assumed for the other half. The computational mesh was refined sufficiently around the burners to resolve the flow field and combustion accurately. The heater was 85 feet long, around 25 feet tall and 10 feet wide and modeled in scale.

The segregated flow solver in STAR-CCM+® is ideally suited for low-speed flows and was used here. The fuel gas mixture in the heater was refinery fuel gas, including hydrogen and hydrocarbons like methane and propane. STAR-CCM+® offers a full suite of combustion models to simulate various combustion phenomena. The multi-

component species model was used to introduce the various fuel-gas components into the heater. The Eddy Break-Up (EBU) model in STAR-CCM+® was used to model the non-premixed combustion of the species by solving the individual transport equations for mean species on the computational mesh. Ignition was not considered based on the characteristic of the heater flame and the standard EBU model was deemed sufficient to model the combustion in conjunction with the realizable k-ε turbulence model. Radiation was accounted for by the choice of the Gray Thermal Radiation model in STAR-CCM+®.

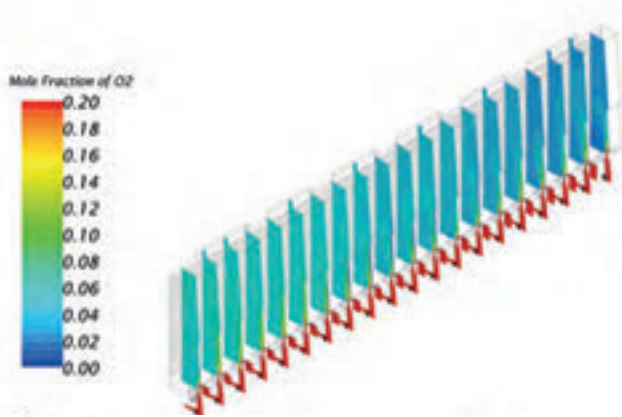


FIGURE 5: Pressure condition changes in time in the gearbox

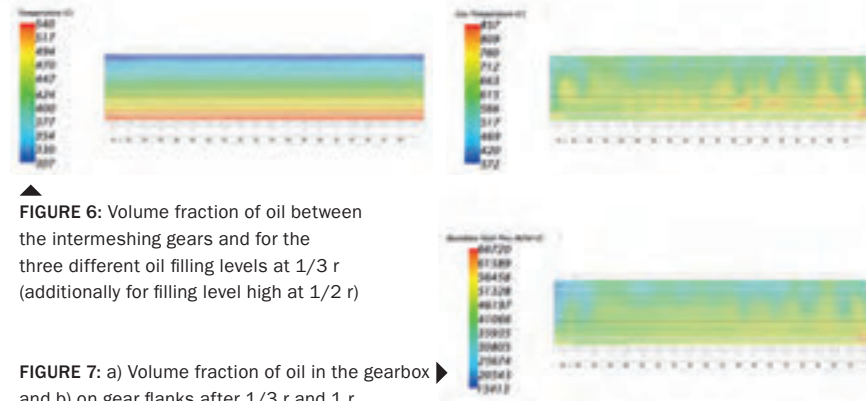


FIGURE 6: Volume fraction of oil between the intermeshing gears and for the three different oil filling levels at 1/3 r (additionally for filling level high at 1/2 r)

FIGURE 7: a) Volume fraction of oil in the gearbox and b) on gear flanks after 1/3 r and 1 r

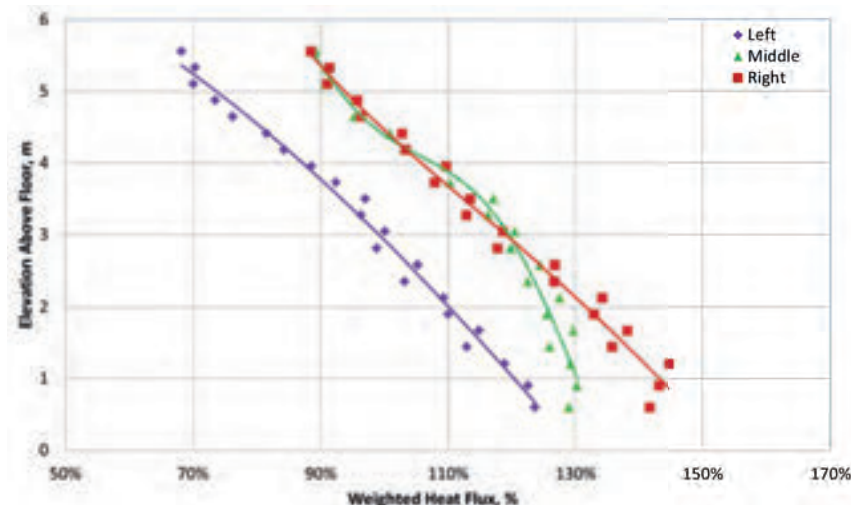


FIGURE 8: Temporal development of the volume fraction of oil on the flanks of gear 1 and gear 2

### IDENTIFICATION OF HEATER ISSUES FROM SIMULATION

Figure 3 shows the predicted combustion flame profile depicted by iso-surfaces of the combustion output species. The combustion air enters the distribution ducts from right to left, leading to the flame height decreasing from right to left as the air available for combustion decreases. The burner at the far left shows anomalous behavior with higher flame length which is caused by a special

duct design at the far left end. The close proximity of the flame (front view) to the side wall was confirmed by visual observation through viewing holes in the heater. Figure 4 depicts the carbon monoxide (left) and unburnt hydrocarbon (right) concentration at the central plane of each burner and shows that the CO burns out quickly, showing that completion of combustion is not an issue. Figure 5 shows the oxygen level at central plane of each burner. Quantitative analysis of

the oxygen concentration shows that excess oxygen is around 5% which is in accordance with the heater design. The process fluid entered the heater from the top and exited at the bottom, resulting in the temperature increasing from top to bottom. A visual analysis of the tube metal temperature as seen in figure 6 confirms this behavior. Flue gas temperature at the tubes shows hot spots on the right side while the left side is cooler. For any heater, a proper uniform distribution of heat flux at the tube surface is necessary for optimal operation. A non-uniform heat flux distribution results in poor heating and makes the hydrocarbons inside the heater prone to coking. Figure 7 shows the heat flux distribution on the tube surface. The left, right and middle sections of the heater are investigated to analyze the heat flux distribution. The weighted heat flux at various locations is compared for the three sections in plot 1. The weighted heat flux represents the ratio of the local heat flux to the overall average heat flux for all tube surfaces. It can be seen that the tube surface on the left is absorbing less heat than the surface on the right side.

### HEATER ISSUES AND RECOMMENDATIONS

For process heaters, it is very typical to see higher heat flux at lower levels where the combustion flame enters the heater as opposed to the higher elevations inside the heater where there is a lesser heat transfer and lower heat flux. From plot 1, it is apparent that at a lower elevation, the left side of the heater has a weighted heat flux of 125%, while this value jumps to 145% on the right side. This shows that the tube surface on the right side is absorbing 20% more heat than the left side, leading to coking of hydrocarbons at these higher temperatures. The heat transfer distribution on the tube surfaces is thus identified as the cause of the poor functioning of the heater. It was recommended to introduce more baffle plates and turning vanes inside the combustion air distribution duct to change the flow pattern. This will result in more uniform air distribution to all the burners, thus reducing the excessive heating of one end of the heater compared to the other. Zeeco used STAR-CCM+® to successfully simulate the heater operation and identify the cause of the heater malfunction. Recommendations were suggested based on the numerical simulations for improved performance. STAR-CCM+® enabled Zeeco to solve an engineering challenge of a customer in a timely, cost-effective manner, reinforcing the capability of STAR-CCM+® to function as a key weapon in the arsenal of any engineering consulting organization.

**A** process heater is a direct-fired heat exchange device. It uses the hot flue gases from combustion of a commonly available fuel in a petrochemical or refinery to heat a fluid flowing through coils. These coils are placed inside the heater. The liquid inside the tubes could be crude oil, naphtha, a mixture of steam and methane or others. In some cases, the heater only heats the fluid. In other cases, the fluid may undergo high temperature reactions to produce valuable chemicals. These chemicals are further processed downstream of the heater. The processes occurring inside the tubes and the combustion occurring in the heater is a coupled phenomenon. It therefore makes these heaters very complex to design and operate. Heat transfer from the burners in the heater needs to be precise to transfer enough heat without causing damage to the tubes or unwanted coking reactions inside the tubes. The heater needs to operate safely, transfer required amount of heat and produce products in correct proportions by promoting desired reactions while minimizing pollutant gas formation such as NO<sub>x</sub>.

The flow inside the coils of the heater could be multiphase or the tubes may be filled with catalysts of various shapes. This adds further complexity to the problem.

STAR-CCM+® offers a wide range of reaction and combustion models to simulate the processes in such heaters. In a new release in near future, CFD analysts will be able to couple the reaction inside the tubes with the combustion phenomenon in the heater in a seamless manner to increase the fidelity of the results. Moreover, the burner design itself can be optimized using rigorous optimization methods using the OPTIMATE™/OPTIMATE+™ add-on. This helps engineers in minimizing the number of experimental trials and arrive at superior designs faster.

# PICKING UP BAD VIBRATIONS: PORTER MCGUFFIE TROUBLESHOOT A VIBRATING HEATER

TITUS SGRO  
CD-adapco™

The bane of most engineers is dealing with physics that have not been considered during the design process and consequently troubleshooting the problem caused by it. This phenomenon is universal across the engineering world, with operating issues in equipment cropping up in countless different ways. Some unanticipated physical behavior can easily be accommodated and fixed. Others, like those often encountered by Porter McGuffie are much more difficult to diagnose and solve.

Porter McGuffie, Inc. (PMI), a Lawrence, Kansas-based computational mechanics and engineering measurement services company, provides engineering solutions backed by FEA and CFD analysis to a wide range of fields. One particular design problem they were asked to resolve was the piping inside a heater unit that was visibly and audibly shaking (and startling its operators). The cause of the shaking in the heater's piping system (figure 1) was unknown. The oscillatory displacement was approximately one inch in each direction under certain operating conditions. This level of vibration was considered too high for safe operation. To limit the vibrations, the unit throughput had to be lowered significantly.

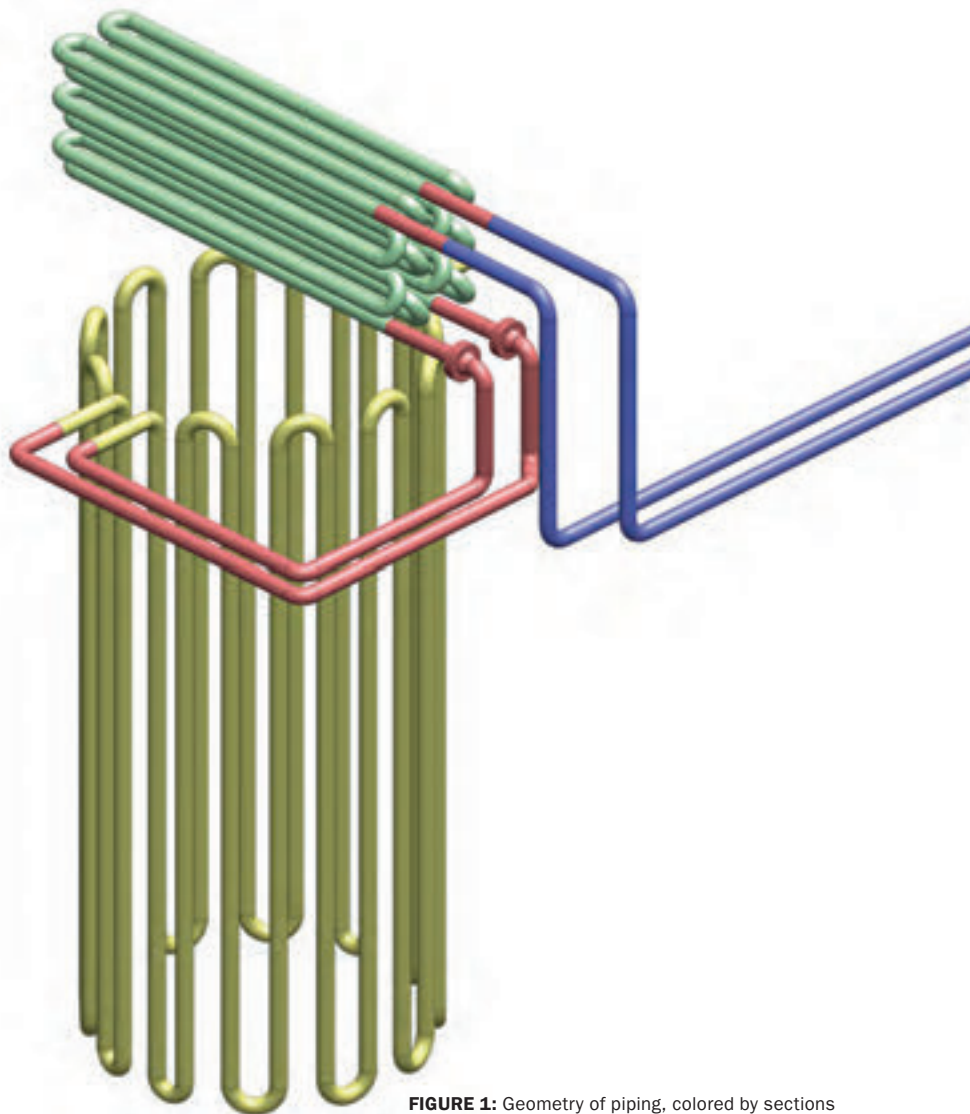
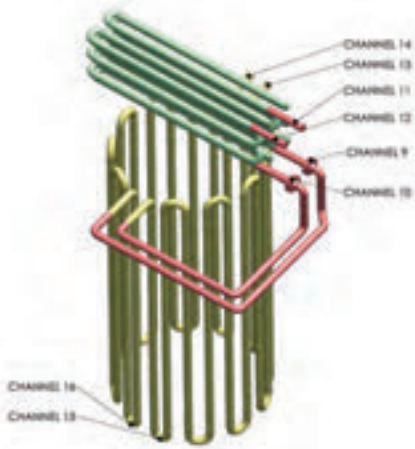
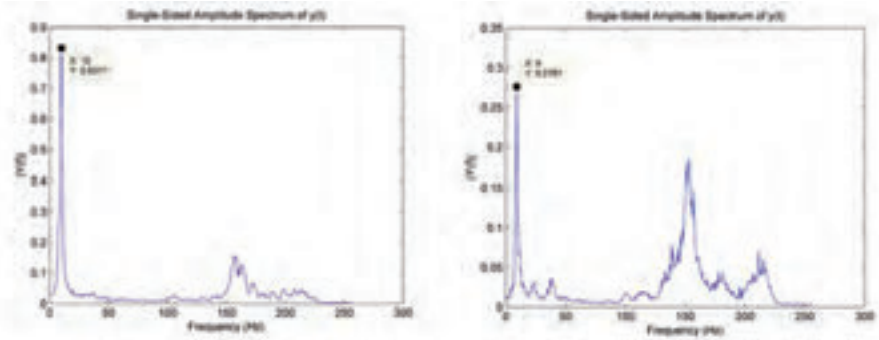


FIGURE 1: Geometry of piping, colored by sections



**FIGURE 2:** Locations of accelerometers on the test system



**FIGURE 3:** Vibration frequency measured at locations 9 and 10

To begin their analysis, PMI visited the site of the heater. They attached accelerometers to the heater’s piping to get precise measurements of the vibration of the pipes. Measurements (obtained at the locations shown in figure 2) indicated that the most significant vibrations were occurring at frequencies of 10 Hz and 9 Hz, as illustrated in figure 3. Later analyses identified these frequencies as the mechanical resonant frequencies of the two separate loops in the system. Additional analysis of the vibration data revealed that the envelope of the vibration amplitude had a periodicity to it. The primary period was approximately 27 seconds in length, and the secondary period was approximately 13.5 seconds in length, as illustrated in figure 4. This amplitude variation traded back and forth between the two loops in the heater, with one loop vibrating at ~10 HZ and then the other at ~9 Hz. This amplitude variation was nearly 180 degrees out of phase between the two loops.

Using this data, PMI was able to correlate the change in vibration levels to the flow of hydrogen in the two-phase distillate stream. To identify the cause of the change in hydrogen flow, PMI performed a CFD analysis on the heater piping system, recreating the entire flow regime in STAR-CCM+® by CD-adapco™. The setup itself made use of STAR-CCM+®’s Eulerian multiphase model to track the gas and liquid phase species in the pipes, as well as the S-gamma submodel to track the size of individual liquid droplets.

To enable tracking of various quantities within sections of the model, five regions were created: the inlet pipe, the convection section, cross-over section, radiant section, and the outlet tee. To accurately read the conditions of the

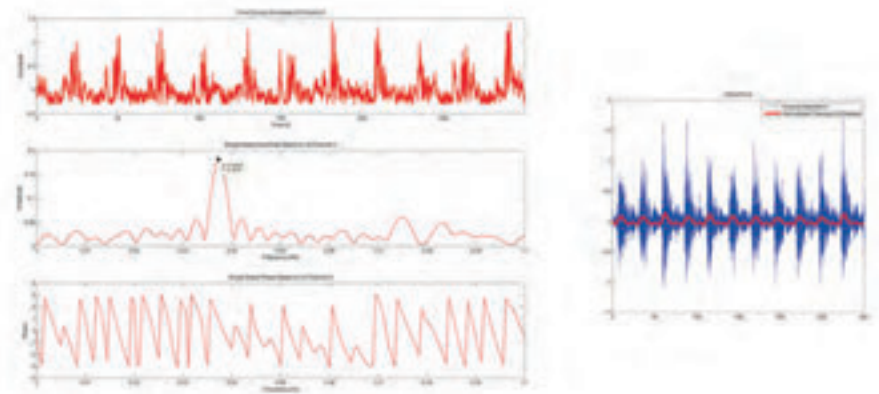


**FIGURE 4:** Analysis to periodicity of vibrational amplitudes

heater, PMI set a considerable number of 3D force monitors at every elbow and pipe within the simulation as well as pressure and mass flow monitors at the entrance to each section for both liquids and gases. Flow regimes were identified within the simulation through visual inspection from still images and animations. Figure 5A shows the Fast Fourier Transform of one of the pressure graphs, with the peak period oscillations of pressure indicated. Figure 5B shows the measured and simulated period of pressure pulses through the radiant and convection sections for each flow configuration. As is clearly shown, there is very good agreement between the simulated and measured frequency calculations, giving credence to the time-domain pressure and force traces queried from the model.

The simulation results indicated that the flow patterns in the convective region, characterized as stratified flow, did not oscillate noticeably. On the other hand,

the radiative section’s flow regime showed significant annular slugging (where the liquid phase flows along the wall with a gas central core) that caused highly unstable flow patterns (figure 6). The slugging pattern that formed matched the frequency of the piping vibrations. These slug patterns also correlated with the pressure pulses measured in the radiant, cross-over, and convection sections. While this would be enough to provide good circumstantial evidence of the cause of the shaking, Porter McGuffie was not satisfied and investigated further, coupling the STAR-CCM+® run with Algor (a finite element analysis code), using PMI proprietary coupling software. Applying the force load data from the CFD simulation, PMI was able to predict the displacement of the pipes (figure 7). The red highlights show the area in the actual heater that was having the most vibrational displacement. Figure 8 shows a comparison of the measured accelerations superimposed over the FEA-predicted accelerations, detailing obvious correlations.

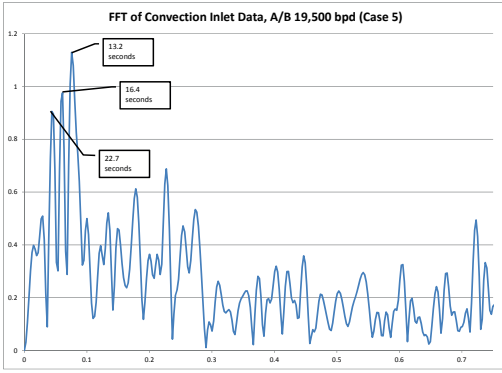


FIGURE 5A: FFT of pressure from time to frequency domain

Case #	Inlet Configuration	Flow Configuration	Approximate Measured Period (s)	Primary CFD Calculated Period(s)
1	Reduced	A/B 14,500	13.3	11
2		A/B 19,500	27	23
3		C/D 14,500	13.3	14
4		C/D 19,500	27	29
5	To Exchanger Outlet	A/B 19,500	27	27
7		A/B 24,500	24.5	22
8		A/B 35,000	N/A	19

FIGURE 5B: Comparison of measured experimental data to CFD results

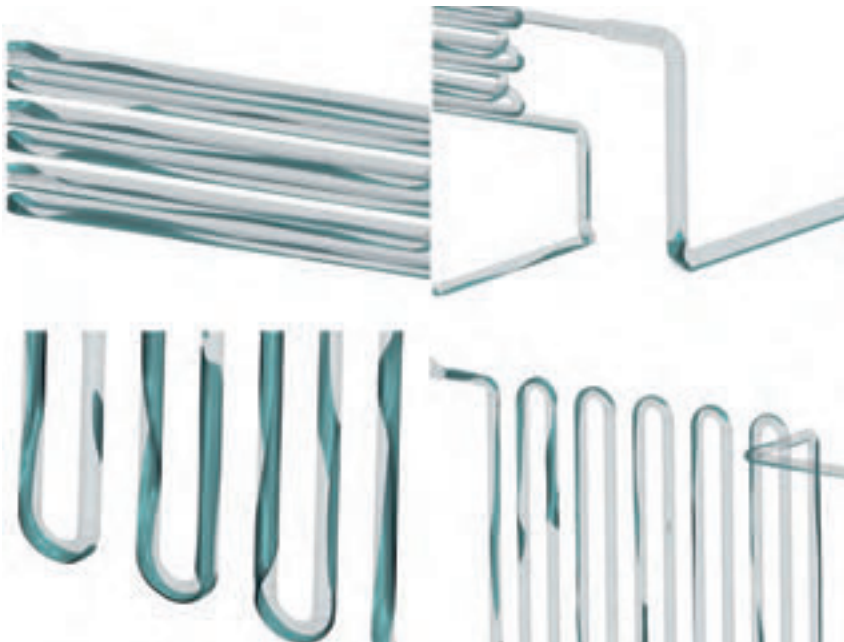


FIGURE 6: CFD calculated flow of liquid in the pipes, showing heavy slugging



FIGURE 7: CFD calculated displacement of flow pipe, accurately predicting locations of heaviest vibrations

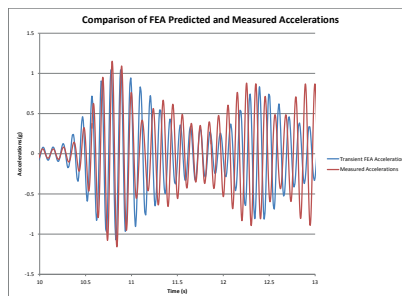


FIGURE 8: Comparison of FEA-predicted accelerations and measured accelerations

Porter McGuffie was able to provide its customer with a detailed explanation of why their heater was exhibiting such high amplitude vibrations. The two-phase flow in the radiant section led to significant

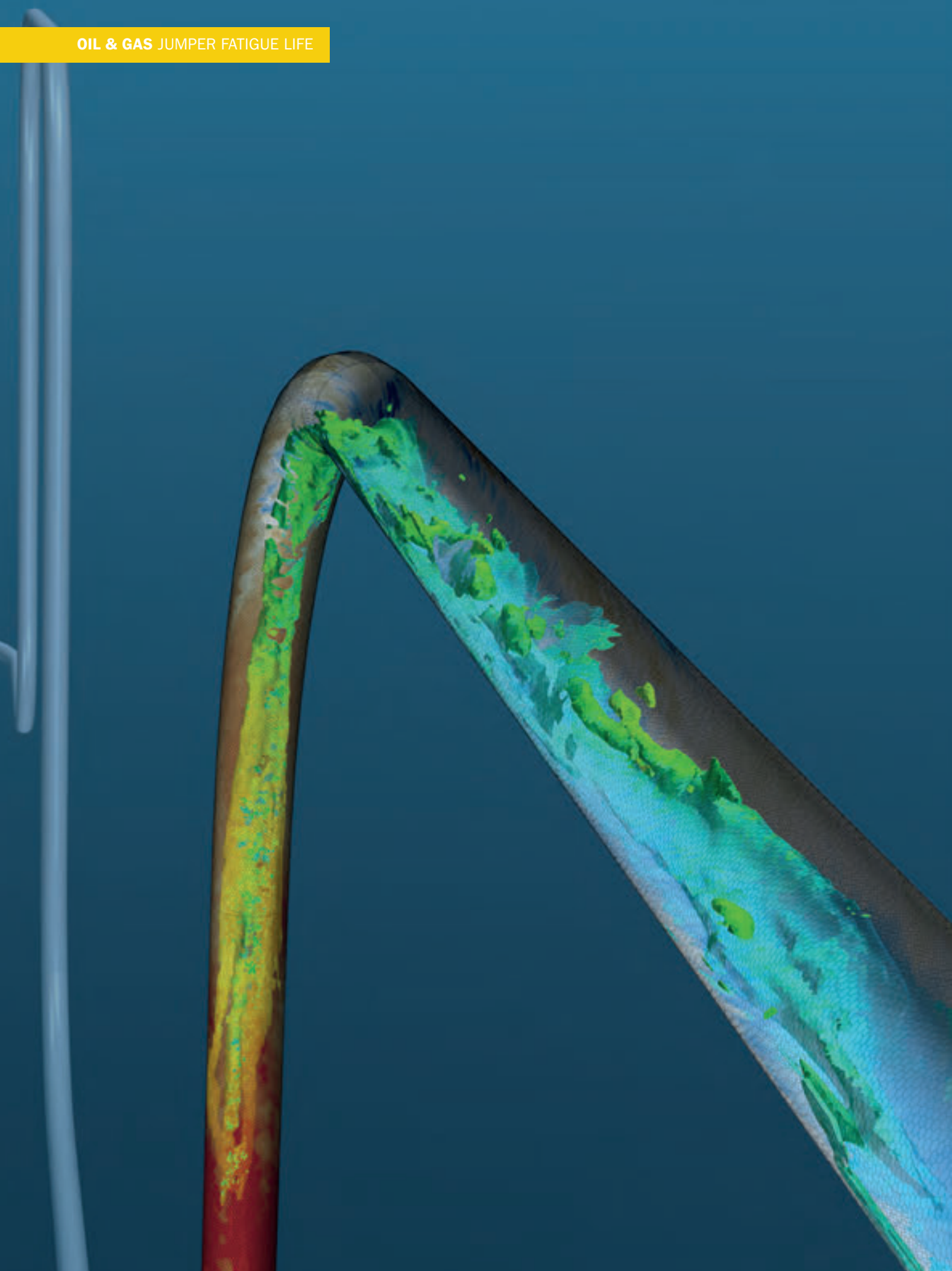
pressure variation in the radiative section of the simulation, which caused mass flow variations in the H2 line. The pressure variation qualitatively agreed with the hydrogen flow oscillation frequency

measured on site. The force magnitudes predicted in the CFD simulation and the structural vibration analysis also lined up well with the measured data. Further experimentation and simulation have shown that while the amplitude of the flow pulsations vary with overall throughput, the frequency of the piping vibration remains constant. Again, this is in good agreement with the measured data. Thus, it is clear that a resonant mode of the piping was being excited.

PMI was able to turn around the measurements and simulations within a few weeks' time using STAR-CCM+. The use of Eulerian Multiphase Model with S-gamma submodel allowed the analysis of a large two-phase system that took approximately one week to run using a few million cells on twelve processor cores. The more traditional Volume of Fluid model method, using the correct grid density, would have required more than 50 billion cells and weeks of run-time per simulation.

Mike Porter, principal engineer at PMI, stated that without simulation with STAR-CCM+, there would have been no way to see what the fluid flow was doing within the pipes, and it would have taken many months of analysis and research to diagnose and correct the problem. All in all, Porter McGuffie was able to do the complete testing, analysis and create a recommended redesign within the span of a few weeks, not the several months' turn-around time common with more traditional methods and tools.

With PMI's suggested changes scheduled to be incorporated this October, it is nearly certain that the subject heater will be able to operate at full capacity. Porter McGuffie will then maintain its record of a 100% success rate for their analysis and design solutions, a claim that most engineering companies and departments within much larger corporations can only envy.



# USING SIMULATION TO ASSESS THE FATIGUE LIFE OF SUBSEA JUMPERS

OLEG VORONKOV, ALAN MUELLER, ALEX READ & SABINE A. GOODWIN  
CD-adapco™

## INTRODUCTION

Structural vibrations of subsea piping systems stem from either external currents passing around the structure (Vortex-Induced Vibration or VIV) or from transient flows of mixtures inside the pipes (Flow-Induced Vibration or FIV). These vibrations compromise the structural integrity of subsea systems and in extreme circumstances can reduce their fatigue life from years down to weeks.

The transient multiphase flow inside subsea piping is complex and gaining insight through physical subsea measurements is expensive and challenging. As a result of this, the industry has relied heavily on simple analysis methods to predict the effects of FIV. These approaches tend to be overly conservative, making the decision process concerning structural integrity of subsea piping systems difficult. This has had a significant economic impact on the Oil and Gas Industry as failure is not an option and thus expensive 'over-design' is common practice for reducing risk, with a price tag of up to hundreds of millions of dollars.

CD-adapco™ is working closely with industry to develop a set of best practices for modeling FIV. This work describes

an example of how Computational Fluid Dynamics (CFD) is being used in complement to other analysis methods by providing higher fidelity information that is otherwise unattainable, to reduce risk, reduce over-design, and increase profit margins.

## TACKLING THE PROBLEM OF FIV WITH SIMULATION

CD-adapco™ is a member of a Joint Industry Programme (JIP) run by the international energy consultancy Xodus Group and the Dutch innovation company TNO to establish and validate best practices for FIV. The ultimate goal of the JIP is to contribute to industrial capability of determining the likelihood of piping fatigue due to excitation from multiphase flow. Potential benefits could include improving screening, simulation and prediction models through the use of CFD and empirical methods. [1]

This work is a demonstration example of slug flow in a jumper, modeled with two-way fully-coupled Fluid Structure Interaction (FSI). The simulations were carried out on a generic geometry of a jumper [3], to make it publicly available to CD-adapco™'s customers.

The multiphase flow encountered in

jumpers covers the complete flow map including slug, annular, dispersed, stratified and wavy flow. For simulation of FIV, it is critical that the movement of the interfaces between different phases in the pipes is accurately captured and thus a multiphase model is required. The Volume of Fluid (VOF) multiphase model available in STAR-CCM+® was used to simulate the transient behavior of the mixture and the development of slugs in the jumper. VOF uses the Eulerian framework and is a practical approach for applications containing two or more immiscible fluid phases, where each phase constitutes a large structure in the system.

A key objective of this work was to address the need to understand the role FSI plays in the fatigue life of subsea structures. The dynamic open architecture in STAR-CCM+® makes it well-suited to help provide answers because it seamlessly enables FSI simulations ranging from one-way coupling of either FIV or VIV all the way up to two-way coupling, including both the internal mixture and external flow of the pipes.

The focus of the simulation work presented here is on FIV using co-simulation (fully-coupled two-way interaction), where STAR-CCM+®

The dynamic open architecture in STAR-CCM+® seamlessly enables FSI simulations ranging from one-way coupling of either FIV or VIV all the way up to two-way coupling, including both the internal mixture and external flow of the pipes.

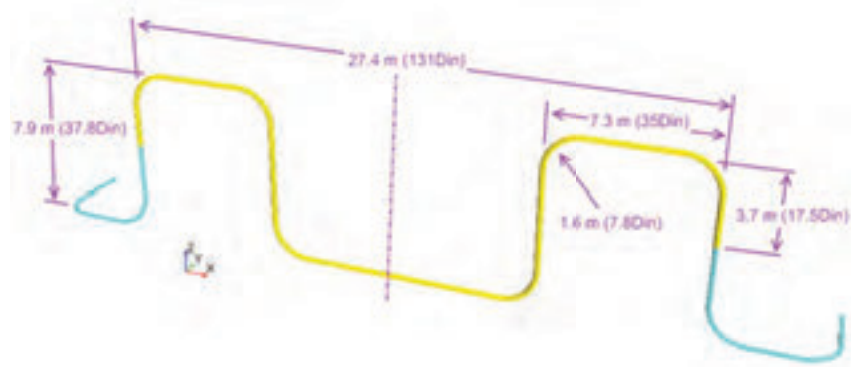


**FIGURE 1:** Jumper geometry in the shape of an M with a circular cross section for FSI co-simulation

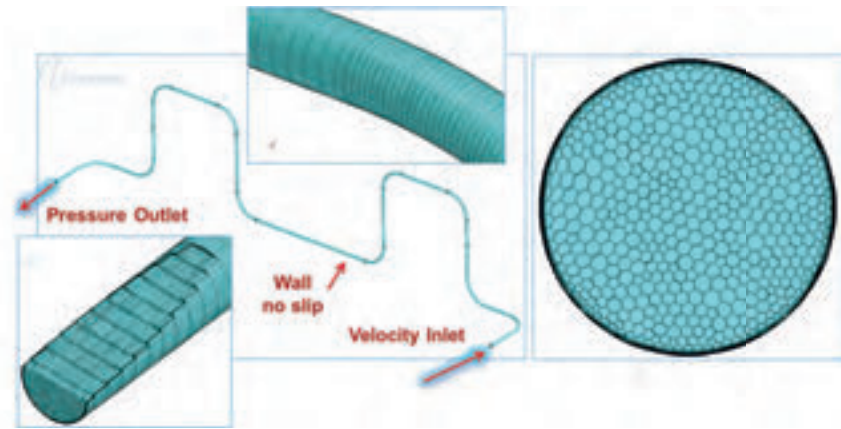


**FIGURE 2:** VOF mesh generated using the generalized cylinder mesher in STAR-CCM+®

handles the multiphase flow and Abaqus FEA (SIMULIA) is used for predicting the dynamic structural deformations of the jumper. The two domains are interconnected using the SIMULIA Co-Simulation Engine (CSE). Although this method is computationally intensive, it demonstrates a more general approach to the end user because it can be deployed for predicting the behavior of complex systems including non-linear structures and highly complicated geometries. Alternatively, because the specific generic jumper geometry for this work is geometrically and structurally relatively uncomplicated (e.g. there is no contact with the sea floor), this particular simulation could also be performed with a simpler approach by, for example, modeling the jumper with beam elements, using 1-way coupling or completely performing the FSI problem in STAR-CCM+® using its structural stress analysis model.

In addition to direct co-simulation coupling with Abaqus, STAR-CCM+® also offers users the ability to customize their FSI simulations by leveraging the power of JAVA to allow them to easily integrate their own legacy codes or their FEA software of choice for FSI simulations.

### COMPUTATIONAL JUMPER GEOMETRY

The generic jumper geometry (figure 1) in this study is made of steel, with a circular cross section and a traditional M-shape [3]. The jumper is clamped on both ends and the multiphase flow passing through the pipes consists of a 50-50% volume mixture of air and water (defined as stratified flow with water on the bottom and air on top at the inlet boundary). Fluid domain (cyan in figure 1) is extended beyond the deformable structure (yellow in figure 1) to avoid influence of boundary conditions on the flow inside the jumper.

For the VOF mesh, the generalized cylinder mesher available in STAR-CCM+® was used in conjunction with the polyhedral volume mesher. This approach works well for this particular application because the geometry consists of cylindrical sections, and the direction of the flow is parallel to the vessel wall. Using extruded prismatic cells reduces the overall cell count, ensures orthogonal cells and improves the rate of convergence. The final VOF mesh has ~4 million polyhedral cells and is depicted in figure 2.

The Abaqus finite element model for the co-simulation consists of 21,000 four-node shell elements and is shown in figure 3. First, a stand-alone structural modal analysis was performed to characterize the dynamic behavior of the structure. The stiffness in each coordinate direction was computed by applying a load to the pipe to get the resulting force-displacement relationship and an eigenvalue analysis was done to obtain the natural frequencies of the jumper. For this case, an equivalent mass representing both the mass from the flow inside the pipes (assuming a uniform mixture of air and water) and the added mass resulting from the displacement of the water surrounding the pipe was used. This added mass coefficient was taken from literature [4], [5]. Figure 4 shows the first four natural modes of the jumper and table 1 lists the frequencies of each mode.

### FIV ANALYSIS WITH STAR-CCM+® AND ABAQUS FEA

STAR-CCM+® was first executed in a stand-alone mode, making the assumption of a rigid and fixed structure.

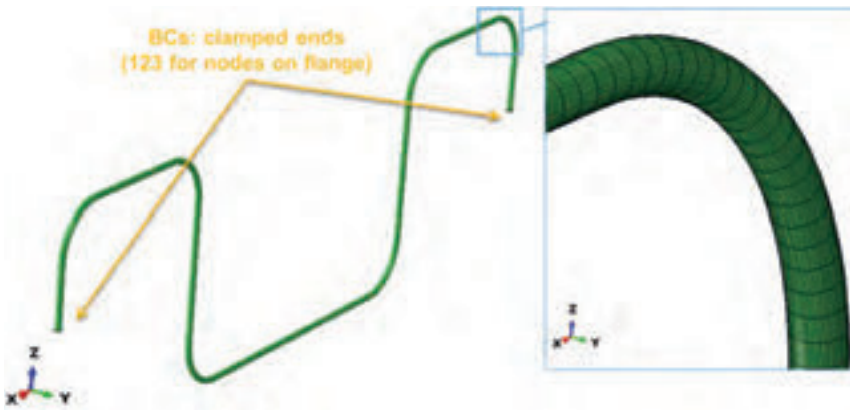


FIGURE 3: FEM model used for co-simulation has 21k 4-node shell elements

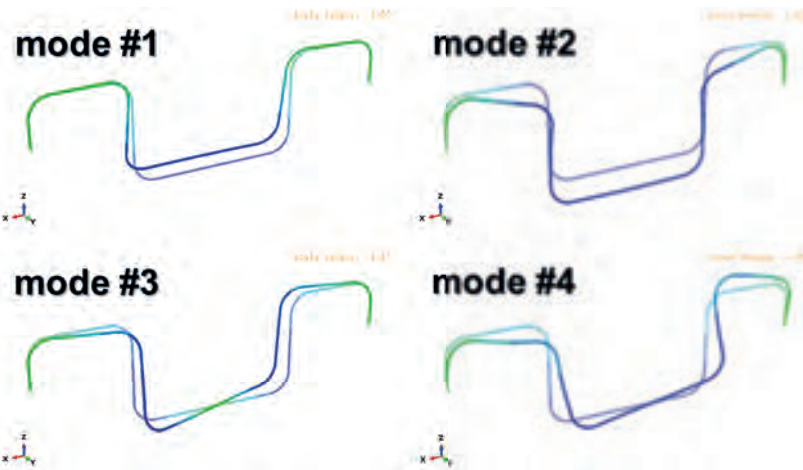


FIGURE 4: First four natural modes of the jumper

EM #	1	2	3	4	5	6	7	8
f, Hz	0.59	1.30	1.70	1.77	2.06	2.07	2.82	6.07

TABLE 1: Natural frequencies for each mode in the jumper.

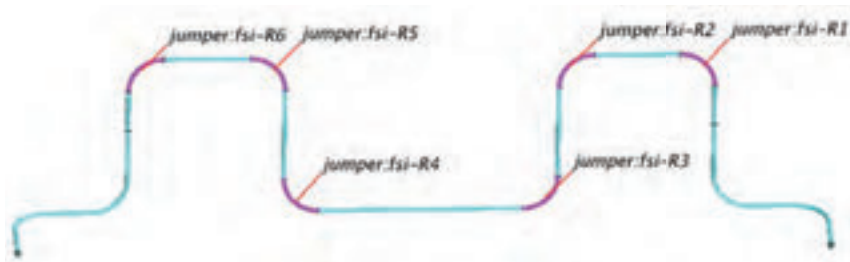


FIGURE 5: Bends in jumper are the primary locations where loading occurs.

These rigid results were used to gain a better understanding of the internal forces due to the mixture in the system and served as the initial solution for the two-way coupled co-simulation.

For co-simulation, on the VOF side, the second order implicit segregated solver using the k-omega SST turbulence model was run unsteady, with a time step providing a Convective Courant Number

value of ~0.5 on most of the phase separation surface. This corresponds to 1/100<sup>th</sup> of the period of the 4<sup>th</sup> natural mode and 1/63<sup>th</sup> of the period of the 7<sup>th</sup> natural mode of the structure and ~1/150<sup>th</sup> of time for the mixture to travel along pipe bend. Gravity was included in the simulation and the inlet velocity was set to 3 m/s, defined as 50-50% stratified flow with water on the bottom and air on top.

The undeformed structure was used as the initial condition for the Abaqus runs. In addition to the added mass described above, the structural model also included a mass proportional damping to account for damping from the external water surrounding the pipes and some additional damping in the joints on jumper ends [5]. The value of the damping coefficient representing the mass proportional damping was obtained by running a fully two-way coupled simulation on a flexible round pipe placed in water. For all simulations, attention was focused on the first seven natural modes of the structure with their natural frequencies ranging from 0.59 to 2.82 Hz (table 1).

The bends in the jumper are the primary locations where significant loading occurs as a result of the large momentum from the change in direction of flow. Figure 6 shows the forces and their Fast Fourier Transform (FFT) on each of the bends depicted in figure 5. It is clear that the multiphase flow encountered by the bends is highly complex with a lot of identifiable peaks in frequency. This means that there are many transient pressure loadings that have the potential to give rise to changing stresses and oscillatory vibrations, thus affecting fatigue and lifetime of the jumper. The primary dominant frequencies observed in the FFT of the forces on the bends were low with time scales of up to ten seconds. These are due to the separation of the phases in the mixture (development of slugs) as it flows through the jumper. Although these frequencies are much lower than the natural modes of the structure, they are a critical component for predicting the fatigue life of the jumper.

Figure 7 visually depicts the water volume fraction for each of the sections in the jumper and shows the evolution of the slugs, starting with the formation of short slugs with an average of ~2 pipe diameters long in the first lift. As the mixture moves through the jumper and arrives at the fourth bend, longer slugs are forming and as they pass the second lift they have reached a length of ~12 pipe diameters long.

When taking a closer look at the dominant slug frequencies (see table 2), once again, the observation is made that the slugs have relatively large time scales with the first dominant frequency around 0.09 Hz. Because of this, each separate slug moving along the pipe produces kind of impulse loading resulting in structural vibrations mainly with structural natural frequencies. This can be seen from the

FFT of jumper displacements at controlled points (figure 8). In addition, one of the slug frequencies is observed to be close to the 1st fundamental mode of the system at 0.54 Hz (table 2).

**PREDICTION OF FATIGUE FAILURE**

Von Mises stresses and displacements for the system were computed and the largest tensile stresses were observed in the cantilevered section of the pipe that is clamped in the simulation and hooks into neighboring equipment in real-life scenarios (see figure 9). This location was thus identified as a prime candidate location for prediction of fatigue failure of the jumper because usually a weld is located at this place and it is subjected to tension at this point.

The time dependent behavior of the stress at this location and its FFT are shown in figure 10. A distinct peak with a dominant frequency occurs at 1.3 Hz and falls close to the frequency of second natural mode. But in addition to this, a low frequency response of 0.09 Hz is once again present, due to the transient motion of slugs in the jumper. Using the results of the stresses at this critical location as an input, the Rain Flow Counting technique was used to estimate the damage to the jumper from the presented portion of altering stress. The result, showing range in stress relative to the mean stress and number of cycles, are depicted in figure 11. The Palmgren-Miner rule, using the S-N curve [2] shown in figure 12, predicted a short fatigue life of only about 5.5 years with a fatigue design factor of 5. This is a good example that demonstrates the value of using high-fidelity simulation to assess fatigue life early in the design process: A potential structural vibration problem is identified up front and additional simulations can be performed at a low cost to redesign the jumper and mitigate the problem.

**CONCLUSION**

Flow induced vibration and its effect on fatigue life of a generic jumper was assessed using a two-way coupled FSI simulation with STAR-CCM+® and Abaqus FEA. Simulations were performed with the multiphase VOF model in STAR-CCM+® and were found to be very robust with minimal numerical problems. The dominant frequencies from the slug formation in this particular jumper geometry were much lower than the natural frequencies of the structure. This suggests that a coupling between the fluid and structure could be treated via a one-way coupling. However, for a one-way coupling, the

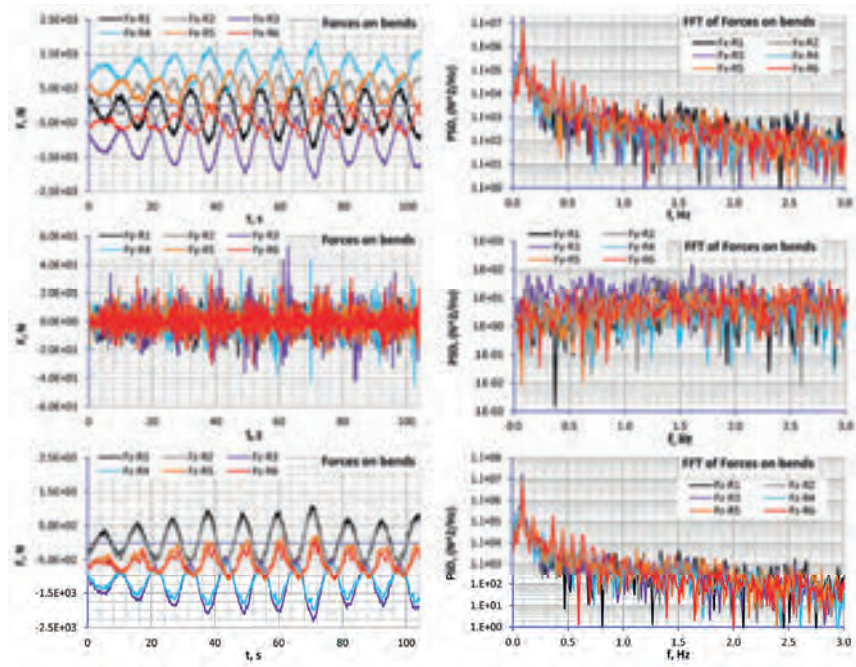


**FIGURE 6:** Forces and their FFT on the six bends defined in the jumper geometry

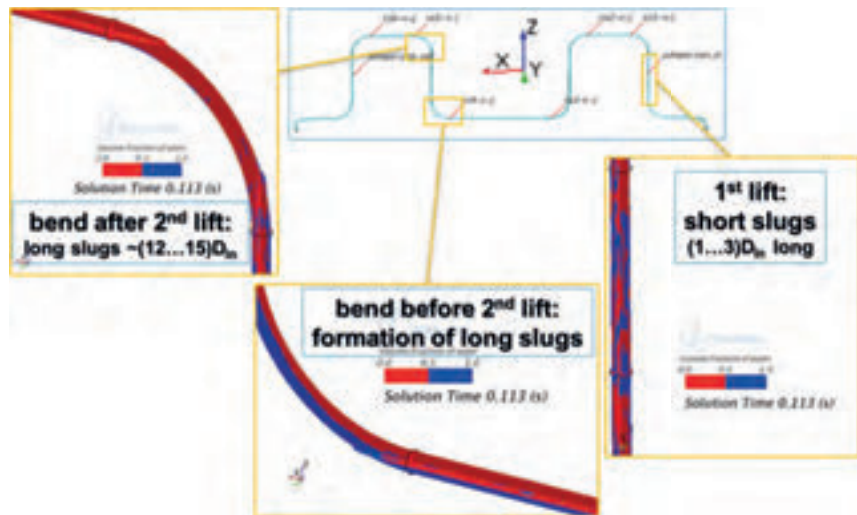


**FIGURE 7:** Slug formation as the mixture travels through the jumper

**Investment in more expensive simulation tools will be very beneficial in failure analysis prediction and prevention of subsea systems. Anticipation of structural integrity early in the design space is expected to help quantify and reduce the amount of conservatism currently used by the Oil and Gas Industry, keeping production flow rates as high as possible, thus increasing their profit margin.**

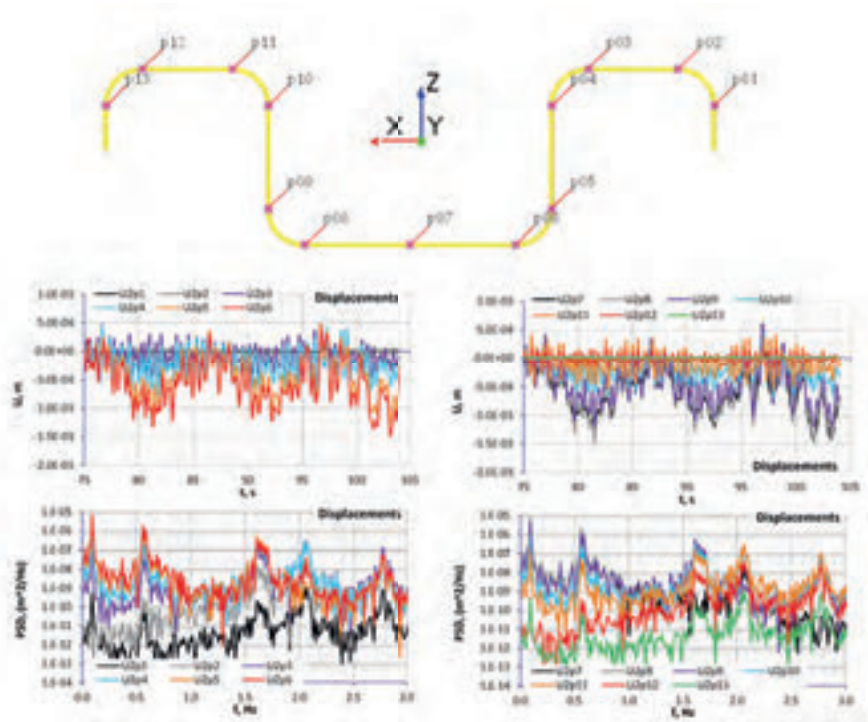


**FIGURE 8:** Monitored points (top), plots of Y-displacement as a function of time (middle) and the corresponding FFT (bottom) at each of the monitored points

1	2	3	4	5	6	
f, Hz	0.089	0.18	0.28	0.37	0.46	0.54

**TABLE 2:** Dominant slug frequencies in the mixture

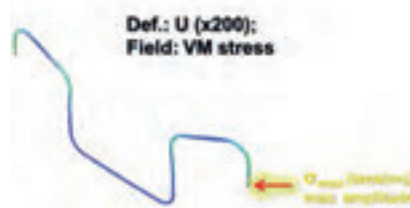


**FIGURE 9:** Location in jumper where the maximum tensile von Mises stresses occur

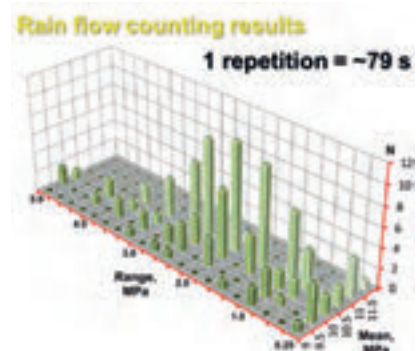


**FIGURE 11:** Fatigue life estimate using the Rain Flow Counting Method

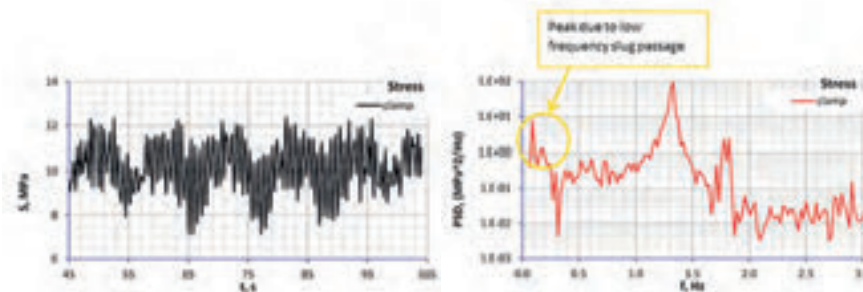


**FIGURE 10:** Time-dependent behavior and corresponding FFT of maximum tensile stress in the jumper

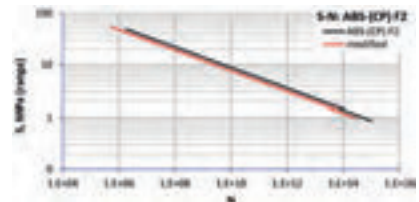
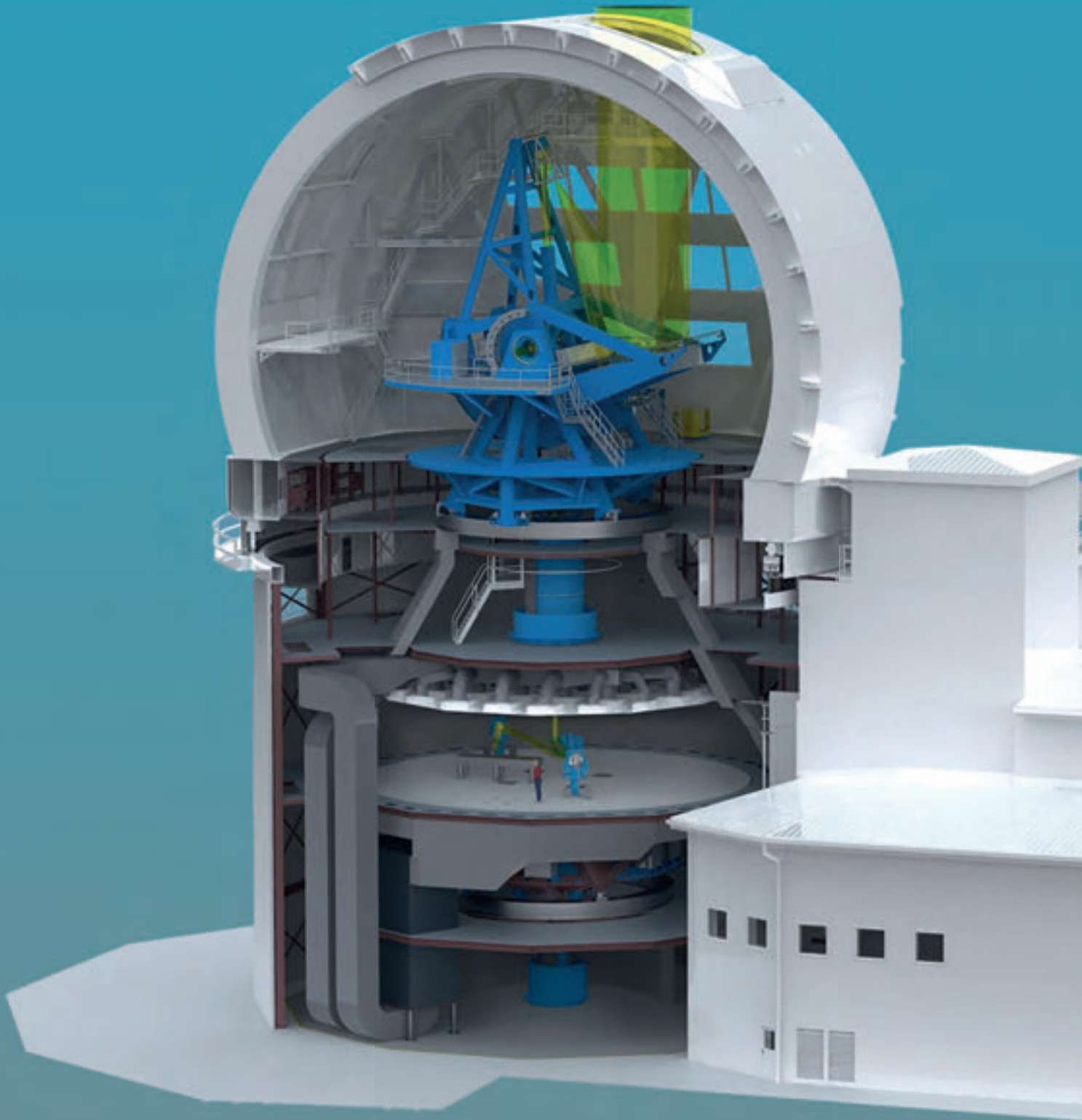


**FIGURE 12:** S-N curve used for fatigue life estimation [1]

**REFERENCES**

[1] <http://www.xodusgroup.com/press/press-releases.html>  
 [2] Guide for the fatigue assessment of offshore structures. American Bureau of Shipping, Houston, TX, USA. November 2010.  
 [3] L. Chica: Fluid Structure Interaction Analysis of Two-Phase Flow in an M-shaped Jumper. University of Houston, College of Technology, Mechanical Engineering Technology. STAR Global Conference 2012. January 28, 2012.  
 [4] J.P. Pontaza, B. Abuali, G.W. Brown, F.J. Smith: Flow-Induced Vibrations of Subsea Piping: A Screening Approach Based on Numerical Simulation. Shell International Exploration and Production Inc., Shell U.K. Limited. SPE 166661. 2013.  
 [5] J.P. Pontaza, R.G. Menon: Flow-Induced Vibrations of Subsea Jumpers due to Internal Multi-Phase Flow. Shell Projects & Technology. OMAE2011-50062.



# BLASTED BY THE SUN: THERMACORE COOLS THE WORLD'S LARGEST SOLAR TELESCOPE

**STEPHEN FERGUSON**  
CD-adapco™



**C**urrently under construction on the Pacific Island of Maui, the 41.5 m tall Daniel K. Inouye Solar Telescope (DKIST) will be the world's largest solar telescope. Once operational, the DKIST will be able to provide the sharpest views ever taken of the solar surface, which will allow scientists to learn even more about the sun and solar-terrestrial interactions. The DKIST will allow astronomers to resolve the extremely small, violently active, magnetic fields that control the temperature of the corona and the solar wind that produce flares and x-ray emissions, and help to improve prediction of the way these "space weather" phenomena influence the earth.

The telescope is currently being built atop the Haleakala volcano on the Pacific island of Maui, which was chosen from a list of 72 possible global locations after two years of monitoring daytime seeing conditions. Haleakala has the darkest, clearest skies, and its tropical location and elevation mean that the telescope sits above the turbulent inversion layer so there is little turbulence to blur its view or moisture to block the infrared spectrum.

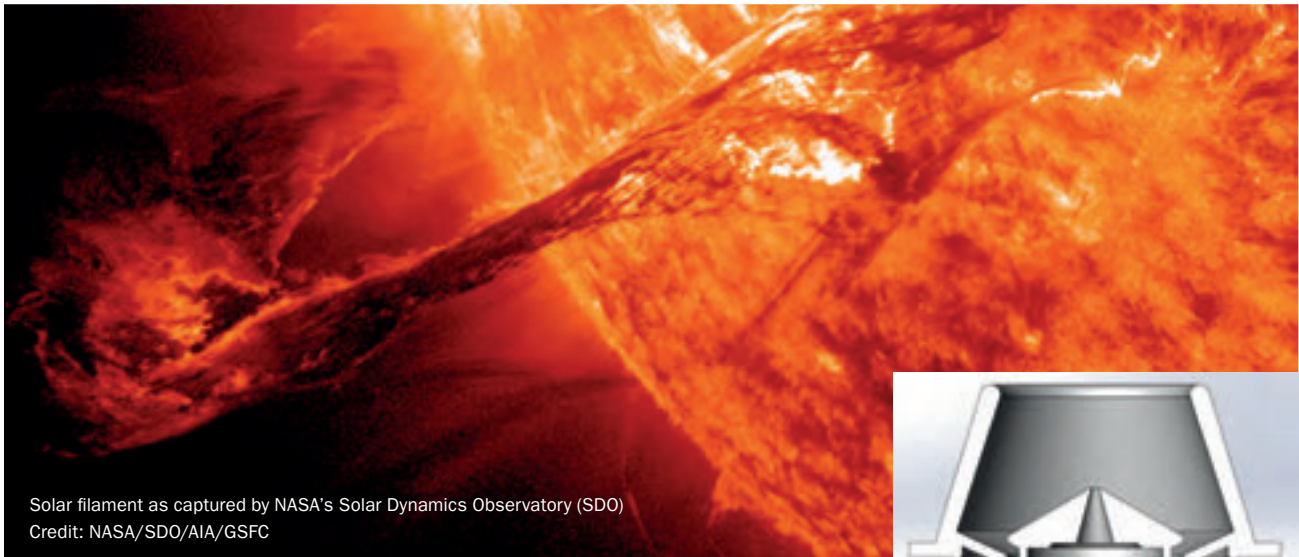
At the heart of the telescope is a huge 13ft (4m) primary mirror which, when combined with adaptive optics technology that reduces the amount of blurring from earth's atmosphere, produces images 33 times sharper than those of common

telescopes. The resolution of the DKIST is comparable with space telescopes, but at a much lower cost and with the benefit of greater accessibility. Unlike a space telescope, it will be relatively easy to upgrade the technology of the DKIST throughout its lifetime.

A solar telescope-specific problem is the heat generated by the tightly-focused sunlight. Unlike most large ground-based telescopes, which are used at nighttime to capture a small number of photons from distant astronomical bodies, the DKIST will spend its working life pointed directly at the sun, absorbing large quantities of focused light and heat energy.

A heat stop is an integral part of the design of solar telescopes, and represents one of its larger engineering challenges. It performs the role of what is called a "field stop" in a conventional telescope, limiting the field of vision to the area with minimal distortion. Located at the prime focus, the heat stop prevents unwanted solar disc light from heating and scattering on subsequent optics. In a solar telescope such as the DKIST, in addition to blocking light, the heat stop must also dissipate huge amounts of thermal energy.

For the upcoming DKIST, the heat load is 2.5 MW/m<sup>2</sup>, reducing the heat load on subsequent optics from an enormous



Solar filament as captured by NASA's Solar Dynamics Observatory (SDO)  
Credit: NASA/SDO/AIA/GSFC

12 kW to a minuscule 300 W (a reduction factor of 40). Designed by Thermacore, the heat stop assembly is actively cooled by an internal system of porous metal heat exchangers that dissipate approximately 1,700 W at peak operating load (see side box for a discussion of porous metal heat exchangers).

The heat stop must not only be able to survive this heat load (without cooling, the heat stop reflector would last only about 30 seconds before catastrophic failure), but also must remain cool enough not to induce any additional turbulence inside the telescope's dome.

One of the obstacles of ground-based astronomical observatories is a phenomenon known as "self-induced seeing". It consists of the degradation of image quality, mostly resulting in an increased blurring of objects and a reduction of contrast in long exposure images. This occurs when thermal and wind disturbances create fluctuating layers of refractive indices within the optical beam path. With this in mind, a small hot object in close proximity to the secondary mirror could have potentially disastrous consequences for the accuracy of the telescope. A key requirement for the system is that the surface temperature of the heat stop must never be more than 10°C higher than the temperature of the ambient air so as to prevent buoyancy-induced flows from creating turbulent disturbances that would result in "self-induced seeing".

As part of the design process, thermacore was required to demonstrate the efficacy and robustness of their heat stop cooling system across the full range of potential

operating conditions, as well as in some "failure mode" scenarios in which the failure of some other component had resulted in the telescope being aligned outside of its design range.

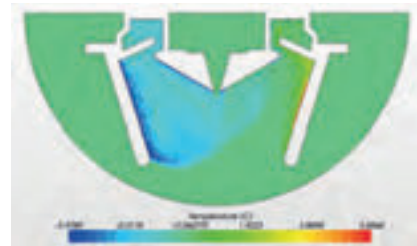
The surface temperatures (and generated flow around the heat stop) depend on a number of interacting physical phenomena. In simulating the heat stop assembly, the Thermacore engineers had to take into account multiphase flow within the porous metal heat exchangers, conjugate heat transfer through the heat stop assembly and the interior wick structure, and both natural convection and radiation heat transfer around the heat stop.

Although some of these configurations provided lower direct thermal loading, Thermacore engineers needed to demonstrate that asymmetries in thermal loading would not lead to local "hot spots" that might generate additional buoyancy-driven flow patterns (the potential source of a "self-induced seeing" problem). Using STAR-CCM+, the Thermacore engineers were not only able to fulfill the design criteria demonstrating that the surface temperature of the reflector could be kept below 10°C above ambient, but they also demonstrated that the criteria was sensible by visualizing the flow patterns generated within the enclosure as a result of natural convection.

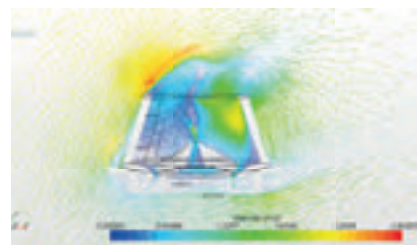
The Thermacore team also examined the influence of various atmospheric wind loading scenarios, predicting flow patterns and heat transfer across a range of possible flow orientations, demonstrating that surface temperatures and turbulence levels would not exceed design criteria.



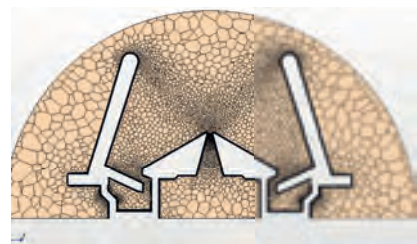
Located at the prime focus, the heat stop limits the field of vision of the telescope and absorbs large amounts of solar energy, preventing it from reaching subsequent optics.



The heat stop must dissipate 1,700 W at peak operating load, without ever allowing the surface temperature to rise by more than 10°C over ambient.

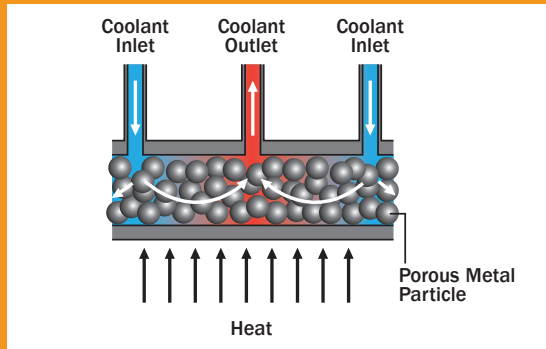


Limiting air disturbance, whether thermally generated or as a result of the wind, plays an important role in reducing "self-induced seeing".



A polyhedral mesh (including fine prism layers) of the fluid space around the heat stop

## ALL ABOUT POROUS METAL HEAT EXCHANGERS



The past decade has witnessed a significant growth in the number of applications for a new category of heat transfer device known as “porous metal heat exchangers”. These devices, when used in conjunction with a pumped single-phase coolant or a pumped gas, employ a porous layer of a thermally conductive medium beneath the heat transfer surface to effect efficient heat transfer. In this device, convective heat transfer to the selected coolant combines with the “fin effect” produced by the large surface area of the conductive porous structure to produce efficient heat transfer. A porous media heat exchanger can be used to dissipate very large heat fluxes, such as those encountered in this solar telescope, or can be used to provide very efficient heat transfer at much lower heat fluxes.

The increased surface area, however, is obtained at the expense of increased flow resistance or pressure drop. To overcome the constricted flow paths, multiple closely-spaced inlets and outlets are used. For example, a section through the wall of a porous metal heat exchanger is illustrated schematically above. In a scale drawing, the circles, which represent grains of metal powder, would be many times smaller than shown. The pore sizes are sufficiently small to prevent a flow “short-circuit” near the walls. The thickness of the porous structure depicted below is typically on the order of 0.020-0.050mm.

A significant effort has been made in recent years to improve the fundamental understanding of convective forced flow heat transfer in porous metal heat exchangers, which has resulted in improved understanding of governing principles, and has thus opened new applications for these devices such as cooling the DKIST solar telescope.

## ABOUT THERMACORE

Founded in 1970, Thermacore specializes in the custom design, development, and manufacturing of innovative, high performance thermal management and material solutions. Thermacore’s thermal management solutions can be found at both the system and component levels for a variety of OEM applications in the Military/Aerospace, Computer, Communications, Industrial, Government, and Medical/Test Equipment markets. With intellectual property (over 100 patents), trade secrets and professional staff (over 50 engineers), Thermacore applies this know-how to solve complex thermal problems for their customers and help to enable their customers’ products.

Thermacore has the industry’s broadest collection of thermal management technologies, products, and services, which include: k-Core encapsulated Annealed Pyrolytic Graphite (APG) based solid conduction heat spreader assemblies and thermal straps (all metal and k-Core based); passive two-phase devices such as heat pipe assemblies, vapor chamber assemblies, thermal ground planes, loop heat pipes, extreme temperature heat pipes, CCHP and VCHP Spacecraft heat pipes, and more; liquid cooled cold plates; aluminum vacuum brazed assemblies, cold plates, heat exchangers, chassis; pumped single and two-phase liquid systems; Intelligent Thermal Management Systems (ITMS); rugged liquid cooling systems (rLCS™); and enclosure heat exchangers. Other unique capabilities include the ability to develop custom refractory metal alloys, cryomilled aluminum and magnesium, and material characterization and testing services.

Thermacore brings unparalleled engineering design expertise and thermal management solution performance, quality, and reliability to help enable our customer’s products and services. Thermacore employs more than 175 employees at six facilities located in the United States (Lancaster, Pennsylvania; Langhorne, PA; Ronkonkoma, NY; Pittsburgh, PA) and the United Kingdom (Ashington, Northumberland). Thermacore facilities are certified to the AS9100, ISO 9001 and ISO 14001 standards.

For information about Thermacore, visit [www.thermacore.com](http://www.thermacore.com).



# FROM GOB TO BOTTLE: BOTTERO SIMULATES THE COMPLETE GLASS FORMING PROCESS

**SIMONE FERRARI**  
Bottero S.p.A.

## INTRODUCTION

**G**lass container production is generally not an easy process to operate and companies often need to invest a significant amount of time and money to ensure they deliver products with appropriate quality. Glass is indeed a material that exhibits an extremely complex behavior often difficult to predict during manufacturing and, until now, the tuning of the production parameters has been completely bound to the operator's experience.

To overcome this sticky situation, Bottero, a process-oriented company operating worldwide in the glass machinery field, has developed a simulation-based methodology in cooperation with university laboratories and production experts. The aim of this work is to provide the glass plants with the necessary support for manufacturing of tools to ultimately achieve a drastic reduction in time required for starting up a process.

Computer simulations are not only useful to gain a better insight and assist in designing optimal bottle shapes, they also offer a good alternative to time-consuming and expensive trial and error procedures commonly encountered by

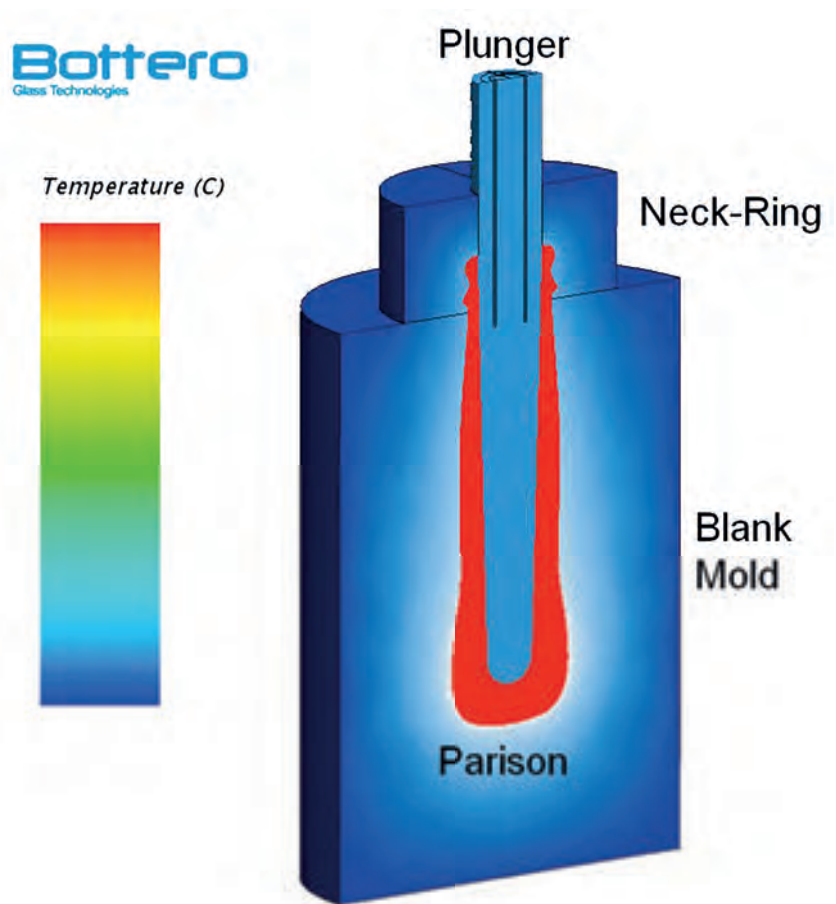


**FIGURE 1:** Three dimensional temperature distribution of the parison as it is created in the blank mold

factories. Representative numerical simulations can help minimize unwanted variations in wall thickness of containers and reduce their weight while maintaining their strength. Simulations also are extremely valuable in optimizing cooling conditions and increasing the production speed. All this has the potential to significantly decrease the cost of the glass manufacturing process.

### THE GLASS CONTAINER FORMING PROCESS

During the process, the container is first formed into an intermediate shape, called the “parison”, and then blown into its final shape. Depending on the different ways of forming the parison, two glass processes exist: the “blow & blow”, where the parison is formed using compressed air, or the “press & blow”, where the parison is mechanically formed with the use of a plunger. Here, the “press & blow” process has been studied and simulated.

When the molten glass leaves the furnace, its temperature is over 1400°C as it goes through the foreheart and then the feeder and is cut into uniform gobs of glass by a shearing and distribution system. After this, each gob is sent to an individual section forming machine where the temperature drops below 1200°C, and the gobs are forced to take the mold shape. The forming machine consists of two sets of molds called the “blank” and “blow” mold.

First, in the blank mold, the gob drops from above and is pressed into the mold shape, forming a thick-walled pre-form or parison. This parison is then removed by a robotic arm from the blank mold, turned upside down and transferred to the second (blow) mold. At this moment, the pre-form starts to stretch towards the bottom of the mold due to gravity. Finally, pressurized air is injected and a vacuum is created to inflate the parison into the final bottle shape. The container is then transferred to an annealing oven where reheating removes the stress produced during forming. After this, the container is cooled under controlled conditions and the process is complete.

### THE NEED OF SIMULATIONS FOR GLASS FORMING

The glass forming process involves high temperatures, and it is extremely sensitive to changes in machine timing, glass composition and environmental conditions. As it is nearly impossible to physically visualize what really happens inside the molds during the different

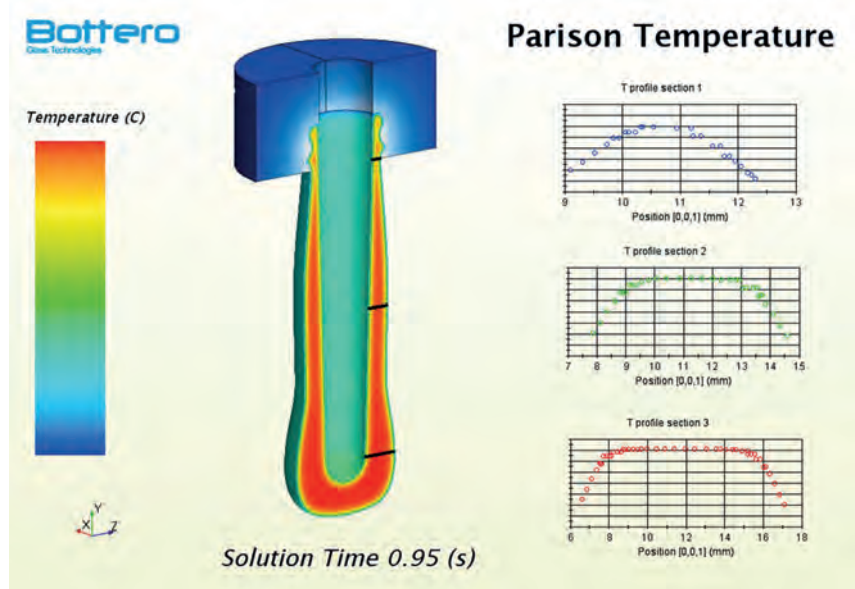


FIGURE 2: Detailed 3D temperature model of the parison, showing realistic vertical temperature trends

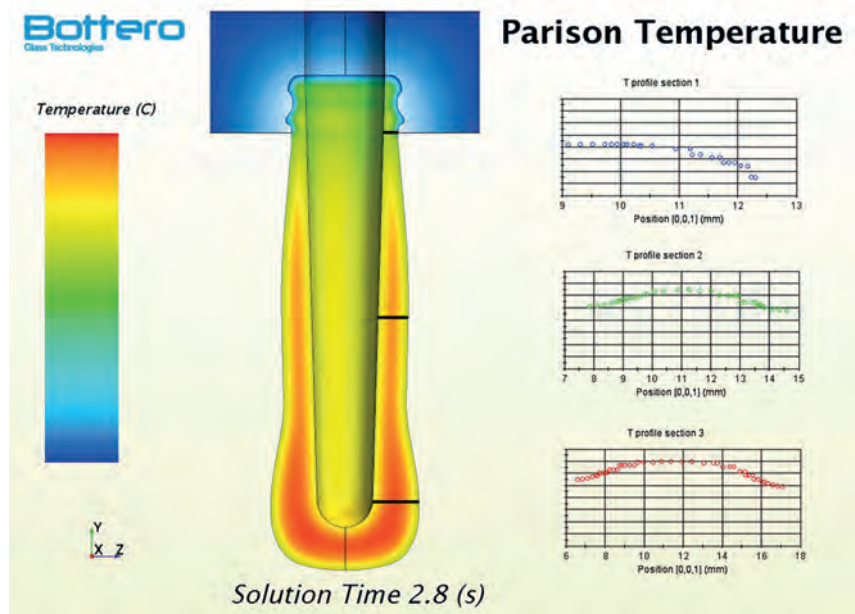


FIGURE 3: Parison temperature during reheating showing temperature redistribution

phases, numerical simulation is the only tool available to help better understand the details of the physics as they occur during the process.

In this work, the results of the simulation are validated experimentally by comparing infrared surface temperature measurements of both glass and equipment and inspecting the final container, the glass distribution (wall thickness) and the presence of possible defects.

In building the simulation methodology, close attention was paid to ensure that the most realistic model possible was used. This means that approximations in the simulations were limited and that the glass forming process was modeled as a tightly coupled thermo-fluid-dynamic process.

In the process, the hot glass yields heat to the molds through conduction and radiation and the glass is only partially emitting/absorbing the infrared light.

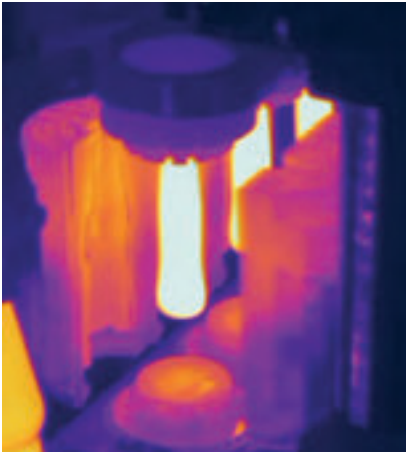


FIGURE 4: Experimental tests were conducted on the glass and confirmed a good correlation with simulations

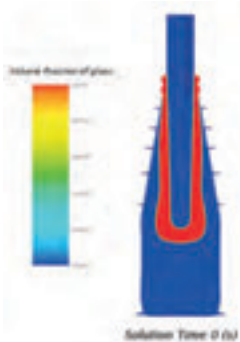


FIGURE 5: Volume fraction of glass in the dynamic model of the parison for simulating shape changes

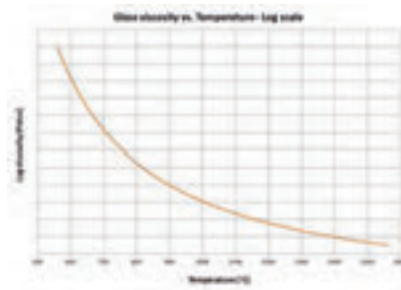


FIGURE 6: Variation of glass viscosity with temperature during the glass forming process

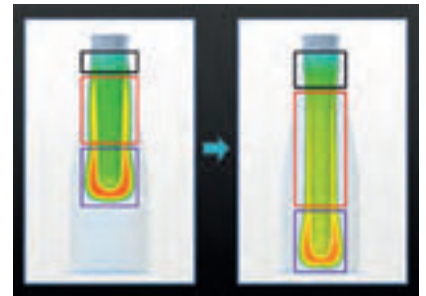


FIGURE 7: Simulation with STAR-CCM+® showing the shape change of the parison in the blow mold

Additionally, a heat exchange also occurs between glass and environment through convection and radiation. These heat exchange interfaces are geometrically complex and drastically change in time during the shaping of the bottle.

**THE MODELING METHODOLOGY**

STAR-CCM+® has made it possible to simulate the complete physical system of this production cycle, starting from a hot glass gob all the way up to the creation of the finished bottle.

A super-computing facility located in Cuneo, Italy (with 25 servers available that operate concurrently on HPC clusters with over 450 cores) facilitated CFD simulations with a very fine volume mesh, resulting in a large number of elements and ensuring a great space resolution to accurately capture the forming process.

The first step in developing the process was to perform unsteady simulations to obtain the three dimensional temperature distribution of the parison created by pressing the glass gob into the blank

mold (figure 1). The numerical model was initialized using the experimental conditions (such as temperature profiles), included all the details of the equipment and solved for both Discrete Ordinate Model (DOM) radiation and conduction.

The contact heat transfer coefficient at the interface between glass and cast iron is not only function of temperature, it also depends on many other parameters (e.g. time, pressure, mold roughness, presence of lubricants, etc.) thus it cannot be considered to be an ideal coefficient. For the simulations, the heat transfer coefficient used was determined by experiment.

The transient simulation led to a detailed 3D temperature model of the parison, and showed realistic temperature trends as expected: the glass was hotter where the parison wall was thicker. This typical vertical temperature trend is required to form a good final product and can be very tricky to control in experiments. As expected, because the glass viscosity highly depends on its temperature, the cold neck zone behaved as solid glass while the hot bottom of the parison was

still soft and easy to work with. A similar approach was used to simulate the reheating of the parison, when the mold opens and the parison temperature redistributes along the thickness for a time period of about two seconds (figure 3).

Simulations with STAR-CCM+® were useful not only for calculating the complete volume temperature (surface and internal) of the parison but also for better understanding of the available thermo-infrared measurements of glass and molds as these give information only on the surface and not on the inner part of the parison. Experimental tests of the glass have been conducted (figure 4) to verify the simulation results, confirming good correlation between simulation and experimental data.

Next, a dynamic model of the parison for predicting the shape changes that occur in the blow mold was built, with the simulations starting from the initial temperature distribution obtained in the previous step. This is one of the most important steps in the glass forming process as it greatly affects the final

bottle shape. The Volume of Fluid (VOF) model in STAR-CCM+® was used to model both fluids in the simulation: glass (dense and viscous) and air that surrounds the parison (figure 5).

The VOF method allowed for accurately modeling the details of the glass and air flow, separated by a well-defined interface (free-surface) and solving for its position in a time-accurate manner at every time-step. Mechanical and thermal properties of the materials were taken into account, including viscosity, density, conductivity and specific heat. Additionally, since the viscosity of glass highly depends on temperature, and the temperature changes with time, the heat flux and temperature distribution in the simulation were solved simultaneously with the motion of the interface.

Using the experimental measurements of the specific glass viscosity as a function of temperature (figure 6) and the temperature profile obtained in the previous step, the mechanical behavior (shape change) of the parison was successfully simulated as it developed in the blow mold. The model consisted of the inner surface of the mold that corresponds to the final bottle shape. A pressure inflow where the air is injected was included on the top and several pressure outflows were present on the sides for creating the vacuum in the final step of the process.

For the first 2.2 seconds in the blow mold, the parison stretches down to the bottom solely due to gravity, so no air is injected. This process, also called stretching, is crucially important to get the right thickness of the bottle wall and it is extremely sensitive to the parison temperature, as it affects the viscosity of glass.

Looking at figure 7, simulations showed that starting from the top of the parison, in the neck region, the glass was cold so it resisted stretching even with a high gravity load from below present. Furthermore, it became clear that the central part of the parison was most responsible for stretching while the bottom (with the lowest gravity load) did not stretch even if glass was soft.

This physical process was successfully simulated thanks to the simultaneous prediction of both the dynamic and thermal features in the STAR-CCM+® model. This allowed for taking the temperature redistribution of the glass during reheating into account (and thus the local time-accurate viscosity change) while stretching occurred.

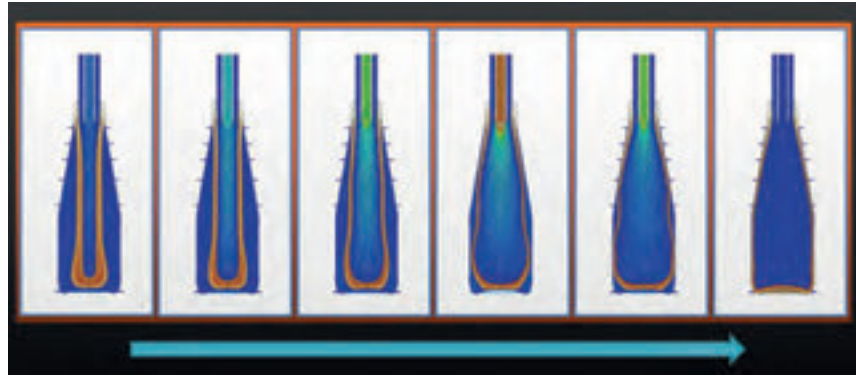


FIGURE 8: Complete simulation with STAR-CCM+® of the glass forming process, starting from the initial glass gob to the final shape

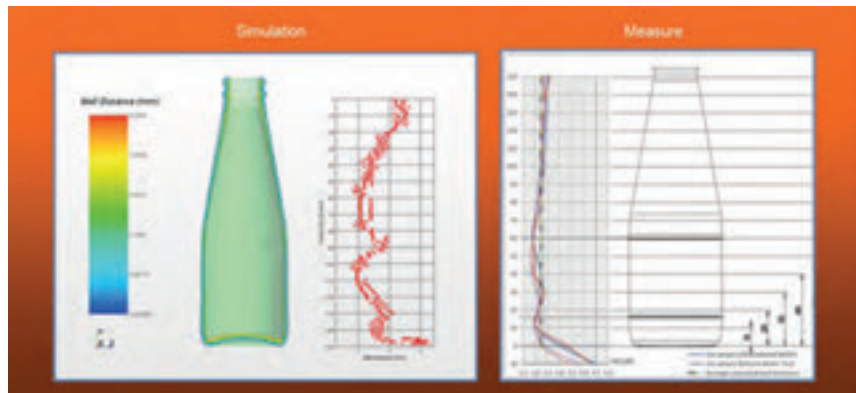


FIGURE 9: Validation of numerical simulations with STAR-CCM+® showing good comparison when comparing wall thickness to real bottles

During the final step in the simulation of the glass forming process, air was injected from the top and a vacuum was created from the side holes to blow the shape into the final bottle, as shown in figure 8. Even though this fast motion is not trivial and presents a challenge, the solver remained stable throughout the simulations.

The simulation results were validated by comparing the wall thickness of real bottles with the values obtained by simulating the process (figure 9). The correlation was very good, confirming that the numerical model is robust, especially considering it is the final result of many consecutive steps. This should come as no surprise since great care was taken to ensure that the numerical model represents a realistic process taking into account the glass (whose properties are strongly influenced by the temperature), the air, the molds and all the production equipment. The glass data has been experimentally measured in a specialized laboratory, and the experimental machine timing was also considered.

## CONCLUSIONS

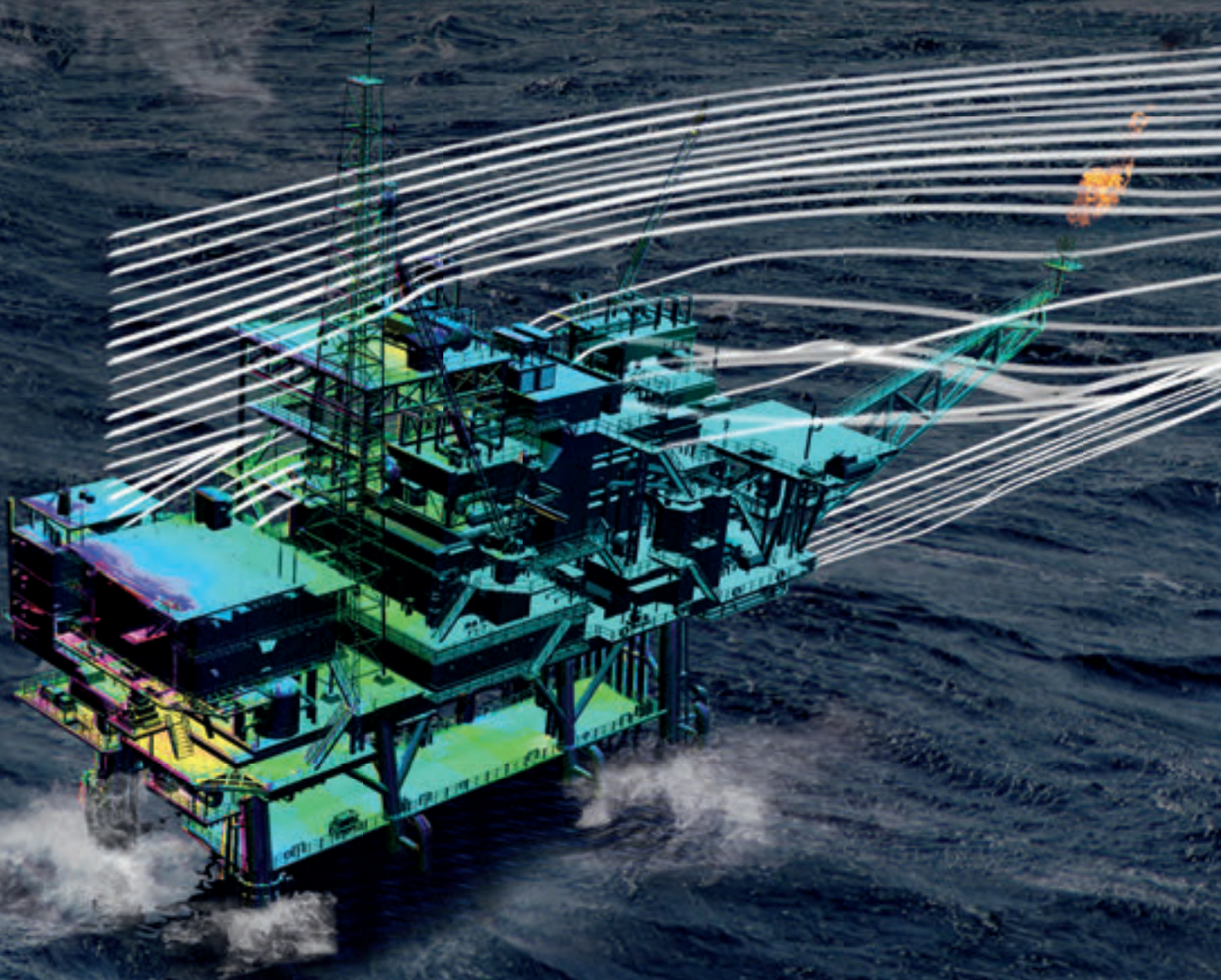
In this study, we presented the numerical implementation of the forming process of glass containers that were previously tested in realistic manufacturing conditions. Both the press and the blow steps of the forming process were modeled using STAR-CCM+®. A realistic non-uniform temperature distribution of the parison was calculated and the final shape of the end product was presented and analyzed.

All calculations were performed in three dimensions, which allows for studying parisons that are not rotationally symmetric, enabling one to assess how a certain imperfection in the initial parison develops over time. The current model is valid for viscous fluids, but it could be modified to, for instance, visco-elastic fluids.

The numerical simulations presented here are extremely valuable to the glass manufacturing industry as they help gain insight into the details of the physics, enable optimization of the production process and will ultimately lead to a significant reduction in manufacturing time and cost.

# SIMULATING SYSTEMS

FLOW – THERMAL – STRESS – EMAG – ELECTROCHEMISTRY – CASTING – OPTIMIZATION  
REACTING CHEMISTRY – VIBRO-ACOUSTICS – MULTIDISCIPLINARY CO-SIMULATION



✉ [info@cd-adapco.com](mailto:info@cd-adapco.com)  
🌐 [www.cd-adapco.com](http://www.cd-adapco.com)



STAR-CCM+





# KIMBERLY-CLARK PUTS THE ELASTIC IN VISCOELASTICITY!

**REZA R. REND & DWAYNE JACKSON**  
Kimberly-Clark Corporation

**SABINE A. GOODWIN**  
CD-adapco™



**FIGURE 1:** Spectrum of materials categorized based on their degree of fluidity or solidity

**M**any industrial products and processes involve the flow of fluids. Some of these fluids are Newtonian in nature as they are well-behaved and display a linear reaction to the external stresses, while others are non-Newtonian with a non-linear response. Non-Newtonian behavior, in turn, can be either purely viscous or viscoelastic. Many of the materials of interest at Kimberly-Clark (KC) are viscoelastic, and as consumer expectations increase and the market becomes more competitive, the need for better understanding of these complex materials has recently taken a front seat. To address this, KC has developed an add-on to STAR-CCM+® to extend its capability and enable modeling of

viscoelastic materials. This add-on was mainly designed for use in early stages of product/process design to improve the fidelity of the model while maintaining a quick turn-around time and at the same time utilizing the post-processing capabilities of STAR-CCM+® to better convey the results to the designers and managers.

## THE WORLD OF RHEOLOGY

Given time, almost every material flows, but for some materials, the time required to flow is so large that we must consider them as solids. We hear stories about glass panes being thicker at the bottom in centuries-old buildings because of fluid behavior of glass at very large

time scales. The reality is that the time required to see any visible change of thickness in a glass due to gravity at room temperatures is millions (and maybe billions) of years and not mere centuries! Forget the “flowing glass” myth and let us categorize materials in such a way that it only considers them to be a fluid if they can flow in a time scale meaningful to us as humans. This categorization can be seen in figure 1.

In engineering circles, we usually deal with either the left side (fluid mechanics) or the right side (solid mechanics) of this spectrum. At KC, however, many of the materials of interest are in the middle of the spectrum and require non-standard simulation tools to study. These

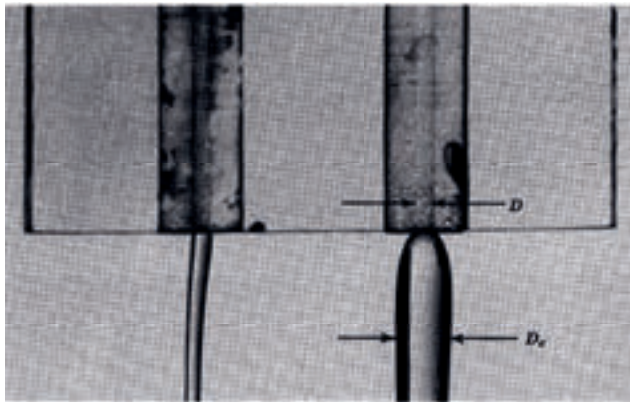


**FIGURE 2:** Diameter change for a Newtonian (left) and viscoelastic (right) fluid after extrusion from an orifice [1]

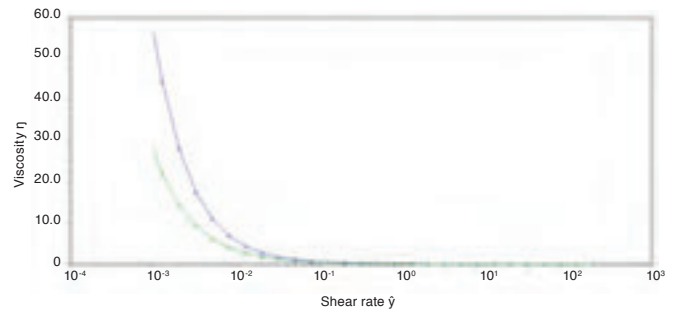


**FIGURE 3:** Variation in dimensionless viscosity for BM mess

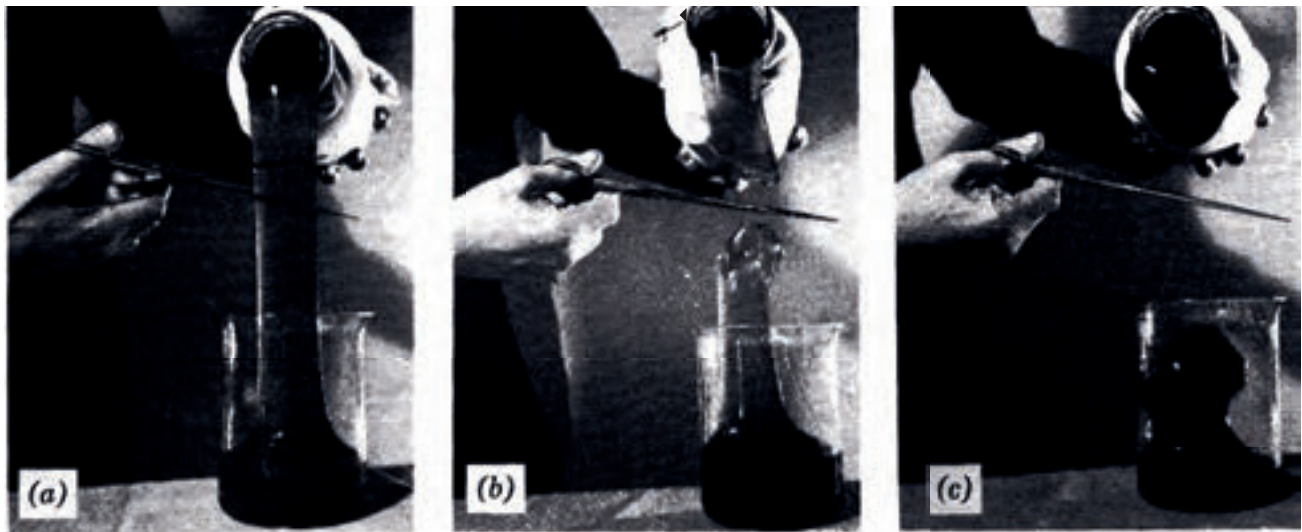


**FIGURE 4:** Spring-back or recoil observed in a viscoelastic fluid flow: (a) The fluid is being poured out of a beaker. (b) The flow is "cut" midstream. (c) The portion of fluid above the cut recoils back to the beaker. [1]

materials are fluid-like in that they flow under an external force, but are solid-like in that they display a memory and an affinity to return to their original shape. The following paragraphs describe two examples of the importance of taking into account the viscoelastic behavior of the material of interest.

The melt spinning process during polymer extrusion for polymeric materials is one example where the significance of viscoelastic behavior comes into play. Let's compare the behavior of a Newtonian fluid and a viscoelastic polymer in a region located downstream of the spinneret (figure 2 [1]): A Newtonian fluid expands only slightly (assuming inertial effects are negligible compared to viscous effects) while the polymer expands significantly and this expansion affects the final fiber diameter. Furthermore, if

we move even further downstream, as the fiber is being drawn or stretched, the quantity that resists this stretch is the fluid's extensional viscosity. For a Newtonian fluid, Trouton [2] has shown that the extensional viscosity is three times the shear viscosity. However, for a viscoelastic fluid, this ratio of three is only achieved at very low strain rates (which is not the case for fiber spinning).

Proper management of Bowel Movement (BM) mess and menstrual fluid (menses) is major functionality of some of KC's products where viscoelasticity also plays an important role. The foundation of most products handling BM mess or menses is a porous medium, and the shear strains encountered by these fluids are usually in the lower end of the curve displayed in figure 3. In this range, the change in viscosity is steep and has to be considered

in product design. Just to add more complexity to an already difficult problem, at low shear strain rates, both BM and menses display highly elastic behavior as well. This is a result of the presence of mucus and long-chained proteins as well as particulates in the fluid. Another important phenomenon to consider in handling viscoelastic materials is recoil. Consider a mass of fluid being pushed through a pore and then the force driving the fluid is suddenly removed. At this instance, if a portion of the fluid remains upstream of the pore, then the rest of fluid can recoil and can be pulled back out of the porous medium (see figure 4 [1])!

**MODELING VISCOELASTICITY**

We can, schematically, use springs and dampers to define linear elastic and viscous materials, respectively.

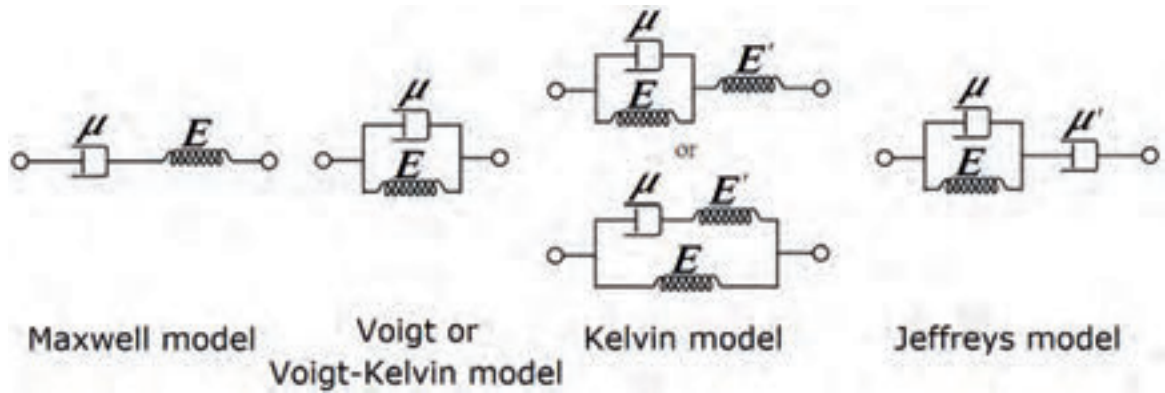


FIGURE 5: Some of the popular linear viscoelastic models schematically displayed as combination of springs and dampers

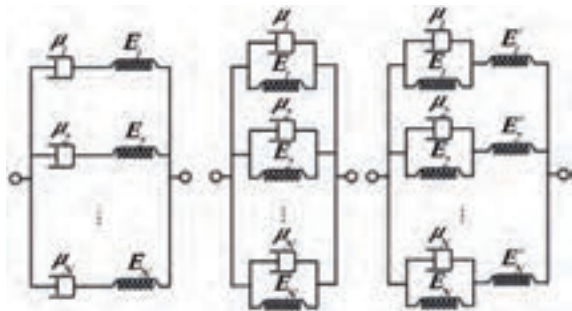


FIGURE 6: Schematic view of multi-mode generalizations of some of the models displayed in figure 5

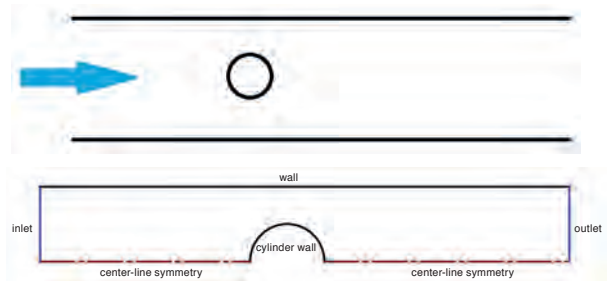


FIGURE 7: (Top) Schematic view of the geometry for a cylinder in cross flow in between two parallel plates and (bottom) imposed boundary conditions for the simulation

Linear viscoelastic materials can be represented by a combination of both springs and dampers and some of the popular models are shown in figure 5. These simple models, however, cannot predict the behavior of a real material well. A simple way of expanding these models is to combine them to create a multi-mode material model (figure 6). However, even these generalized models fail to predict many of the phenomena observed in real viscoelastic flows. To answer these shortcomings, multi-mode nonlinear models have to be utilized. Depending on the material, different models (constitutive equations) can be selected and the appropriate constitutive equation can be obtained from literature or by fitting a model to experimental data.

**IMPLEMENTATION IN STAR-CCM+®**

All rheological models available in STAR-CCM+® are only capable of modeling Newtonian or purely viscous non-Newtonian fluids. To accommodate simulation of viscoelastic materials, KC has developed an add-on (JAVA macro) to STAR-CCM+®. Although this implementation is not expected to result

in the highest possible accuracy (this would require direct modifications to the solver in STAR-CCM+® to better discretize the constitutive equations), the ease of use of this package with a very short learning curve and quick implementation was the motivation behind this work.

STAR-CCM+® uses a finite volume method to discretize the Navier-Stokes equations (which are the momentum balance equations for a Newtonian fluid). For comparison, the Navier-Stokes and Cauchy (generic momentum balance) equations in x-direction written in a Cartesian coordinate system are, respectively:

$$S = \left( \frac{\partial \tau_{xx}}{\partial x} + \frac{\partial \tau_{xy}}{\partial y} + \frac{\partial \tau_{xz}}{\partial z} \right) - \mu \left( \frac{\partial^2 u}{\partial x^2} + \frac{\partial^2 u}{\partial y^2} + \frac{\partial^2 u}{\partial z^2} \right) \quad (i)$$

$$\rho \left( \frac{\partial u}{\partial t} + u \frac{\partial u}{\partial x} + v \frac{\partial u}{\partial y} + w \frac{\partial u}{\partial z} \right) = - \frac{\partial p}{\partial x} + \mu \left( \frac{\partial^2 u}{\partial x^2} + \frac{\partial^2 u}{\partial y^2} + \frac{\partial^2 u}{\partial z^2} \right) + S \quad (ii)$$

As it can be seen, Eq. (i) and Eq. (ii) are very similar except for the second term on the right-hand side. STAR-CCM+® allows the user to define a source term (S) for each component of the momentum equation. Therefore, the following source term can be used to convert Eq. (i) to Eq.(ii):

$$\rho \left( \frac{\partial u}{\partial t} + u \frac{\partial u}{\partial x} + v \frac{\partial u}{\partial y} + w \frac{\partial u}{\partial z} \right) = - \frac{\partial p}{\partial x} + \left( \frac{\partial \tau_{xx}}{\partial x} + \frac{\partial \tau_{xy}}{\partial y} + \frac{\partial \tau_{xz}}{\partial z} \right) \quad (iii)$$

A similar approach can be used for the other components of the momentum equation. Doing so will introduce six more unknowns to the system of equations to be solved (six components of the symmetric stress tensor:  $\tau_{xx}$ ,  $\tau_{xy}$ ,  $\tau_{xz}$ ,  $\tau_{yx}$ ,  $\tau_{yz}$  and  $\tau_{zx}$ ). These unknowns follow the constitutive equation for the viscoelastic material; therefore STAR-CCM+® has to be instructed to solve these extra six equations. One of the means to do so is to utilize the capability of STAR-CCM+® to solve user-defined scalar transport equations. These equations are in the form of a generic partial differential equation with time derivative, convective and diffusive terms.

As the constitutive equations do not contain a diffusive term, they can be converted to the following form:

$$\frac{\partial \phi}{\partial t} + \mathbf{u} \cdot \nabla \phi = S_\phi$$

Where  $\phi$  denotes each of the stress tensor components and  $S_\phi$  is the source

term corresponding to each component of the constitutive equation containing any term other than the time derivative and convective term. This format is the same as one used by STAR-CCM+® in its scalar transport module. Therefore, the user has to only define the source terms for each component, and use these newly-defined scalar quantities to derive the source terms for each momentum equation component.

In order to simplify this process, a JAVA macro has been developed to define all the necessary user scalar transport equations, their source terms for numerous constitutive equations, their link to the momentum sources, and the required settings to define all these in a given STAR-CCM+® simulation.

The JAVA macro also allows for definition of multi-mode materials. This requires six extra scalar transport equations for each mode of the model. For example, if a simulation involves a polymer that can be modeled by a five-mode Oldroyd-B constitutive equation, the macro will define 30 scalar transport equations that need to be solved simultaneously with the momentum and continuity equations.

**BENCHMARK RESULTS**

A cylinder in cross flow in a parallel plate channel (figure 7) has been chosen as a benchmark because of availability of results in the literature [3]. It needs to be noted here that the method proposed can be applied to much more complex problems involving laminar incompressible flow.

This problem was solved for a single-mode Oldroyd-B fluid with very low-Reynolds-number laminar flow and varying Deborah Numbers (De) of up to 0.9 (De characterizes the fluidity of materials under specific flow condition).

When De is close to zero, the flow is considered Newtonian and there is no need to use a viscoelastic solver. However, this case was run viscoelastic anyway in order to assess the accuracy of the implementation of solving the additional equations. The velocity contour can be seen in figure 8 and accurately matches to the Newtonian result within 0.2%.

Next, De was set to 0.3 and the velocity contour of the resulting solution can be seen in figure 9. The results are similar to those in figure 8, but the maximum velocity is higher, and the flow is starting to look slightly asymmetric with respect to a

vertical plane passing through the axis of the cylinder.

The velocity contour for De=0.9 can be seen in figure 10. The higher maximum velocity and the asymmetry are now even

more pronounced. This asymmetry is somewhat similar to the case of medium-Reynolds number flow of a Newtonian fluid where inertial effects cause an asymmetry in the flow pattern because of flow separation downstream of the cylinder.

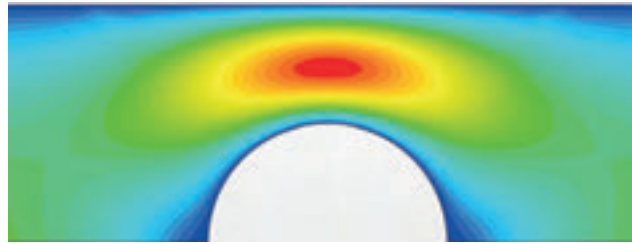


FIGURE 8: Velocity contour for the case of De=0.0

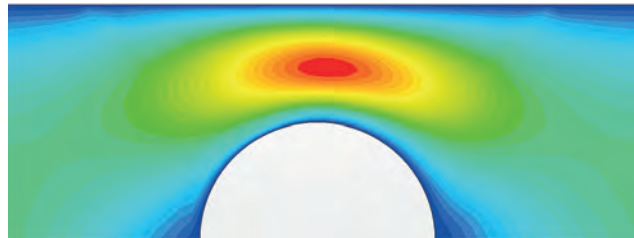


FIGURE 9: Velocity contour for the case of De=0.3

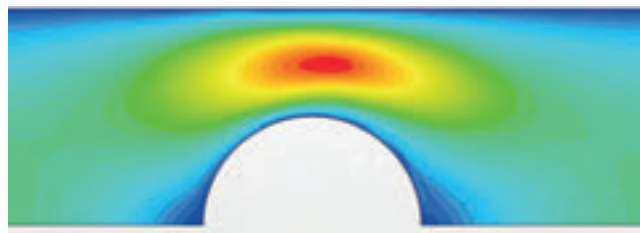


Figure 10: Velocity contour for the case of De=0.9

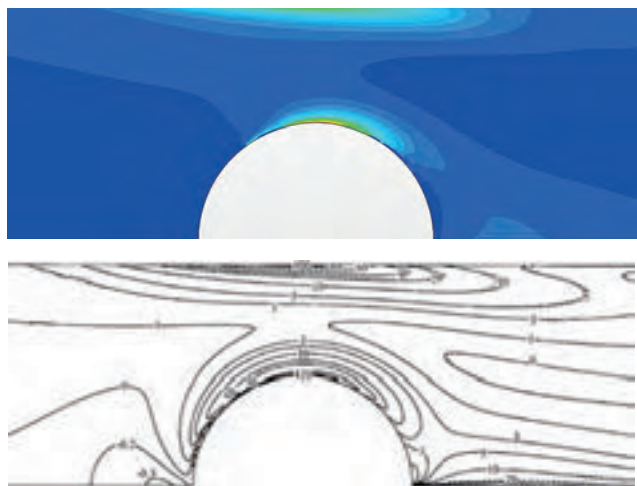
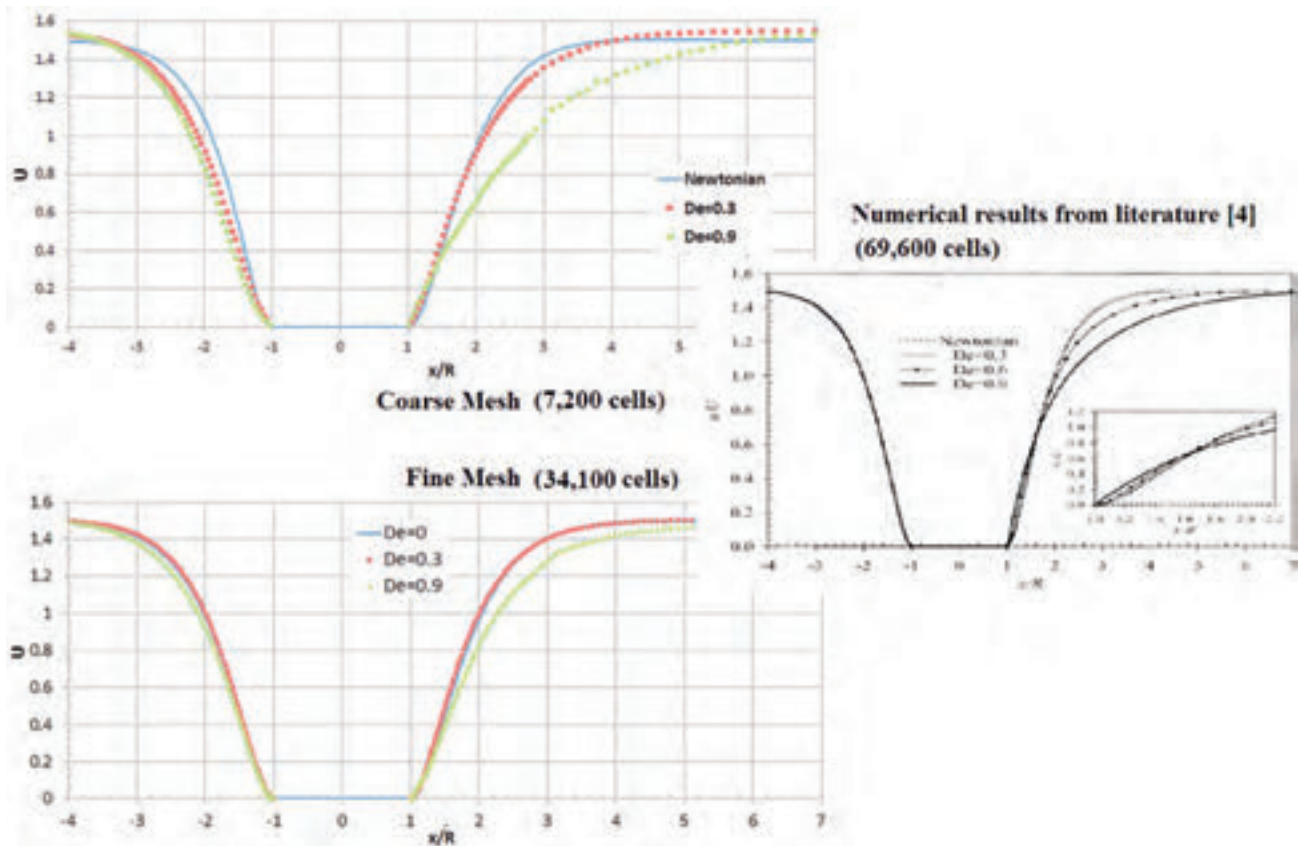


FIGURE 11: First normal stress difference comparison between STAR-CCM+® solution (top) and results from literature (bottom)



**FIGURE 12:** Center-line velocity as a function of normalized distance from the center of the cylinder. Negative locations are upstream of the cylinder.

However, in the case of figure 10, there is no recirculation zone behind the cylinder, the flow separation does not exist, and the asymmetry and the higher maximum velocity can be attributed to the non-zero first normal stress difference (a phenomenon only observed in viscoelastic fluids).

Figure 11 shows a side-by-side view of first normal stress difference ( $\tau_{xx} - \tau_{yy}$ ) contours obtained by STAR-CCM+® and in the literature [3] for  $De=0.9$ . The results are qualitatively very similar.

A comparison of center-line velocity of STAR-CCM+® and literature [3] results can be seen in figure 12. The observed trends are similar, but the STAR-CCM+® results predict a change of velocity upstream of the cylinder for  $De=0.9$  while no significant change is seen in literature. As mentioned earlier, these discrepancies are expected as this implementation is limited in how the

constitutive equations can be formulated because no changes to STAR-CCM+® are made. As seen in figure 12, mesh refinement has a very large effect on the accuracy of the solution of the additional governing equations. Further improvement can be made by increasing the mesh density, but this will also considerably increase the solution time which is in contrast with the goal of quick analysis in early stages of product/process design.

## CONCLUSION

A method was introduced to implement a viscoelastic fluid flow capability into STAR-CCM+®. Ability to easily model problems involving complex geometry, ease-of-use of the software and good pre- and post-processing capabilities of STAR-CCM+® were the motivation behind this implementation. The JAVA macro for STAR-CCM+® was only around 800 lines long, was developed in hours, and can

be used easily with future releases of the code. Implementing a viscoelastic solver directly into a CFD code would allow for a more accurate result, but the effort would take several days of coding and this implementation would have to be updated for each new version of the CFD code. This implementation with a JAVA macro into STAR-CCM+® will be very useful in early stages of product or process development, where time is of the essence. Accuracy of the model can be improved by refining the underlying mesh, but this will also increase the solution time considerably.

Work is underway to improve the numerical method by taking advantage of the most recent advances in the field of numerical rheology. This improved high-elasticity handling will allow the user to solve problems involving geometric singularities (sharp corners) and high deformation rates independent of the elasticity of the fluids involved.

## REFERENCES

- [1] A. S. Lodge: "Elastic Liquids", Academic Press, New York (1964), Figures on page 237 and 242.
- [2] J. Wisniak: "Frederick Thomas Trouton: The Man, the Rule, and the Ratio", Chem. Educator, Vol. 6, pp. 55-61, 2001.
- [3] M. A. Alves, F. T. Pinho and P. J. Oliveira: "The Flow of Viscoelastic Fluids Past a Cylinder: Finite-Volume High-Resolution Methods", Journal of Non-Newtonian Fluid Mechanics, Vol. 97, pp. 207-232, 2001.

**TRAINING TO FIT INTO YOUR SCHEDULE & LOCATION:**

[www3.cd-adapco.com/training](http://www3.cd-adapco.com/training)

**TRAINING VENUES**

- Detroit - United States
- Houston - United States
- Seattle - United States
- London - United Kingdom
- Nuremberg - Germany
- Paris - France
- Turin - Italy
- Bangalore - India
- São Paulo - Brazil
- Yokohama - Japan
- Osaka - Japan
- Seoul - South Korea
- Shanghai - China

**CHOOSE FROM ONE OF THE FOLLOWING COURSES:**

- JAVA™ Scripting - Process Automation
- STAR-CCM+® Wizard Creation
- Computational Fluid Dynamics (CFD) for the Chemical Industry
- Vehicle Thermal Management
- Effective Heat Transfer
- Introduction to Particle Modeling using the Discrete Element Method
- Lagrangian Multiphase Flow Modeling
- Advanced Engineering Optimization (Coming Soon)
- Internal Combustion Engine Analysis
- Turbomachinery Engineering (Coming Soon)
- Applied Computational Dynamics
- External Vehicle Aerodynamics (Incompressible) (Coming Soon)
- Aeroacoustics
- High Speed Aerodynamics (Coming Soon)
- Virtual Building Analysis (Including Fire Simulation)
- Advanced Meshing
- Offshore Computational Engineering
- Battery Modeling
- SPEED™ Machine Design
- STAR-Cast
- Cabin Comfort Analysis (Thermal, Acoustic, HVAC Systems)
- Electronics Thermal Management
- Wind Turbine Analysis

## TRAINING COURSES

Training adds incredible value to the software you have purchased and comes highly recommended by all. Courses are regularly held at CD-adapco™ offices around the world including Detroit, Houston, Seattle, London, Nuremberg, Paris, Turin and others. The courses listed on our website can be scheduled to suit your requirements. To take advantage of this, please request information from your account manager.

Courses are held in small groups and the number of available places can be checked online at:

[www3.cd-adapco.com/training/calendar](http://www3.cd-adapco.com/training/calendar)

Just click on the course you are interested in to get an overview on the dates, locations, and availability. If the course is not scheduled in an office near you, then why not take it via distance learning, CD-adapco™'s internet-based remote learning service. To find out more or to get a course scheduled to suit your requirements, please contact your account manager.

View your local course offerings, customer testimonials and register for an upcoming course at [www3.cd-adapco.com/training](http://www3.cd-adapco.com/training).

To register for a course complete the online registration or request a faxable form from your local support office.

<b>USA:</b> info-us@cd-adapco.com	(+1) 631 549 2300	<b>India:</b> info-in@cd-adapco.com	(+91) 804 034 1600
<b>UK:</b> info-uk@cd-adapco.com	(+44) 20 7471 6200	<b>China:</b> info-cn@cd-adapco.com	(+86) 216 100 0802
<b>France:</b> info-fr@cd-adapco.com	(+33) 141 837 560	<b>Brazil:</b> info-br@cd-adapco.com	(+55) 113 443 6273
<b>Germany:</b> info-de@cd-adapco.com	(+49) 911 946 433	<b>Japan:</b> info-jp@cd-adapco.com	(+81) 45 475 3285
<b>Italy:</b> info-it@cd-adapco.com	(+39) 011 562 2194	<b>South Korea:</b> info-kr@cd-adapco.com	(+82) 2 6344 6500

**Specialized Courses:**

New specialized courses relating to application-specific areas are developed throughout the year. Please contact your account manager for more information.

**STAR-Tutor Interactive:**

STAR-Tutor Interactive offers a broad range of tutorials and elective short courses which are delivered by our highly qualified team via live streaming feed. These virtual classes extend and focus knowledge built up from the introductory STAR-CCM+® class to cover specific engineering analysis areas. For more information, please contact your account manager.

**Note:**

In most situations, it will be possible to register trainees on the course of their choice. However, if requests for places are received too close to the course date, this may not be possible. Availability of places can be obtained online or by contacting your local office.

**CHECK OUT THIS LINK FOR COURSE AVAILABILITY:** [www3.cd-adapco.com/training/calendar](http://www3.cd-adapco.com/training/calendar)

# SIMULATING SYSTEMS



CD-adapco™ is the world's largest independent CFD-focused provider of engineering simulation software, support and services. We have over 30 years of experience in delivering industrial strength engineering simulation.

We employ more than 800 talented individuals, working at 30 different offices across the globe.

## Corporate Headquarters

CD-adapco™  
60 Broadhollow Road  
Melville, NY 11747  
USA  
☎ +1 631 549 2300  
✉ [info@CD-adapco.com](mailto:info@CD-adapco.com)  
🌐 [www.CD-adapco.com](http://www.CD-adapco.com)

## Americas

Austin • Cincinnati • Detroit • Houston • Los Angeles • New Hampshire  
Orlando • São Paulo • Seattle • State College • Tulsa

## Europe

Glasgow • London • Lyon • Nuremberg • Paris • Rome • Toulouse • Turin • Vienna

## Asia-Pacific

Bangalore • Beijing • Busan • Chennai • Pune • Seoul • Shanghai • Shin-Osaka • Shin-Yokohama • Singapore

## Resellers

### Australia

CD-adapco™ Australia  
[info@CD-adapco.com.au](mailto:info@CD-adapco.com.au)

### Israel

ADCOM Consulting Services  
(Shmuel Keidar Ltd.)  
[info@adcomsim.co.il](mailto:info@adcomsim.co.il)

### New Zealand

Matrix Applied Computing Ltd.  
[sales@matrix.co.nz](mailto:sales@matrix.co.nz)

### Russia

SAROV Engineering Center  
[info@saec.ru](mailto:info@saec.ru)

### South Africa

Aerotherm Computational Dynamics  
[martin@aerothermod.co.za](mailto:martin@aerothermod.co.za)

### Turkey

A-Ztech Ltd.  
[info@a-ztech.com.tr](mailto:info@a-ztech.com.tr)



RECYCLED PAPER. VEGETABLE INKS.

[www.cd-adapco.com](http://www.cd-adapco.com)



2 FOR 1 OFFER - IF YOU REGISTER AND PAY YOUR TICKET BEFORE DECEMBER 31, 2014  
YOU WILL RECEIVE A VOUCHER TO REGISTER A SECOND PERSON FOR FREE.\*

# STAR Global Conference 2015

SAN DIEGO



DESIGN EXPLORATION

# MARCH 16 - 18

## THE BIGGEST ENGINEERING SIMULATION EVENT OF THE YEAR



✉ [info@cd-adapco.com](mailto:info@cd-adapco.com)  
🌐 [www.cd-adapco.com](http://www.cd-adapco.com)



\* Full price paid registrations received before December 31, 2014 only.